INVESTIGATION OF THE FUNCTIONS OF THE NDC80 KINETOCHORE COMPLEX IN BUDDING YEAST

by

LINA MA

A THESIS SUBMITTED IN PARTIAL FULFILLMENT OF THE REQUIREMENTS FOR THE DEGREE OF

DOCTOR OF PHILOSOPHY

in

THE FACULTY OF GRADUATE STUDIES

(Genetics)

THE UNIVERSITY OF BRITISH COLUMBIA

(Vancouver)

October 2010

Abstract

Kinetochores are multi protein complexes comprised of inner kinetochore proteins that assemble on centromeric DNA sequences and outer kinetochore proteins that bind to microtubules. Kinetochores are responsible for accurate transmission of genetic information during each cell division. In the budding yeast *Saccharomyces cerevisiae*, the highly conserved Ndc80 kinetochore complex has been well characterized in terms of its roles in chromosome-microtubule attachment and spindle checkpoint. The work presented in this thesis suggests that the Ndc80 complex has additional cellular roles.

The kinetochore is required to prevent spindle expansion during S phase in budding yeast, but the mechanism of how the kinetochore maintains integrity of the bipolar spindle in S phase is not well understood. In Chapter 2, I demonstrate that a mutation in Spc24, a component of the Ndc80 complex, causes lethality when cells are exposed to the DNA replication inhibitor hydroxyurea (HU) due to premature spindle expansion and segregation of incompletely replicated DNA. Overexpression of Stu1, a CLASP-related MT-associated protein or a truncated form of the XMAP215 orthologue Stu2 rescues *spc24-9* HU lethality and prevents spindle expansion. Stu1 and Stu2 localize to the kinetochore early in the cell cycle and Stu2 kinetochore localization depends on Spc24. I propose that mislocalization of Stu2 results in premature spindle expansion in S phase stalled *spc24-9* mutants.

In Chapter 3 and Chapter 4, I present data suggesting that the Ndc80 complex has a role

in the cAMP/PKA glucose signaling pathway and actin regulation. Firstly, I identified genetic interactions between Spc24 and the components of cAMP/PKA pathway and demonstrated that *spc24* mutants have defects in PKA signaling in response to glucose depletion. Interestingly, most of the temperature sensitive mutant alleles of the Ndc80 complex are rescued by non-glucose carbon sources. Finally, I present actin defects in *spc24* mutants and genetic interactions between *spc24* mutants and mutants of proteins involved in actin turnover, nucleation or polarity establishment. Further investigation on the mechanism and rationale behind the kinetochore-cytoskeleton interactions will be an intriguing avenue for future research.

Preface

Chapter 2 is modified from a published paper "Ma L., McQueen J., Cuschieri L., Vogel J., Measday V, Spc24 and Stu2 Promote Spindle Integrity When DNA Replication is Stalled, Molecular Biology of the Cell, 18(8): 2805-2816 (2007)". I did the experiments described in this chapter with the following exceptions: The spot assay in Figure 2.1(A) and images in Figure 2.1(B) and 2.14 were performed by Vivien Measday. Jennifer McQueen performed all the experiments shown in Figure 2.4. Timelapse imaging in Figure 2.9, 2.10 and 2.11 were performed by Jennifer McQueen (Measday lab), Lara Cuschieri (Vogel lab) and Jackie Vogel at McGill University. The paper was written by Vivien Measday. Copyright of the paper belongs to American Society for Cell Biology (ASCB) and the link to the publication on-line is: http://www.molbiolcell.org/cgi/content/full/18/8/2805?maxtoshow=&hits=10&RESULTFORMAT=&author1=Lina+Ma&andorexacttitle=and&andorexacttitleabs=and&andorexactfulltext=and&searchid=1&FIRSTINDEX=0&sortspec=relevance&resourcetype=HWCIT.

Table of contents

List of tables

List of figures

List of symbols and abbreviations

Δ	deletion (symbol for a gene knockout)
α-factor	alpha-factor
APC	anaphase promoting complex
bp	base pair
cAMP	cyclic AMP
Cdc	Cell division cycle
Cdk	cyclin-dependent kinase
CFP	Cyan Fluorescent Protein
CH	calponin-homology
ChIP	chromatin immunoprecipitation
cMT(s)	cytoplasmic microtubule(s)
DAPI	4’,6-diamino-2-phenylindole
FACs	fluorescence activated cell sorting
FH	formin-homology
GAP	GTPase activating protein
GEF	GDP-GTP exchange factor
GFP	Green Fluorescent Protein
GPCR	G protein coupled receptor

HCS	high copy suppressor
IP	immunoprecipitation
kb	kilobase pair(s)
kD	kilodaltons
LatA	latrunculin A
min.	minute(s)
MT(s)	microtubule(s)
NPCS	non-preferred carbon source
PAGE	polyacrylamide gel electrophoresis
PCR	polymerase chain reaction
PKA	protein kinase A
SAC	spindle assembly checkpoint
S. cerevisiae	*Saccharomyces cerevisiae*
SL	synthetic lethal
SPB	spindle pole body
SS	synthetic sick
ts	temperature sensitive
VFP	Venus Fluorescent Protein

Nomenclature

Wild-type alleles in *Saccharomyces cerevisiae* are represented by italicized capital letters (e.g. *SPC24*), while mutant recessive alleles are denoted in lower case italics (e.g. *spc24-9*). Gene products are written with the first letter capitalized (e.g. Spc24).

Acknowledgements

I want to greatly thank Dr.Vivien Measday for her striking particularity and for giving me the opportunity to come to Canada and work in her lab. Thanks for waiting for me for over two hours in the airport on the first day I landed in Canada. Thanks for teaching me all the methods that I needed to learn. Thanks for reading all my proposals, committee meeting reports and thesis and making precise comments every time. Thanks for helping me prepare for my comprehensive and listening to my practice before each presentation. Thanks for prolonging my vacation every time when I visited China. Thanks for all the sweet gifts for the birth of my baby and each Christmas. More importantly, I am grateful that she always saw the end of the tunnel, especially when I didn't. Her talent always sheds light on my research and accelerates my pace for publishing a paper.

I also want to thank Liz Conibear, Jim Kronstad and Geoffrey Wasteneys for agreeing to be members of my thesis committee, squeezing in time to attend my committee meetings and sharing suggestions whenever we met.

A very special thanks goes to my program director Hugh Brock for introducing me to the world of genetics, telling me what a real scientist is and what the life will be, and giving me the self-confidence to start a PhD. And thanks the program secretary Monica Deutsch for all the information and official letters.

The Measday lab is a great place to work and the support from everybody at any given time is more than one could expect. We are a small team but super warm. Thanks Nina Piggott, for ordering all the reagents I need and making the lab so neat and organized, and thanks for making all the delicious cakes when celebrating everyone's birthday. Thanks Jennifer McQueen, for flying to Montreal and working day and night on the live imaging for my paper. Thank Angel Chang for all the nice biscuits. Thanks Krystina Ho for our delightful chats and help for my writing. Thanks Mike Anderson for teaching me the tips for powerpoint. Thanks Ravi, Nick, Linda, Steve and Dheva for making the media.

I also want to thank Hieter lab especially the following people: Thanks Irene for all the reagent help, thanks Jan, Kirk and Ben for sharing ideas and the help with microscope, thanks Karen and Jessica for teaching me how to use the FACs machine.

I want to thank my husband Hongwei Song, for doing as much housework as possible and taking care of Bryan when I was busy. Thanks to my parents, for agreeing to let their only

child going abroad, suffering their missing and holding the longing for the short reunion every two or three years. Thanks to my son Bryan, your smile, sweet and smart always makes me happy and feel that all my effort is deserved.

Chapter 1 General Introduction

1.1 Cell division

Life has the ability to pass on its genetic material to the daughter cell by cell division. Cell division involves the division of the nucleus (mitosis) and of the cytoplasm (cytokinesis) of a cell. Errors in chromosome transmission lead to aneuploidy (an abnormal number of chromosomes) and even cell death. Therefore, highly conserved machineries and mechanisms orchestrate cell cycle events to ensure proper chromosome transmission and promote genome stability.

1.1.1 Life cycle in the budding yeast

The budding yeast *Saccharomyces cerevisiae* is a small, unicellular eukaryote that provides a perfect tool for studying mitotic events. It is easy to utilize genetic and biochemical experimental methods in budding yeast. Budding yeast grows rapidly when supplied with full nutrients and is able to alternate between a haploid and diploid state. Haploid cells have two mating types, MATa and MATα, which can mate with each other and generate diploid zygotes. In response to starvation diploid cells can sporulate and germinate to form four haploid cells (Figure 1.1) (Morgan, 2007).

1.1.2 Mitotic cell cycle

During cell division, chromosomes undergo a cycle of replication and segregation that is synchronized with the cell cycle. The mitotic cell cycle is divided into four phases, named G1, S (DNA replication), G2 and M (mitosis) (Figure 1.2). M phase has two substages: metaphase and anaphase. In metaphase, duplicated chromosomes (sister chromatids) achieve bipolar attachment to the mitotic spindle via the kinetochore, which is a multiprotein complex connecting centromere DNA and spindle microtubules. In anaphase, the sister chromatids are pulled apart from each other and segregated into the mother cell and the daughter cell. The key machinery to define the boundaries between these phases is the cyclin dependent kinase (CDK) complex, which is activated by cyclin binding. The levels of Cdks are constant but the levels of cyclins oscillate during the cell cycle, therefore Cdk/cyclin complexes perform different and specific tasks depending on the cyclin partner. In budding yeast, there are nine cyclins (Cln1-3, Clb1-6) but only one CDK, called Cdc28 (Cdk1) (Figure 1.3A). Successive activation and inactivation of Cdc28/cyclin is required for ensuring proper progress during the cell cycle (Figure 1.3B) (Morgan, 2007).

Budding yeast must achieve a critical cell size in G1 prior to entering a new cell cycle. The G1/S cell cycle transition, termed START, occurs upon initiation of budding, replication of the 16 chromosomes and spindle pole body (SPB) duplication. SPBs are embedded in the nuclear envelope throughout the cell cycle, which is different from higher eukaryotes whose nuclear envelope is broken down during centrosome duplication (animal cells) or after spindle pole

formation (plant cells). SPBs nucleate microtubules both inside and outside of the nucleus. Cytoplasmic microtubules project towards the cell cortex where they perform an important function by generating forces required for spindle orientation. Intranuclear microtubules are composed of 32 kinetochore microtubules which each attach to one kinetochore, and 8 overlapping polar microtubules (Tanaka, *et al*., 2005; Morgan, 2007).

Prometaphase is defined as the stage when replicated chromosomes are transported to the spindle through the interaction between kinetochores and microtubules (Tanaka, *et al.*, 2005). In yeast an accurate boundary between S phase and prometaphase is hard to define (McAinsh, *et al*., 2003; Tanaka, *et al*., 2005). During metaphase cells prepare the duplicated sister chromatids for a proper division. Unlike in higher eukaryotes, where chromosomes align at the metaphase plate between the spindle poles, yeast chromosomes are distributed along the metaphase spindle. The reason for this is precocious splitting of the sister chromatids around the centromere region while chromatid arms are still held together. This process is also known as biorientation, because kinetochores of two sister chromatids have to attach to spindle microtubules emanating from opposite SPBs (Straight, 1997; Tanaka, *et al*., 2005). Once the checkpoints monitoring the correct attachment between kinetochore and microtubules are satisfied, the cell is ready to transit from metaphase to anaphase and to separate the sister chromatids. The anaphase promoting complex (APC) is activated by Cdc20 and thereafter ubiquitinates proteins which are subsequently targeted for degradation by the 26S proteasome. One target of APC^{Cdc20} is securin which inhibits the protease separase. Ubiquitination of securin releases separase to cleave Scc1,

which is one of the four subunits of the cohesin complex bundling sister chromatids (Morgan, 2007; Peters, *et al*., 2008). After release from cohesin, sister chromatids rapidly move to opposite spindle poles in anaphase A. Anaphase B is characterized by the subsequent separation of the poles and elongation of the mitotic spindle (Straight, *et al.*, 1997). Telophase is defined as the stage when the spindle reaches its maximum length and is subsequently disassembled, followed by the separation of the cell and the nucleus into two during cytokinesis (Tanaka, *et al*., 2005; Morgan, 2007) (Figure 1.2).

1.2 Kinetochore

The kinetochore is defined as the complex of proteins that binds centromeric DNA and provides a platform for microtubule attachment that mediates chromosome movement and checkpoint signaling (Maney, *et al.*, 2000). The budding yeast kinetochore is the best characterized and kinetochore architecture is highly conserved among higher eukaryotes (Kitagawa & Hieter, 2001; Przewloka & Glover, 2009; Santaguida & Musacchio, 2009).

1.2.1 Centromere

Kinetochore proteins are required to assemble on a specific region of the chromosomes to ensure correct segregation. The region for assembly can be restricted to one site (monocentric chromosomes) or extended over the whole chromosome (holocentric chromosomes, e.g.

Caenorhabditis.elegans) (Madddox, *et al*., 2004). In budding yeast a relatively short stretch of 125 base pairs (bp), which is referred to as the centromere (Figure 1.4), is necessary and sufficient to direct the assembly of a kinetochore. By comparison, in fission yeast and vertebrates centromeres are spread over several kilobases or megabases (regional centromeres). Furthermore, the centromeric DNA sequence in budding yeast is conserved whereas no conserved centromere sequence is determined in other eukaryotes (Santaguida & Musacchio, 2009). These differences make the centromere of budding yeast much more accessible for genetic manipulations.

1.2.2 Kinetochore assembly

The budding yeast kinetochore consists of more than 65 proteins which assemble in a hierarchical order as several multiprotein subcomplexes. According to their relative position between centromere and spindle microtubules, they are often grouped into three categories — inner kinetochore, centre kinetochore and outer kinetochore protein complexes. Inner kinetochore proteins interact directly with centromeric DNA and provide a platform for the assembly of other kinetochore proteins. Outer kinetochore proteins bind directly to the spindle microtubules, and central kinetochore proteins are linkers for inner and outer kinetochore layers (Westermann, *et al.*, 2007). This classification is consistent with a model that suggests that the kinetochore is built up from the centromere towards the microtubule attachment site in an inside-out manner (Santaguida & Musacchio, 2009). However, these categories only provide an approximate position and sometimes it is difficult to assign protein complexes strictly to one of

these layers. The core protein complexes are described in more detail in the following paragraphs and a simplified scheme of the kinetochore architecture is given in Figure 1.5 (Bloom, *et al*., 2010).

In budding yeast, the inner kinetochore is composed of the centromere binding factor 3 (CBF3) complex and the Cse4-nucleosome and is essential for the recruitment of all other kinetochore proteins (Santaguida & Musacchio 2009). The CBF3 complex, which consists of Ndc10, Cep3, Ctf13 and Skp1, interacts directly with CDEIII (see Figure 1.4) and is the primary determinant for kinetochore construction since all analyzed budding yeast kinetochore proteins depend on CBF3 for association with the centromere (Westermann, *et al.*, 2007). Although the CBF3-like complex seems to be restricted to fungi with a sequence-defined centromere, Skp1 is functionally conserved between yeast and humans (Kitagawa & Hieter, 2001). In addition, Ndc10 alone can also bind to CDE II and probably serves as a foundation for recruiting other kinetochore proteins to the centromere (Espelin, *et al.*, 2003).

The relatively uncharacterized Ctf19 complex consists of more than 10 proteins and four of these proteins, Ctf19, Okp1, Mcm21 and Ame1, copurify as a subcomplex called COMA. Only Okp1 and Ame1 are required for viability and Mcm21 is essential for pericentromeric cohesion in ensuring kinetochore biorientaion (Westermann, *et al*., 2007; Santaguida & Musacchio, 2009; Ng, *et al.*, 2009).

The Spc105 complex consists of Spc105 and Kre28 (YDR532C) and is poorly described in budding yeast (De Wulf, *et al.*, 2003; Necrasov, *et al.*, 2003). Homologs in different

eukaryotes are known as Spc7, KNL-1 or Blinkin. It was shown that this complex tightly interacts with two other complexes, the MIND (Mtw1-Nnf1-Nsl1-Dsn1) and Ndc80 complexes, and with components of the spindle assembly checkpoint. Studies of the *D. melanogaster* Spc105 protein suggest a role in providing a platform within the outer kinetochore upon which various other kinetochore proteins can assemble (Schittenhelm, *et al.*, 2009). In budding yeast, Spc105/Kre28 was suggested to have essential roles in both bipolar attachment and recruitment of spindle checkpoint components (Pagliuca, *et al.*, 2009).

The budding yeast proteins Mtw1, Dsn1, Nnf1 and Nsl1 form the MIND-complex. Mutants in complex subunits result in chromosome missegregation and insufficient tension between sister kinetochores. The MIND complex interacts with Cse4, Mif2 and Ndc80 and is conserved from yeast to humans (Euskirchen, *et al.*, 2002).

One of the best characterized kinetochore components is the Ndc80 complex, which I will describe in more detail later (see 1.2.4). In budding yeast, the MIND, Ndc80 and Spc105 complexes likely interact tightly to form the highly conserved KMN network (KNL1, Mis12, Ndc80) as a core kinetochore microtubule binding complex (Cheeseman and Desai, 2008). The combined protein network was shown to bind with higher affinity to microtubules than the single complexes and likely forms a microtubule binding site for attaching kinetochores to dynamic microtubules (Tanaka & Dasai, 2008).

The budding yeast Dam1 complex is a fungal-specific outer kinetchore complex, that consists of ten proteins: Dam1, Ask1, Dad1, Dad2, Dad3, Dad4, Duo1, Spc19, Spc34 and Hsk3

(Hofmann, *et al.*, 1998; Enquist-Newman, *et al.*, 2001; Cheeseman, *et al.* 2001; Cheeseman, *et al.*, 2002; De Wulf, *et al.*, 2003; Janke, *et al.*, 2002; Li, *et al.*, 2002) . The complex has an important role in mediating kinetochore-microtubule interactions and chromosome segregation. Dam1 is a target of the Ipl1 kinase, which plays an important role in the correction of improper kinetochore-microtubule attachments (Cheeseman, *et al*., 2001; Li, *et al*., 2002; Pinsky, *et al.*, 2006; Westermann, *et al*., 2007). Biochemical analysis and *in vitro* studies revealed the formation of a ring around a microtubule formed by 16 single heterodecameric Dam1 complexes. The ring diffuses along the microtubule lattice and moves processively with a depolymerizing end of a microtubule (Westermann, *et al*., 2005; Wang, *et al*., 2007; Grishchuk, *et al.*, 2008; Lampert, *et al.*, 2010; Tien, *et al.*, 2010).

Microtubule associated proteins (MAPs) and motor proteins are also present at kinetochore structures and play additional roles in chromosome attachment and segregation. These MAPs include Stu2 (XMAP215), Bik1 (CLIP170) and Bim1p (EB1), which recognize and bind to plus ends of microtubules and regulate microtubule dynamics (Berlin, *et al*., 1990 ; Schwartz, *et al*., 1997 ; Wang and Huffaker, 1997; Tirnauer, *et al*., 1999 ; Kosco, *et al.*, 2001; Hwang, *et al*., 2003 ; Miller, *et al*., 2006 ; Wolyniak, *et al*., 2006 ; Al-Bassam, *et al.*, 2006; Gardner, *et al*., 2008 ; Zimniak ,*et al*., 2009*et al*; Blake-Hodek, *et al*., 2010). Motor proteins like Kar3, Kip1, Kip3 and Cin8 play a role in chromosome segregation by crosslinking spindle microtubules or organizing chromosome movements, but their exact function during mitotic processes is not fully understood (McAinsh, *et al*., 2003; Westermann, *et al*., 2007; Gardner, *et*

al., 2008).

1.2.3 Regulation of kinetochore-microtubule attachment

During metaphase, sister chromatids must attach to the microtubules from opposite SPBs in order to ensure equal distribution of DNA to both cells. Mature, bipolar attachments generate tension across kinetochores. Errors in attachment or tension are recognized by two mechanisms. Aurora B/Ipl1 and its partner INCENP/Sli15 respond to the absence of tension by stimulating kinetochore-microtubule detachment which liberates kinetochores to attach to the opposite pole (Biggins and Murray, 2001; Tanaka, *et al*., 2002; Pinsky & Biggins, 2005; Liu & Lampson, 2009; Kelly & Funabiki, 2009). However, Aurora B/Ipl1 does not repair all the attachment errors and the spindle assembly checkpoint (SAC) is required to block the metaphase-anaphase transition until all the chromosomes have attained bipolar attachment to the mitotic spindle (Taylor and McKeon, 1997; Gillett & Sorger, 2001; Warren, *et al.*, 2002). Even though the function of the SAC is well established, it is unclear whether the checkpoint responds only to chromosome detachment or to the loss of tension as well.

In budding yeast, the key components of the SAC pathway are Mad1, Mad2, Mad3 (BubR1 in humans), Bub1, Bub3 and Mps1 (Hoyt, *et al*., 1991; Li & Murray, 1991; Weiss, *et al*., 1996). This checkpoint is extremely sensitive. One unattached kinetochore is sufficient to activate the checkpoint (Ault, *et al*., 1991; Ault, *et al*., 1992). In higher eukaryotes, the SAC is essential and all the checkpoint proteins localize to kinetochores in prometaphase cells. In

budding yeast the *BUB* and *MAD* genes are non-essential however other genes involved in the spindle checkpoint, such as Mps1 and Ipl1 are essential (reviewed in Lew & Burke, 2003). Bub1 and Bub3 associate with kinetochores until metaphase. However, Mad2 is only recruited to unattached kinetochores upon microtubule depolymerization or kinetochore disruption, but does not associate with the kinetochore in a normal cell cycle (Hoyt, *et al*., 1991; Li, *et al*., 1991; Gillett, *et al*., 2004; Musacchio & Salmon, 2007; Santaguida, *et al*., 2009).

Kinetochores are required for SAC activation. The complete inactivation of CBF3 leads to a failure of checkpoint control and prevents Mad and Bub proteins from associating with kinetochores (Goh & Kilmartin, 1993; Gardner, *et al*., 2001). However, hypomorphic mutations in CBF3 subunits which causes a partial loss of gene function engage the checkpoint (Doheny, *et al.*, 1993). Therefore, the checkpoint is sensitive to partially inactive kinetochores but the signaling complexes cannot form in the absence of the kinetochore.

1.2.4 The Ndc80 complex

The Ndc80 complex contains four proteins – Ndc80, Nuf2, Spc24 and Spc25 – all of which are essential and localize exclusively to kinetochores based on fluorescence microscopy imaging (Wigge & Kilmartin, 2001; He, *et al*., 2001; Janke, *et al*., 2001). All the Ndc80 complex components are evolutionarily well conserved and are also required for chromosome segregation in human cells, *Xenopus* and other organisms (Table 1.1) (Zheng, *et al*., 1999; Howe, *et al*., 2001;

Janke, *et al*., 2001; Wigge, *et al*., 2001; DeLuca, *et al*., 2002; Le Masson, *et al*., 2002; Hori, *et al*., 2003).

The structure of Ndc80 complex was first determined by electron microscopy (Wei, *et al*., 2005). It forms a long dumbbell shape with globular domains at the ends and an elongated coiled-coil domain in between (Figure 1.6A) (Ciferri, *et al*., 2005; Wei, *et al*., 2005). The Spc24/Spc25 subcomplex forms a dimer that interacts with Ndc80/Nuf2 with their N-terminal coiled-coil domains and interacts with other kinetochore proteins via their C-terminal globular domains (Joglekar, *et al*., 2009; Wan X, *et al*., 2009). The Ndc80/Nuf2 subcomplex binds microtubules directly with their N-terminal globular domains (Cheeseman, *et al*., 2006; Wei, *et al*., 2007; Ciferri, *et al*., 2008) whereas their C-terminal coiled-coil domains interact together and form a tetramerization domain that meets the Spc24/Spc25 dimer (Ciferri, *et al*., 2005; Wei, *et al*., 2005) (Figure 1.6A,C).

In budding yeast, there are approximately 8 copies of the Ndc80 complex on each microtubule attachment site (Joglekar, *et al.*, 2006). A recent study with Ndc80 complex coated beads proposed that the Ndc80 complex undergoes biased diffusion towards the minus end of a depolymerizing microtubule (Powers, *et al.*, 2009) (Figure 1.6E). However, how the Ndc80/Nuf2 subcomplex binds the microtubule remains unclear. Structural analyses reported that the microtubule binding domain of Ndc80/Nuf2 consists of one unique unstructured tail in Ndc80 and two calponin-homology (CH) domains, which have high affinity with the acidic C-terminus of tubulin (Cheeseman, *et al*., 2006; Wei, *et al*., 2007; Ciferri, *et al*., 2008; Powers, *et al*., 2009),

whereas other studies argue that the CH domain is not necessary for microtubule binding (Wilson-Kubalek, *et al*., 2008; Guimaraes, *et al*., 2008; Miller, *et al*., 2008).

Besides directly binding microtubules, the Ndc80 complex plays a role in the regulation of kinetochore-microtubule attachment as a target of the Aurora B/Ipl1 kinase (DeLuca, *et al*., 2006; Cheeseman, *et al*., 2006; Pinsky, *et al.,* 2006; Akiyoshi, *et al.,* 2009). The Aurora B/Ipl1 mediated phosphorylation of Ndc80, probably in the N-terminal unstructured region of the protein, reduces Ndc80 microtubule binding ability (DeLuca, *et al*., 2006; Cheeseman, *et al*., 2006; Wei, *et al*., 2007). Preventing Ndc80 from Aurora B/Ipl1 phosphorylation leads to overstretched kinetochores due to the stabilization of the kinetochore-microtubule attachments, high frequency of merotelic kinetochores (a sister chromatid attached to both poles) and overstabilized plus end microtubules (Cimini, *et al*., 2006; DeLuca, *et al*., 2006). In addition, the Ndc80 complex is also involved in the Ipl1 dependent corrective detachment of kinetochores in an indirect manner. Tien *et al.* (2010) have demonstrated that the Dam1 complex promotes Ndc80 complex tracking along the microtubules and that this interaction is abolished by Ipl1 phosphorylation of Dam1 when the kinetochores lack tension.

A second role of the Ndc80 complex is signaling attachment defects to the spindle checkpoint. The Ndc80 complex is essential for recruiting the SAC proteins Mad1, Mad2 and Mps1 to unattached kinetochores (Martin-Lluesma, *et al*., 2002; DeLuca, *et al*., 2002; Hori, *et al*., 2003; DeLuca, *et al*., 2003; McCleland, *et al*., 2003; Bharadwaj, *et al*., 2004; Meraldi, *et al*., 2004; McCleland, *et al*., 2004; Gillett, *et al*., 2004). Depleting Ndc80 or Nuf2 in mammalian

cells dramatically reduces the protein levels of Mad1 and Mad2, but a Mad2-dependent mitotic arrest is still triggered probably due to the residual kinetochore recruitment of the checkpoint proteins (DeLuca, *et al.*, 2002; Hori, *et al.*, 2003; McCleland, *et al.*, 2003; Bharadwaj, *et al.*, 2004; Martin-Lluesma, *et al.*, 2002; DeLuca, *et al.*, 2003). Complete depletion of Ndc80 complex subunits or interference with their function abolishes the SAC (McAinsh, *et al.*, 2003; McCleland, *et al.*, 2004; Meraldi, *et al.*, 2004; Guimaraes, *et al.*, 2008). Overexpression of Ndc80 in a mouse model leads to hyperactivation of the SAC and tumor formation (Diaz-Rodr ǵuez, *et al.*, 2008). It remains unknown how checkpoint proteins associate with kinetochores and sense attachment problems, but two-hybrid interactions have been detected between yeast Spc25 and Mad1 (Newman, *et al.*, 2000) and between human Ndc80 and Mad1 (Martin-Lluesma, *et al.*, 2002) and synthetic growth defects between *mad1*Δ and *spc24* ts alleles (Montpetit B, *et al.*, 2005). Moreover, recruitment of Bub1 and Bub3 to centromeres requires some but not all members of the Ndc80 complex, indicative of a requirement of the Ndc80 complex in SAC (Gillett, *et al.*, 2004).

1.3 Summary

Kinetochores are large, complicated structures whose function is vital to the fidelity of chromosome segregation. Although much is known about the structure of the Ndc80 complex, all its known activities are restricted to kinetochore-microtubule attachment and spindle checkpoint functions. The major goal of my thesis work was to investigate novel roles of the Ndc80 complex

by utilizing *spc24* temperature sensitive (ts) alleles in budding yeast.

Objective 1: Since the *spc24-9* kinetochore mutant prematurely elongates its spindle in response to hydroxyurea (HU) which stalls DNA replication, a potential role for Spc24 in the DNA replication checkpoint and spindle stability was studied. In Chapter 2, I performed a high copy suppressor (HCS) screen to identify genes that when overproduced would rescue the HU sensitivity of *spc24-9*. I further studied one of the genes identified in this screen, the Stu2 microtubule binding protein, and characterized the roles of Spc24 and Stu2 in maintaining spindle stability by quantitative and time-lapse fluorescence analysis.

Objective 2: Previous studies from the Measday lab have shown a genetic interaction between *spc24-9* and two components of cAMP/PKA pathway, and two other studies have demonstrated an interaction between kinetochore proteins and cAMP/PKA pathway (Dubacq, *et al*., 2002; Li, *et al*., 2005). Therefore, the relationship between the Ndc80 complex and the cAMP/PKA pathway was of interest to study. In Chapter 3, I analyzed cAMP/PKA pathway activity through two of its targets, trehalose levels and Msn2 phosphorylation, in *spc24* mutant strains and compared the growth of different kinetochore ts mutants on different carbon sources by cell dilution assay.

Objective 3: Some of *spc24-9* mutant cells have an elongated bud at the non-permissive temperature which suggested that the Swe1-dependent morphogenesis checkpoint was activated in these mutants. Indeed I found that Swe1 levels were stabilized in *spc24-9* cells at restrictive temperature. The objective of this chapter was to characterize why the morphogenesis

checkpoint is activated in *spc24-9* mutants. I focussed my analysis on genetic interactions with mutants in actin patch and cable formation and key polarity determinants and fluorescence imaging of the septin scaffold and the actin cytoskeleton.

Table 1.1 Homologs of Ndc80 complex in multiple organisms.

	S. cerevisiae	***S. pombe***	***C. elegans***	***Xenopus***	***H. sapiens***
Ndc80 complex	Ndc80	Ndc80	Ndc-80	xNdc80	HsNdc80
	Nuf2	Nuf2	Jim-10	xNuf2	HsNuf2
	Spc24	Spc24	Kbp-4	xSpc24	HsSpc24
	Spc25	Spc25	Kbp-3	xSpc25	HsSpc25

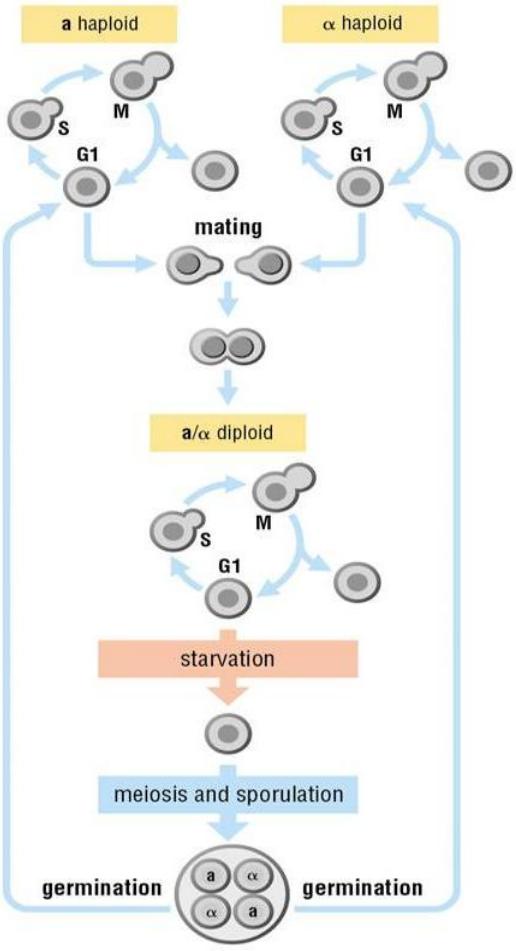

Figure 1.1 Life cycle of *Saccharomyces cerevisiae*

(Cited from D. Morgan, 2007, by permission © Oxford University Press, 2010)

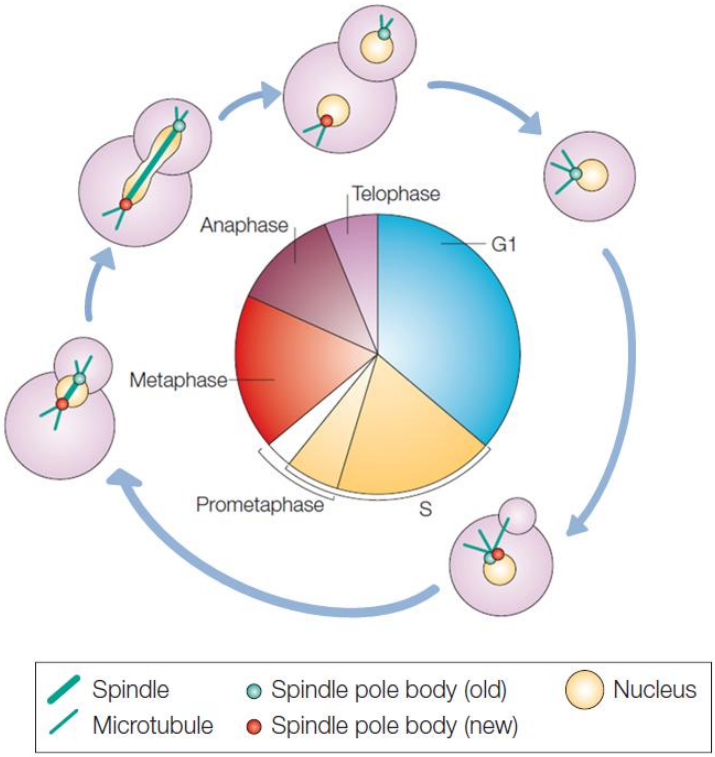

Figure 1.2 Mitotic cell cycle stages of budding yeast

(Modified from Tanaka *et al*., 2005, by permission © Nature Publishing Group)

A

Cell-Cycle Control Cyclins

Species	Cyclin class (with Cdk partner) G1	G1/S	S	M
S. cerevisiae	Cln3 (Cdk1)	Cln1,2 (Cdk1)	Clb5,6 (Cdk1)	Clb1,2,3,4 (Cdk1)

B

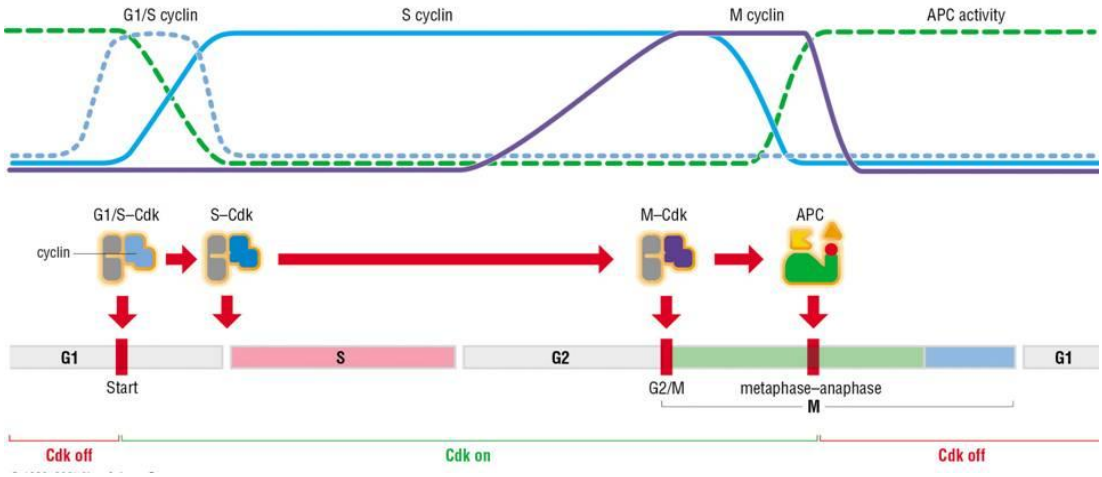

Figure 1.3 A simplified view of the cell-cycle control system

A. Cyclins in budding yeast.

B. Oscillations of cyclins (top) and cyclin-Cdk complexes (bottom) drive cell-cycle events. (Cited from D. Morgan, 2007, by permission © Oxford University Press, 2010)

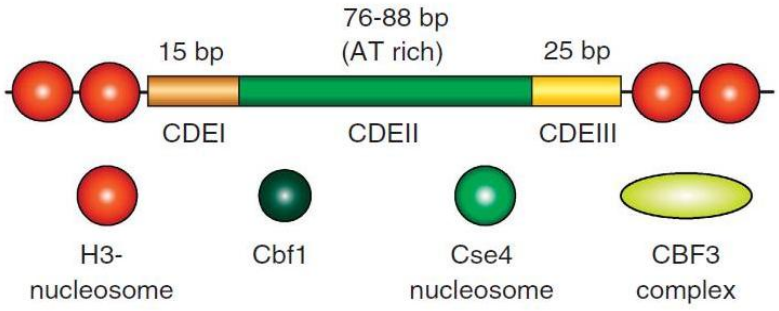

Figure 1.4 Centromere of *Saccharomyces cerevisiae*

The centromere of budding yeast is divided into three regions: CDEI, recruits a dimer of the Cbf1 transcription factor (Bram and Kornberg, 1987); CDEII surrounds the Cse4-nucleosome (Meluh *et al*, 1998; Keith and Fitzgerald-Hayes, 2000); CDEIII, which is bound by the CBF3 complex(Lechner and Carbon, 1991). (Cited from Santaguida & Musacchio, 2009**,** by permission © Nature Publishing Group)

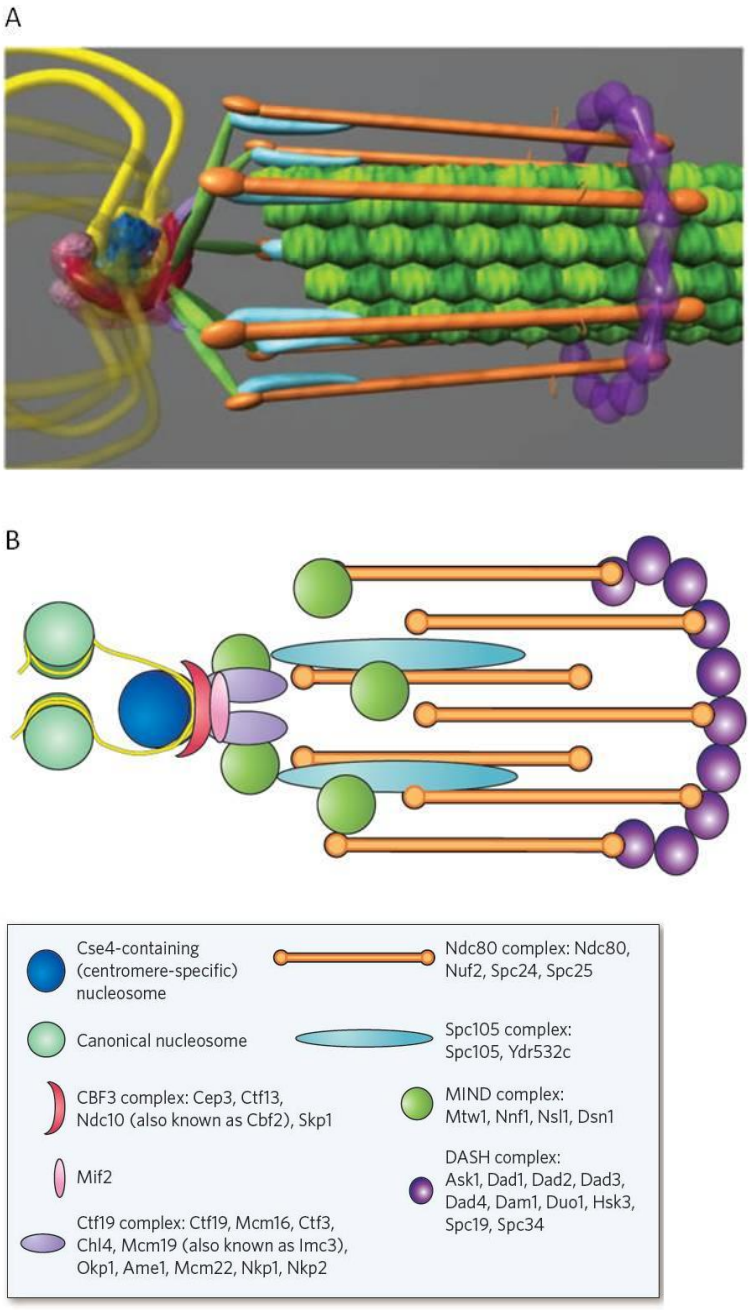

Figure 1.5 Protein architecture of the *Saccharomyces cerevisiae* kinetochore

A. The *S. cerevisiae* kinetochore image derived from *in vivo* super-resolution microscopy (Joglekar *et al*., 2009). The left part: yellow strands: DNA; dark blue: histone; dark pink: CBF3 complex; light pink sphere: centromeric DNA. The right part: central green structures: microtubules; purple ring: DASH complex; orange rods: Ndc80 complex. The linker complexes: light blue: Spc105 complex; green: MIND complex; small purple: Ctf19 complex.
B. A schematic model of the kinetochore structure in A. (Cited from Bloom & Joglekar, 2010, by permission © Nature Publishing Group)

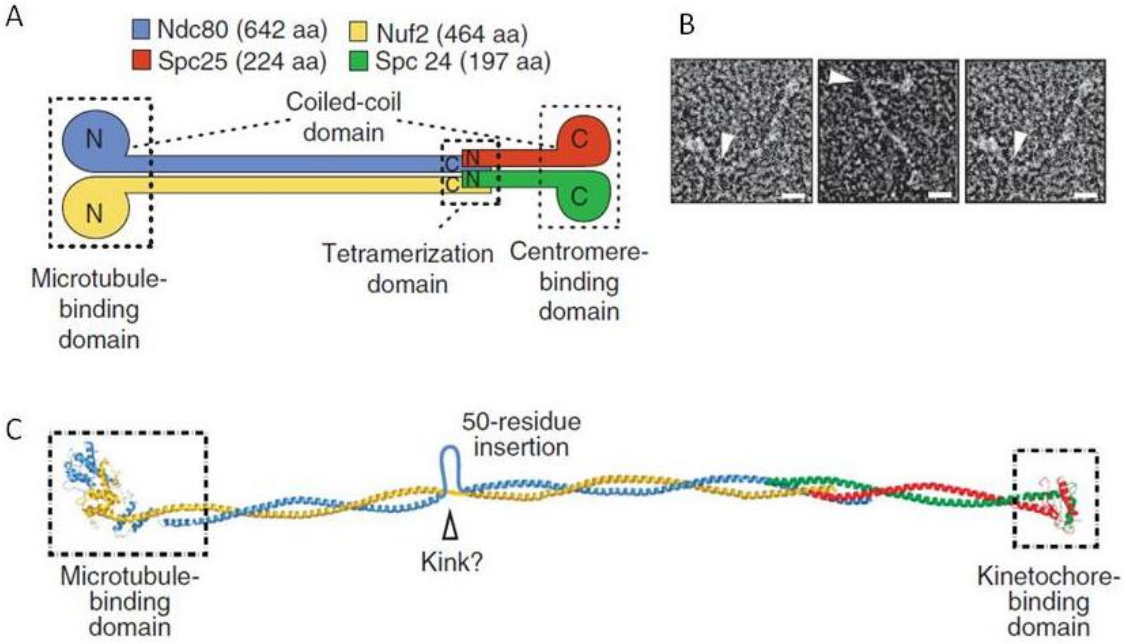
A
Ndc80 (642 aa)
Nuf2 (464 aa)
Spc25 (224 aa)
Spc 24 (197 aa)
Coiled-coil domain
N
N
C
C
N
C
C
N
Microtubule-binding domain
Tetramerization domain
Centromere-binding domain
B
C
50-residue insertion
Kink?
Microtubule-binding domain
Kinetochore-binding domain
D
GMPCPP
GMPCPP + Ndc80 complex
E
–
+
Biased diffusion

Figure 1.6 The molecular machinery of kinetochore–microtubule attachment

(A) Topology of the Ndc80 complex. aa, amino acids. N and C indicate the N- and C-termini, respectively. The image is reproduced from Ciferri *et al* (2008).
(B) Electron microscopy images of negatively stained Ndc80 complexes. The arrowheads point to the kink along the shaft. Scale bar: 10nm. The images are reproduced from Wang *et al* (2008).
(C) A model of the full length Ndc80 complex.
(D) The Ndc80 complex forms rod-like projections on the microtubule lattice. Left: the control microtubules stabilized with a non-hydrolysable GTP analogue GMPCPP. The middle image is the negatively stained GMPCPP microtubules in the presence of 5 mM Ndc80 complex (C. elegans). Right: traces of the EM images representing the angled rod-like complexes bound to the lattice. Scale bars:200 nm. The images are reproduced from Cheeseman *et al* (2006).
(E) A biased diffusion model of the Ndc80 complex proposed by Powers *et al* (2009). Kinetochores (showed as red hollow discs) diffuse along the lattice by the interaction with five microtubule-binding elements. "+" and "–" refer to the plus end and minus end, of the microtubules, respectively.
(Adapted from Santaguida & Musacchio, 2009, by permission © Nature Publishing Group)

Chapter 2 Spc24 and Stu2 Promote Spindle Integrity when DNA Replication is Stalled[1]

2.1 Introduction

Preserving the integrity of the genome is a fundamental requirement for eukaryotic cell viability. DNA replication must be completed prior to segregation of the chromosomes to prevent the transmission of partially replicated chromosomes to daughter cells. In the budding yeast *Saccharomyces cerevisiae*, cells undergo a closed mitosis and the MT organizing centres, which in yeast are called spindle pole bodies (SPBs), are embedded in the nuclear envelope. SPB duplication begins at G1 and spindle formation begins during S phase when duplicated SPBs separate from each other (Adams and Kilmartin, 1999; Jaspersen and Winey, 2004). Because chromosomes remain attached to kinetochore MTs throughout the cell cycle, spindle expansion must be restrained until all sixteen chromosomes have duplicated and kinetochores on sister chromatids have formed bipolar MT attachments. When DNA replication is stalled by HU treatment, cells arrest with a large bud, an undivided nucleus is positioned at the mother-bud neck and a short bipolar spindle forms (Allen *et al.*, 1994). Maintaining a short spindle is

[1] Chapter 2 is a modified version of a published paper: Ma L., McQueen J., Cuschieri L., Vogel J., Measday V, Spc24 and Stu2 Promote Spindle Integrity When DNA Replication is Stalled, Molecular Biology of the Cell, 18(8): 2805-2816 (2007). By permission © The American Society for Cell Biology. See details in Preface.

crucial for cell survival during HU induced arrest, which activates the DNA replication checkpoint effectors Mec1 and Rad53 (Kolodner *et al.*, 2002). When *mec1* and *rad53* mutants are treated with HU, the DNA replication checkpoint is not activated and as a result replication forks are not stabilized, the spindle expands and unequal division of incompletely replicated nuclear material occurs – all of these events contribute to cell lethality (Allen *et al.*, 1994; Weinert *et al.*, 1994; Lopes *et al.*, 2001).

In human cells, stalled replication forks activate the ATM (ataxia telangiectasia mutated) and Chk2 kinases, which are Mec1 and Rad53 homologs respectively, and arrest the cell cycle by inhibiting mitotic entry (Canman, 2001). Until recently, it was presumed that *mec1* and *rad53* mutants enter mitosis prematurely upon HU treatment. However, two recent studies have shown that this is not the case, suggesting that spindle expansion is actively restrained when DNA replication is stalled (Krishnan *et al.*, 2004; Bachant *et al.*, 2005; Krishnan and Surana, 2005). Two mechanisms, which are not mutually exclusive, have been proposed for how spindle expansion is prevented during the DNA replication checkpoint. One mechanism suggests that spindle associated proteins are regulated in a Mec1/Rad53-dependent manner (Krishnan and Surana, 2005). Spindle expansion and nuclear division of *mec1-1* mutants is reduced in cells carrying mutations of the kinesin-5/BimC ortholog Cin8 and XMAP215 ortholog Stu2 (Krishnan *et al.*, 2004). The second mechanism proposes that tension imposed by the bipolar attachment of kinetochores to MTs emanating from opposite SPBs is responsible for maintaining a short spindle upon inhibition of DNA replication (Bachant *et al.*, 2005).

In budding yeast, each kinetochore, a multi-protein complex that resides on centromere (*CEN*) DNA, attaches to a single MT (McAinsh *et al.*, 2003). After chromosome replication, kinetochores on sister chromatids must attach to MTs emanating from opposite SPBs in order to achieve bipolar attachment. The SPB pulling force opposes the cohesion complex holding sister chromatids together and creates tension that physically separates *CEN* regions during metaphase (Goshima and Yanagida, 2000; He *et al.*, 2000; Pearson *et al.*, 2001). The kinetochore not only attaches to spindle MTs but is also capable of regulating MT dynamics and spindle stability before and during mitosis. Firstly, MT associated proteins such as Stu2 and kinesin-related motor proteins localize to and function at kinetochores (He *et al.*, 2001; McAinsh *et al.*, 2003; Tanaka *et al.*, 2005; Tytell and Sorger, 2006). Secondly, the Dam1 outer kinetochore complex encircles MTs and mutations in Dam1 components severely affect MT dynamics (Cheeseman *et al.*, 2001; Miranda *et al.*, 2005; Westermann *et al.*, 2005; Shimogawa *et al.*, 2006). Thirdly, a group of kinetochore proteins called chromosome passenger proteins relocalize from kinetochores to the spindle midzone during anaphase and regulate spindle stability and cytokinesis (Bouck and Bloom, 2005).

During her postdoctoral studies in Dr. Hieter's lab, Dr. Measday identified an HU sensitive *spc24-9* kinetochore mutant that prematurely elongates its spindle upon HU treatment. By performing a high copy suppressor (HCS) screen, I have identified ten genes that when over-expressed rescue the HU sensitivity and spindle expansion defect of the *spc24-9* mutant strain. I characterized the rescue function of two of these genes – Stu1, a MT associated protein

that shares a region of similarity to the CLASP/Mast/Orbit sub-family of MT plus-end tracking proteins and Stu2 which is a member of the conserved Dis1/XMAP215 family of MT plus end binding proteins (Inoue *et al.*, 2000; Yin *et al.*, 2002; Gard *et al.*, 2004). I demonstrate that both Stu1 and Stu2 are localized to the kinetochore early in the cell cycle and that Stu2 kinetochore binding depends on Spc24. By performing quantitative and time-lapse analysis of Stu2 fluorescence on spindles during HU treatment, we show that spindle expansion in *spc24-9* cells correlates with mis-localization of Stu2. I propose that localization of Stu2 to the kinetochore in cells when DNA replication is stalled is imperative for maintaining a short spindle and preventing separation of incompletely replicated DNA.

2.2 Materials and methods

2.2.1 Strain construction

Standard methods for yeast culture and transformation were followed (Guthrie and Fink, 1991). Rich medium (YPD), and supplemental minimal medium (SC) were used (Kaiser *et al.*, 1994) as well as FPM (minimal media supplemented with adenine and 6.5g/L sodium citrate) for microscopy analysis (Pot *et al.*, 2005). Yeast strains used in this study are described in Table 2.2. Genes were deleted or epitope tagged using standard yeast methods (Longtine *et al.*, 1998).

2.2.2 HCS screen

I transformed a 2μ yeast genomic DNA library carrying 6-8kb genomic DNA fragments (Connelly and Hieter, 1996) into the *spc24-9* strain and plated 40,000 colonies onto SC-URA plates to select for the presence of the library plasmid. I then replica plated the colonies to 0.1M HU (Sigma) SC-URA plates and incubated at 30^{o}C to identify colonies that could rescue the HU lethality of *spc24-9* mutants. Library plasmids were rescued from colonies growing on the 0.1M HU SC-URA plates and transformed back into *spc24-9* mutants to confirm the HU rescue phenotype. Plasmids were then sequenced using T3 and T7 primers to identify the flanking sequences of the genomic insert.

2.2.3 Plasmid construction - subcloning of HCS genes

The coordinates of the genomic DNA identified in the HCS screen rescue plasmids and their subsequent subclones to confirm identity of the gene are as follows: *STU1*Δ*N*: Chr.II, 151363-158219; *STU1*Δ*N* subclone: Chr.II, 153753-158219; *STU2*Δ*N*: Chr.XII, 230442-237078; *STU2*Δ*N* subclone: Chr.XII 233569-237078; *KIP2*: Chr.XVI, 252390-259933; *KIP2* subclone: Chr.XVI, 257172-259933; *GIC1*: Chr.VIII, 220246-228530; *GIC1* subclone: Chr.VIII, 220246-222771; *RCK2*: Chr.XII, 634230-640397; *RCK2* subclone: Chr.XII, 634230-636611; *HCM1*: Chr.III, 224203~231351; *MCK1*: Chr. XIV, 52447-58767; *DMA1*; Chr.VIII, 337353-344031; *DMA1* subclone: Chr. VIII, 337353-342008. *DMA1* was confirmed as the gene responsible for rescue by digesting the *DMA1* subclone with EcoRI followed by Klenow

treatment to create a frameshift in the *DMA1* gene. Full length *MCK1* was a gift from Dr. Phil Hieter (Shero and Hieter, 1991), full length *HCM1* was a gift from Dr. Trisha Davis (Zhu *et al.*, 1993), and full length *STU1* and *STU2* were gifts from Dr. Tim Huffaker (Pasqualone and Huffaker, 1994; Wang and Huffaker, 1997).

2.2.4 Microscopic analyses

Immuno-fluorescence

Cells shown in Figures 1, 3, 4 and 5 were imaged using a Zeiss Axioplan 2 microscope equipped with a CoolSNAP HQ camera (Photometrics, Tucson, AZ) and Metamorph (Universal Imaging, West Chester, PA) software. The indirect immunofluorescence microscopy studies in Figures 1 and 4 were performed as described previously (Hyland *et al.*, 1999) with the following modifications. Cells were synchronized in G1 at 25^{o}C using α-mating factor (5 μg/ml) (BioVectra), released into 0.2M HU for 3 hours at 30˚C and fixed with a final concentration of 3.7% formaldehyde for 1 hour. Spindles were visualized by staining with Yol 1-34 rat antitubulin antibody (1:50) (Serotec, Oxford) followed by fluorescein-conjugated goat anti-rat secondary antibody (1:2000). Single focal plane images were acquired with a 100X objective.

Analysis of GFP-centromeres, Stu1-VFP and Stu2-VFP localization in fixed cells

CEN15-green fluorescent protein (GFP)-tagged [Figure 2.4, (Goshima and Yanagida, 2000)], cells were synchronized with α−mating factor and LacI-GFPHIS

LacO::URA3-*CEN15*(1.8) was activated with 30mM 3-aminotriazole in SC–HIS media. Cells were released into indicated concentrations of HU in FPM media for 3 hours. Cells were washed and fixed in a total concentration of 2% formaldehyde for 15 min. Image stacks were acquired with a 100X objective at a step of 0.2 µm to span the entire cell. Stu1-VFP fluorescence (Figures 5) was imaged as described above with the following alterations. Cells were grown in FPM media at 30^{o}C, synchronized with α-mating factor and released to 30^{o}C. After 30 min., samples were taken every 15 min. and fixed in 70% ethanol. Stu2-VFP in fixed cells (Figure 2.10) was imaged with a WaveFX spinning disc confocal microscope (Quorum Technologies) as previously described (Cuschieri *et al.*, 2006) without agar pads. Optical sections (0.5 µm) were acquired through a ±2.5 µm z-plane (total of 5.0 µm stack) using Volocity 3DM acquisition software (Improvision, UK).

2.2.5 Live cell analysis

For live-cell imaging of Stu2-VFP fluorescence intensities and spindle length measurements (Figure 2.11 and Figure 2.9), overnight cultures were grown in YPD (containing 2X adenine sulfate) at 25˚C to a cell density of ~0.3-0.4 OD_{600} units ml^{-1}. Cultures were then diluted to 0.2 OD_{600} units ml^{-1} and grown for an additional generation. Cells were arrested with 5 µg/ml of alpha factor for 1.5 hr at 25˚C, washed and then released into media containing 0.2 M HU for 1.5 hours at 25˚C. 1 ml samples of each strain were taken and re-suspended in ~ 50 µl of

30˚C pre-warmed media containing 0.2 M HU. Cells were mounted on a pre-warmed 30˚C heated stage and allowed to equilibrate for 15 min prior to imaging.

Multi-channel 4D imaging of Spc29-CFP and Stu2-VFP fluorescent fusion proteins was performed using a WaveFX spinning disc confocal system (Quorum Technologies, Guelph ON) as previously described (Cuschieri *et al.*, 2006). A Tokai Hit stage warmer was used to shift cells from 25˚C to 30˚C. Image acquisition commenced 15 min. after the stage reached 30˚C. Optical sections (0.5 µm) were acquired through a ±2.5 µm z-plane (total of 5.0 µm stack) at 2 min. intervals for 30 min. using Volocity 3DM acquisition software (Improvision, UK).

2.2.6 Spindle length measurements

Calculation of spindle lengths in fixed and live cell analyses shown in Figures 7 and 8 was performed using Volocity Classification (Improvision, UK). Spindle lengths (in µm) were measured in triplicate for each time point and the average value and standard error of the mean determined. Lengths were determined by measuring the linear distance (µm; in x, y, z) between the mid-point of one SPB (Spc29-CFP channel) to the midpoint of the opposite SPB. All spindle lengths were measured in the XYZ plane view using the line length measurement tool. Average spindle lengths and standard errors were calculated using Excel software.

2.2.7 Stu2-VFP fluorescence measurement

For Stu2-VFP fluorescence measurements shown in Figures 7 and 8, image stacks were

acquired using an exposure of 91 msec/frame (providing an un-saturated image). For both fixed and live cell analyses, fluorescence intensity was measured by rastering a 4x4 voxel volume along the length of the long axis of the spindle (4x4 voxel: spindle fluorescent unit), including both SPBs. Background subtraction as performed as follows: the fluorescence in a 4x4 voxel volume positioned in the cytoplasm was measured, and subtracted from each fluorescence units acquired along the spindle resulting in corrected spindle fluorescence units (arbitrary units). For live cell analyses, background fluorescence was determined for each time point. The corrected fluorescence per unit length (fluorescence/μm) was calculated. Background subtractions, corrected fluorescence values and standard deviations were calculated using Excel software.

2.2.8 ChIP assays (Chromatin immunoprecipitation)

ChIP experiments and primers used for PCR analysis were performed as described previously (Measday *et al.*, 2002; Pot *et al.*, 2003). The linear range for PCR analysis was determined and dilutions used for Figure 2.2A were T (total chromatin,1:200), immunoprecipitation (IP, 1:1); Figure 2.2B, T (1:200), IP (5:1); Figure 2.2C, T (1:200), IP (5:1). Dilutions used for Figure 2.8A were T (1:780), IP (1:6); Figure 2.8B, T (1:780), IP (1:2.5); Figure 2.8C and 6D T (1:125), IP (1:1).

2.3 Results

2.3.1 Spc24 is required for viability and preventing spindle expansion during HU arrest

The budding yeast Ndc80 central kinetochore complex, which is composed of the four coiled-coil proteins, Ndc80, Nuf2, Spc24 and Spc25, is required for proper attachment of chromosomes to spindle MTs and activation of the spindle checkpoint in the presence of defects in attachment (Janke *et al.*, 2001; Wigge and Kilmartin, 2001; Le Masson *et al.*, 2002; Montpetit *et al.*, 2005; Pinsky *et al.*, 2006). It has recently been shown that the kinetochore has a role in maintaining a short (1.5-2 μm) spindle when DNA replication is stalled by treatment of cells with HU (Bachant *et al.*, 2005). Previously, Dr. Measday created two mutants in the coiled-coil region of Spc24 (*spc24-8* and *spc24-10*) and one mutant in the C-terminus of Spc24 (*spc24-9*) (Montpetit *et al.*, 2005). Dr. Measday tested these alleles for viability in the presence of HU at semi-permissive temperature (30^{o}C) and found that the growth of the *spc24-9* mutant is sensitive to levels of HU that do not inhibit the growth of *spc24-8* and *spc24-10* mutants and the wild type strain (Figure 2.1A). Next, Dr. Measday monitored the spindle length and bulk segregation of DNA in *spc24* mutants arrested in G1 and released into 0.2M HU media. This analysis revealed that 100% of wild type and 98% of *spc24-8* and *spc24-10* mutants maintain a short spindle and undivided nuclei after 3 hours exposure to HU, however the majority (76%) of *spc24-9* mutants displayed elongated spindles and segregated nuclei (Figure 2.1B, C). Her data suggests that the *spc24-9* mutation results in a defect in the function of the Ndc80 complex in preventing expansion of the spindle in cells with partially replicated DNA.

2.3.2 Characterization of the kinetochore in spc24-9 mutants

The Ndc80 complex is composed of two subcomplexes – Nuf2/Ndc80 and Spc24/Spc25 – that are linked via their coiled-coil domains (Wei *et al.*, 2005). The C-terminal mutation in *spc24-9* lies within the Spc24 globular domain (Montpetit *et al.*, 2005; Wei *et al.*, 2005). To determine the state of the kinetochore and the Ndc80 complex in *spc24-9* mutants, I performed chromatin immunopreciptation (ChIP) assays using a member of the inner kinetochore CBF3 complex, Ndc10 and the Ndc80 protein. I found that Ndc10 was able to interact with centromere (*CEN*) DNA in *spc24-9* cells at both restrictive temperature (37^{o}C) and after three hours of 0.2M HU treatment at 30^{o}C, suggesting that the core kinetochore is still intact in *spc24-9* mutants (Figure 2.2A, lanes 10 and 12). Ndc80, however, showed a clear defect in its ability to associate with *CEN* DNA in *spc24-9* cells both at 37^{o}C and after three hours of 0.2M HU treatment at 30^{o}C (Figure 2.2B, lanes 10 and 12). In corroboration with our ChIP data, I found that Ndc80-VFP localization was also perturbed in *spc24-9* mutants at 37^{o}C and is even more affected in HU arrested cells (Figure 2.3). 80% of HU treated *spc24-9* mutants showed diffuse and weak Ndc80-VFP staining suggesting that the Ndc80 complex is disrupted when *spc24-9* cells are exposed to 0.2M HU (Figure 2.3).

2.3.3 Bipolar attachment is not a requirement for maintaining a short spindle in HU treated cells

Previous studies have suggested that specific kinetochore mutants display inappropriate

spindle expansion during HU exposure due to their inability to establish kinetochore-MT bipolar attachment and thus appropriate tension on the spindle (Bachant *et al.*, 2005). Using a *CEN15*-GFP marked strain, Jennifer McQueen found that a similar percentage of wild type, *spc24-9* and *spc24-10* cells displayed bipolar attachment in cells released from a G1 block to 30^{o}C (Figure 2.4A). Thus, *spc24-9* kinetochores are capable of bipolar attachment to spindle poles during a normal cell cycle at the same temperature (30^{o}C) that results in *spc24-9* HU lethality. Whether or not kinetochores attain bipolar attachment in a wild type strain in the presence of partially duplicated DNA (as a result of treatment with HU) is unclear. We reasoned that exposing cells to increasing concentrations of HU would increase replication fork stalling (.05M-0.3M HU) and impact the number of *CENs* that were replicated (Clarke *et al.*, 2001). Jennifer monitored *CEN15* separation as a sign of bipolar attachment using *CEN15*-GFP and Spc29-CFP tagged wild type and *spc24-9* mutant strains. Wild type cells treated with the lowest concentration of HU (.05M HU) exhibited *CEN15* bipolar attachment in 60% of cells after 3hours (Figure 2.4B). Importantly, *spc24-9* mutants displayed the same percentage of separated *CEN15* foci suggesting once again, that *spc24-9* mutants are capable of bipolar attachment (Figure 2.4B). Similar to previous studies, Jennifer found that separated *CEN15* foci were detected in 23% of wild type cells exposed to 0.1M HU yet only 4% of separated *CEN15* foci were seen in 0.2M HU treated wild type cells (Goshima and Yanagida, 2000; Krishnan *et al.*, 2004). The majority of wild type cells treated with the highest concentration of HU (0.3M HU) contained one *CEN15* focus that colocalized with one SPB suggesting either that

CEN15 had not yet replicated or had replicated but had not yet established bipolar attachment (Figure 2.4C). Previous work has demonstrated that unreplicated monocentric minichromosomes also remain in the close vicinity of one SPB (Dewar *et al.*, 2004). Thus the ability of *CEN15* to attain bipolar attachment is not correlated with maintaining a short spindle during the DNA replication checkpoint.

2.3.4 Identification of HCS genes that rescue spc24-9 HU lethality

To understand why Spc24 is required for viability when DNA replication is stalled, I performed a HCS screen to identify genes that, when overexpressed, could suppress the lethality of *spc24-9* cells exposed to HU. Ten genes were identified in our HCS screen (Table 2.1). Multiple isolates of *SPC24* and its interacting partner *SPC25* were recovered (Janke *et al.*, 2001; Wigge and Kilmartin, 2001). I also identified four genes encoding proteins that regulate spindle dynamics – MT associated proteins Stu1 and Stu2, the kinesin-related motor protein Kip2 and a protein involved in spindle positioning called Dma1 (Roof *et al.*, 1992; Pasqualone and Huffaker, 1994; Wang and Huffaker, 1997; Fraschini *et al.*, 2004). Two protein kinases were isolated – Mck1, which has a role in chromosome segregation and Rck2 which has a role in the osmotic stress response pathway (Neigeborn and Mitchell, 1991; Shero and Hieter, 1991; Bilsland-Marchesan *et al.*, 2000). I identified Gic1 which has roles in cell polarity and mitotic exit (Brown *et al.*, 1997; Chen *et al.*, 1997; Hofken and Schiebel, 2004). Finally, I identified the Hcm1 transcription factor, which has also been isolated in a variety of synthetic lethal screens

pertaining to the cell division cycle and chromosome segregation (Zhu and Davis, 1998; Horak *et al.*, 2002; Sarin *et al.*, 2004; Montpetit *et al.*, 2005; Daniel *et al.*, 2006). Interestingly, Hcm1 has recently been shown to activate expression of spindle and chromosome segregation proteins specifically in S phase (Pramila *et al.*, 2006). All the HCS genes were able to rescue the HU lethality of two other alleles of the Ndc80 complex, *ndc80-1* and *spc25-1*, however, none of them was able to rescue the inviability of a *mec1* mutant on HU plates (data not shown). Therefore, the HCS genes suppress the HU specific defects of Ndc80 complex mutants but do not suppress *mec1*, a key effector of the DNA replication checkpoint.

2.3.5 HCS rescue occurs through restraining spindle expansion

I next determined if the HCS genes rescued *spc24-9* HU lethality by restraining spindle expansion and thus premature chromosome segregation. *spc24-9* mutants carrying the HCS rescue plasmids were synchronized in G1 phase, released into HU for 3 hours and immunofluorescence was performed to analyze chromosome segregation and spindle morphology. All of the HCS genes were able to restore a single nuclei phenotype to *spc24-9* HU treated cells (Figure 2.5D). The *STU1* and *STU2* rescue clones that I identified lacked the N-terminal 97 and 252 amino acids of Stu1 and Stu2, respectively (herein referred to as *STU1*Δ*N* and *STU2*Δ*N*). I tested if high copy full length *STU1* or *STU2* expression plasmids were capable of rescuing *spc24-9* HU lethality. Expression of full length *STU2* was clearly not able to rescue either the HU lethality or chromosome segregation defects of *spc24-9* mutants

suggesting that the N-terminal truncation is an important feature of the *STU2ΔN* rescue activity (Figure 2.5A, D). Expression of full length *STU1* was able to rescue *spc24-9* HU lethality and chromosome separation at levels above vector alone, but not as well as the *STU1ΔN* clone (Figure 2.5A, D).

I reasoned that expression of *STU2ΔN* might be rescuing the spindle expansion defect in HU treated *spc24-9* mutants by destabilizing MTs. Consistent with this hypothesis, *STU2ΔN* clone lacks the entire TOG1 domain of Stu2 which binds tubulin heterodimers (Al-Bassam *et al.*, 2006; Al-Bassam *et al.*, 2007). Previous work has shown that Stu2 promotes microtubule polymerization whereas expression of Stu2 lacking its TOG1 domain, which still binds MTs, results in decreased mitotic spindle length and slows down anaphase spindle elongation (Al-Bassam *et al.*, 2006). I asked if Stu2ΔN localization is similar to endogenous Stu2 by tagging Stu2ΔN with VFP (which still retains its *spc24-9* HU rescue activity) and endogenous Stu2 with CFP. Indeed I found that Stu2ΔN-VFP localization overlapped with Stu2-CFP in both wild type and *spc24-9* mutants in log phase or HU treated cells, consistent with previous data demonstrating that Stu2ΔTOG1-GFP still binds MT plus ends (Figure 2.6, (Al-Bassam *et al.*, 2006)). To test if depletion of Stu2 activity using another mutant form of Stu2 is also capable of preventing spindle expansion in *spc24-9* cells, I combined *spc24-9* with the *stu2-10* Ts mutation (Severin *et al.*, 2001) and tested the double mutant for separation of nuclei upon HU treatment. Only 8% of *stu2-10 spc24-9* mutants segregated nuclei after 3 hours of HU treatment compared to 59% of *spc24-9* mutants (Figure 2.5E). Therefore functional Stu2 is

required for the spindle expansion defect in *spc24-9* mutants. Although *stu2-10 spc24-9* double mutants maintained a short spindle during HU treatment, they were lethal on HU plates at 30^{o}C (Figure 2.5B) suggesting that the defects in both Stu2 and Spc24 prevent cell cycle recovery after HU exposure.

Stu2 interacts with two other MT plus-end tracking proteins, Bim1 and Bik1 (Chen *et al.*, 1998; Lin *et al.*, 2001; Wolyniak *et al.*, 2006). Since we had previously shown that *bim1 spc24-9* mutants have a synthetic growth defect (Montpetit *et al.*, 2005), I deleted *BIK1* in *spc24-9* cells and analyzed growth phenotypes. The *bik1 spc24-9* double mutant rescued the nuclei separation defect of HU treated *spc24-9* mutants and both the HU (at 30^{o}C) and Ts (at 33^{o}C) lethality of *spc24-9* mutants (Figure 2.5C, E). Therefore the activity of Stu2 and Bik1 is responsible for the spindle expansion and subsequent nuclei separation and lethality of *spc24-9* cells upon HU exposure.

We also determined if Stu1 is required for the spindle expansion activity in *spc24-9* HU treated cells by creating a *stu1-5 spc24-9* double mutant (Yin *et al.*, 2002). The *stu1-5 spc24-9* mutant behaved in a similar manner to *spc24-9* mutants and elongated their spindles when treated with HU suggesting that, unlike Stu2 and Bik1, Stu1 activity is not required for spindle expansion in HU exposed *spc24-9* mutants. Although both *spc24-9* and *stu1-5* individual mutants grow well at 30^{o}C on rich media (YPD), the double mutant is synthetically lethal at 30^{o}C (Figure 2.5D). In addition, the *spc24-9 stu1-5* double mutant is viable at 25^{o}C in rich media but inviable when grown on HU plates (Figure 2.5D). The sensitivity of *spc24-9 stu1-5*

double mutants to HU and the synthetic lethal interaction between *spc24-9* and *stu1-5* mutants suggests that Stu1 and Spc24 have a joint or parallel role in restraining spindle expansion during the DNA replication checkpoint.

2.3.6 Stu1 localizes to kinetochores prior to anaphase

Stu1, which was originally isolated as a suppressor of a *tub2* (β-tubulin) mutation, interacts with Tub2 and localizes to the spindle midzone in anaphase spindles (Pasqualone and Huffaker, 1994; Yin *et al.*, 2002). However, the localization of Stu1 in relation to a SPB marker has not been assessed. I imaged Stu1 fused to VFP in relation to the Spc29-CFP SPB protein by synchronizing cells in G1 phase with mating pheromone, then releasing into the cell cycle and fixing cells every 30min. The budding yeast spindle reaches a length of 1.5-2 μm prior to entering anaphase (Pearson *et al.*, 2001). Prior to anaphase, I detected three evenly distributed patterns of Stu1-VFP localization in fixed cells - a bilobed distribution pattern in between the Spc29-CFP foci which is a hallmark localization pattern for a kinetochore protein (Figure 2.7, top row) (He *et al.*, 2001; Measday *et al.*, 2002), a single focus located closer to one of the SPBs (Figure 2.7, second row) and a continuous signal inbetween SPBs (Figure 2.7, third row). In agreement with previous results, I also found that Stu1-VFP localized to the midzone of anaphase spindles (Figure 2.7, fourth row) (Yin *et al.*, 2002). Finally, in telophase, I observed a dispersed Stu1 signal near the SPBs (Figure 2.7, bottom row).

Our localization data suggests that Stu1 may interact with the kinetochore. I tested if

Stu1 localizes to the kinetochore by performing Stu1-Myc chromatin immunoprecipitation (ChIP) assays from logarithmically growing cells. Stu1-Myc specifically associated with *CEN1* and *CEN3* DNA but not with a non-*CEN* locus, *PGK1* (Figure 2.8A, lane 4). I performed a Stu1-Myc ChIP assay in a *spc24-9* mutant strain at both permissive (25^{o}C) and restrictive (37^{o}C) temperature (Figure 2.8B). Stu1-Myc is still able to associate with *CEN* DNA at restrictive temperature suggesting that Stu1 does not require Spc24 to bind kinetochores (Figure 2.8B, lane 4). In summary, our localization and ChIP data demonstrate that Stu1 localizes to kinetochores early in the cell cycle in an Spc24 independent manner and relocalizes to the spindle around the time of the metaphase to anaphase transition.

2.3.7 Stu2 localizes to kinetochores early in the cell cycle

In anaphase cells, Stu2-GFP localizes to the cytoplasmic side of the SPB and along the spindle MTs as determined by immunoelectron microscopy (Kosco *et al.*, 2001). In addition, Stu2 has been shown to colocalize with kinetochores and SPBs and bind *CEN* DNA in metaphase cells (He *et al.*, 2001). We analyzed Stu2-VFP localization in short (<1.5μm) spindles (acquired at the time of bud emergence) and during normal spindle expansion using time-lapse microscopy (Figure 2.9). We observed that Stu2-VFP signal displayed a bilobed pattern between Spc29-CFP foci in short spindles (Figure 2.9, image 10b). Time-lapse microscopy using longer exposures (which saturate Stu2-VFP spindle fluorescence) revealed that Stu2-VFP also tracks on astral microtubules and transiently associates with SPBs as astral MT shorten (data

not shown). Our imaging data is consistent with Stu2 localizing primarily to kinetochores and/or the nuclear spindle prior to metaphase. Once spindles had lengthened (>2 μm), we detected co-localization of Stu2-VFP with Spc29-CFP as well as Stu2-VFP at the spindle midzone as previously described (Figure 2.9, image 0c) (He *et al.*, 2001; Kosco *et al.*, 2001). The localization of Stu2 to kinetochores early in the cell cycle suggests that defects in kinetochore function when DNA replication is stalled by HU treatment may significantly affect Stu2 activity.

2.3.8 Stu2 is mislocalized in HU treated spc24-9 cells

We tested if Stu2 localization to the kinetochore depends on functional Spc24 by using both ChIP and microscopy analyses. Stu2-Myc displayed a decreased ability to interact with *CEN* DNA in *spc24-9* cells as I increased the temperature from permissive (25^{o}C) to semi-permissive (30^{o}C) conditions (Figure 2.8D, lanes 8 and 10). Stu2-Myc did not co-precipitate with *CEN* DNA in *spc24-9* mutants shifted to restrictive temperature (37^{o}C) suggesting that Stu2 requires Spc24 to interact with the kinetochore (Figure 2.8D, lane 12). Although Stu2 requires Spc24 for proper *CEN* localization in logarithmically growing cells, this does not necessarily reflect the situation when cells are exposed to HU. I performed a Stu2-Myc ChIP assay in wild type and *spc24-9* cells after treating cells with HU for three hours at 30^{o}C. Stu2 interaction with *CEN* DNA was highly reduced in *spc24-9* mutants compared to wild type cells (Figure 2.8C, compare lanes 2 and 4). Thus Spc24 is required for Stu2 to efficiently interact with *CEN* DNA in both log phase and HU treated cells. To test if Stu2

localization is perturbed in *spc24-9* cells, Jennifer McQueen, Lara Cuschieri and Dr. Jackie Vogel performed a quantitative analysis of Stu2-VFP fluorescence during HU exposure. Cells were released from a G1 pheromone block into HU at 25^{o}C, shifted to 30^{o}C and fixed after 60min of incubation. At this time point, spindle expansion had clearly begun in *spc24-9* cells as spindle lengths averaged 2.5 μm in mutant cells compared to 1.8 μm in wild type cells (Figure 2.10B). Analysis of individual cells revealed that Stu2 remained as bilobed foci in wild type cells whereas Stu2 signal was clearly mis-localized along the spindle midzone (cs) or next to one pole (monopolar) in *spc24-9* cells (Figure 2.10A, 3-dimensional render, rotated). Analysis of Stu2-VFP fluorescence on the spindle indicated that Stu2-VFP fluorescence intensity decreased significantly in the *spc24-9* mutant relative to wild-type (Figure 2.10C). Stu2-VFP also re-distributed from discrete foci to diffuse fluorescence along the length of the spindle (Figure 2.10A); thus Stu2-VFP fluorescence on the spindle per unit length (μm; see Materials and Methods for details) was used for the comparison of Stu2-VFP in wild type versus *spc24-9* cells. In general, this analysis revealed that spindles in the *spc24-9* mutant had decreased Stu2-VFP fluorescence and were longer, suggesting that spindle expansion correlates with mis-localization of Stu2 (Figure 2.10C). However, low levels of Stu2-VFP fluorescence were found on both long and short spindles in *spc24-9* cells suggesting that the relationship between spindle length and Stu2 levels was not absolute. More specifically, it was not clear if the observed spindle expansion observed in *spc24-9* cells was permanent or represented oscillations in spindle length.

To further explore the dynamics of Stu2 interaction with the spindle and spindle

expansion, Jennifer McQueen, Lara Cuschieri and Dr. Jackie Vogel analyzed dynamic changes in Stu2-VFP fluorescence and spindle length in living cells using time-lapse microscopy. For this analysis, HU-arrested wild type and *spc24-9* mutant cells were shifted to 30^{o}C on the microscope stage and the HU arrest maintained throughout the time-lapse by mounting the cells in FP medium supplemented with HU. This analysis revealed that spindle length remains relatively static in wild-type cells, with an average net change (either shrinking or elongating) in length of 0.40 ± 0.125 μm during the time-lapse for all cells (n=4) analyzed (Figure 2.11A and 2.11C). Spindle length at the start of the time-lapse was not significantly different between wild-type and *spc24-9* cells, and was similarly static in *spc24-9* cells (n=4 cells/strain) during the first 5 min. of the time-lapse (Figure 2.11B). In contrast with wild-type cells, spindle length increased significantly (1.45 ± 0.638 μm) in the *spc24-9* mutant over time (Figure 2.11B and 2.11C). At 18 min. after the shift to 30˚C, a net increase in spindle length occurred in all four *spc24-9* cells; in each cell spindle length had increased (0.9 – 2.3 μm; mean length increase of $1.3. \pm 0.66$ μm) relative to length at the start of the time lapse and relative to all four wild-type cells (Figure 2.11B and 2.11D). For this reason, we chose to compare the intensity of Stu2-VFP fluorescence on the spindle at time 0 and at 18 min. Stu2-VFP fluorescence was significantly decreased in *spc24-9* cells compared to wild type cells (Figure 2.11E), suggesting that mis-localization of Stu2 is correlated with the spindle expansion observed (Figure 2.11D). Finally, we detected significant oscillation of spindle length between 10- 28 min. in *spc24-9* cells (Figure 2.11B), suggesting that mis-localization of Stu2 results in transient spindle expansion.

The transient nature of this defect is consistent with the observation of a sub-population of *spc24-9* cells with short spindles and mis-localized or low Stu2-VFP levels.

2.4 Discussion

The kinetochore is required to restrain spindle expansion in budding yeast when DNA replication is stalled however the mechanism by which kinetochores maintain spindle length in this state is not well understood. I identified genes that when over-expressed, rescue the lethality and spindle expansion defects of the *spc24-9* kinetochore mutant when exposed to HU. Two MT plus end binding proteins, the CLASP related protein Stu1 and XMAP215 homologue Stu2, were identified and their interactions with the kinetochore were explored further. I demonstrated that Stu1 localizes to kinetochores early in the cell cycle and relocalizes to the spindle midzone after metaphase and that Stu2 binds to the kinetochore in a Spc24-dependent manner. In addition, inappropriate spindle expansion in HU-treated *spc24-9* cells can be prevented by inhibiting Stu2 activity. I propose that mislocalization of Stu2 in *spc24-9* cells enables spindle expansion during the DNA replication checkpoint.

Kinetochore-MT bipolar attachment and the DNA replication checkpoint. DNA microarray studies have suggested that most *CENs* are replicated upon exposure to HU (Yabuki *et al.*, 2002; Feng *et al.*, 2006). Thus budding yeast *CENs* may be capable of attaining bipolar attachment during HU treatment. However, the data presented in Figure 2.4 of this Chapter

suggests that bipolar attachment may not be the only mechanism by which kinetochores maintain short spindles during HU arrest. Firstly, wild type and *spc24-9* cells display similar percentages of *CEN15*-GFP bipolar foci when treated with different concentrations of HU yet only *spc24-9* spindles expand (Figure 2.4B). Secondly, when wild type cells are treated with high concentrations of HU, a single *CEN15*-GFP focus is detected that clearly colocalizes with one SPB (Figure 2.4C). These data are similar to previous studies demonstrating that a GFP marked unreplicated minichromosome colocalizes with one SPB after SPB separation (Dewar *et al.*, 2004). Although the data do not distinguish between replicated and unreplicated *CEN15*, *CEN15* is clearly attached to one pole, yet the spindle remains short. Thus the ability to attain bipolar attachment during HU treatment is not correlated with restraining spindle expansion.

Stu2 activity enables spindle expansion in spc24-9 HU treated cells. I isolated a truncated version of the XMAP215 homologue, *STU2* (*STU2*Δ*N*), in my *spc24-9* HCS screen that lacks the N-terminal 252 amino acids of Stu2 (Table 2.1). I propose that over-expression of *STU2*Δ*N* rescues *spc24-9* HU lethality by restraining MT dynamics induced by mis-localization of Stu2. *STU2*Δ*N* lacks the N-terminal TOG1 domain that binds tubulin heterodimers but retains the TOG2 domain that binds MT plus ends (Al-Bassam *et al.*, 2006). Previous studies have shown that Stu2 lacking its TOG1 domain binds MT plus ends but cannot promote plus end MT growth suggesting that *STU2*Δ*N* inhibits *spc24-9* HU spindle expansion via the same mechanism (Al-Bassam *et al.*, 2006). The *spc24-9* mutant and the resultant mislocalization of

Stu2 (see next section) is an important feature of *STU2ΔN*'s rescue function because overexpression of *STU2ΔN* does not inhibit spindle expansion in a wild type cell cycle (Figure 2.12). Another possible Stu2ΔN rescue mechanism, which is not mutually exclusive with the previous mechanism, is that over-expression of *STU2ΔN* is titrating out a Stu2 interacting protein that is mediating spindle expansion in *spc24-9* HU cells. Stu2 interacts with the CLIP-170 ortholog, Bik1, at the C-terminus of Stu2 (Wolyniak *et al.*, 2006). I find that deletion of the Stu2 interacting protein Bik1 rescues the *spc24-9* spindle expansion defects and HU lethality at 30^{o}C and that the *bik1 spc24-9* double mutant grows at a higher temperature than the *spc24-9* mutant alone (Figure 2.5C, 2.5E). Thus, inhibition of Stu2 or Bik1 plus end MT activity prevents spindle expansion when *spc24-9* mutants are under HU arrest.

Stu2 retention at the kinetochore is important for maintaining a short spindle when DNA replication is stalled. My data suggests that Stu2 activity is required for spindle expansion in *spc24-9* HU treated cells. The *stu2-10 spc24-9* double mutant no longer displays inappropriate spindle expansion when exposed to HU (Figure 2.5E). Why is Stu2 able to promote spindle expansion in HU treated *spc24-9* cells but not wild type cells? I propose that the inability to recruit and retain Stu2 at the kinetochore in *spc24-9* mutants enables Stu2 to promote MT dynamics. My ChIP data suggest that the interaction of Stu2 with *CEN* DNA is perturbed in *spc24-9* mutants both in log phase cells and during HU treatment (Figure 2.8C and 6D). In agreement with my studies, Stu2 does not associate with *CEN* DNA at restrictive

temperature in an *ndc80-1* Ts mutant (He *et al.*, 2001). Thus the Ndc80 complex is required for recruitment of Stu2 to the kinetochore. Jennifer McQueen, Lara Cuschieri and Jackie Vogel performed a detailed analysis of Stu2-VFP fluorescence and spindle length in both live and fixed *spc24-9* HU treated cells. Shortly after shift to restrictive temperature (30^{o}C for *spc24-9* cells exposed to HU), they detected spindle expansion and mis-localization of Stu2-VFP as well as its diffusion along the axis of the spindle (Figure 2.10). Stu2-VFP also displayed variable localization patterns including movement to one pole and to the spindle midzone in these cells (Figure 2.10A). The time-lapse analysis revealed that HU treatment induces *spc24-9* mutants to undergo oscillations in spindle length, unlike wild type cells where relatively little change in spindle length is detected (Figure 2.11). A window of time was identified when the spindle was at an average maximum length in these analyses and Stu2-VFP fluorescence levels were quantified at this time. Stu2-VFP fluorescence was significantly reduced compared to wild type cells suggesting a correlation between reduction in Stu2-VFP fluorescence and spindle expansion (Figure 2.11E). The oscillations observed also explain why short spindles with decreased Stu2 are observed in populations of *spc24-9* cells. Finally, oscillations in spindle length were also detected in HU exposed *rad53* mutants, suggesting that activation of the DNA replication checkpoint regulates spindle dynamics and in the absence of the checkpoint this restraint is compromised (Bachant *et al.*, 2005). Our studies have uncovered the role of an effector of the checkpoint, Stu2, in restraining spindle dynamics while localized at the kinetochore.

The role of Stu2 during the DNA replication checkpoint. Does Spc24 participate in regulating spindle expansion only during the DNA replication checkpoint or also during an unperturbed cell cycle? To address this question we measured spindle length in a wild type versus *spc24-9* mutant after release from a G1 block to restrictive temperature (Figure 2.13). We found that early in the cell cycle, *spc24-9* mutants had longer spindles than wild type cells consistent with a defect in the S phase checkpoint during a normal cell cycle. As cells progressed, *spc24-9* spindle expansion lagged behind wild type cells suggesting a delay in anaphase. These data are consistent with our analysis of DNA content during a synchronous cell cycle at restrictive temperature which demonstrated that *spc24-9* cells progress more rapidly through S phase than wild type cells (compare 60 min. time point between wild type and *spc24-9*, Figure 2.14). However, once DNA has replicated in *spc24-9* cells, a 2N content of DNA is maintained for two hours before 1N DNA content is once again detected [Figure 2.14, (Montpetit *et al.*, 2005)]. Thus *spc24-9* cells accelerate through S phase but are delayed in anaphase.

Mechanism of spindle expansion in *rad53* and *mec1* mutants. The results shown here suggest that the kinetochore regulates spindle integrity during an HU induced DNA replication checkpoint by sequestering proteins such as Stu2 that regulate MT dynamics. Why then do *mec1* and *rad53* mutants elongate their spindles during the DNA replication checkpoint? A previous study used a *CEN* transcription read through assay to demonstrate that the kinetochore is still capable of blocking access to the transcription machinery in a *rad53-21* strain suggesting

that the inner CBF3 kinetochore complex that binds DNA is still intact (Bachant *et al.*, 2005). Ndc10, a CBF3 component, is also present on *CEN* DNA in *spc24-9* cells suggesting that the spindle expansion is not due to defects in inner kinetochore assembly (Figure 2.2A). Not all central kinetochore mutants display *CEN* transcription read through thus the central kinetochore may be compromised in *rad53* or *mec1* mutant strains (Doheny *et al.*, 1993). *mec1-1* HU treated cells display upregulation of *STU2* and *CIN8* mRNA and protein levels suggesting that increased levels of MT regulatory proteins may contribute to spindle expansion in *mec1-1* cells (Krishnan *et al.*, 2004). Our data suggest that mis-localization of Stu2 by disruption of a central kinetochore complex also causes spindle expansion during the DNA replication checkpoint.

By using HU as a method to stall cells in the process of DNA replication, I have uncovered a role for the kinetochore in regulating spindle dynamics in S phase. I have discovered a role for Spc24 in recruiting Stu2 to the kinetochore to mediate MT dynamics prior to metaphase. Mutation of Spc24 results in mis-localization of Stu2 and deregulation of spindle dynamics when DNA replication is stalled and likely during an unperturbed S phase as well. I propose that the kinetochore regulates spindle integrity during an HU induced DNA replication checkpoint by sequestering proteins such as Stu2 that play central roles in controlling spindle MT dynamics.

Table 2.1 HCS screen of *spc24-9* HU lethality

HU rescue[a]	Gene Name	ORF	Biological Process[d]
+	*DMA1*	YHR115C	Spindle position and orientation
+	*RCK2*	YLR248W	Oxidative and osmotic stress signaling
+	*STU1* truncated[b]	YBL034C	MT dynamics
+ +	*GIC1*	YHR061C	Cell polarity
+ + +	*KIP2*	YPL155C	Mitotic spindle positioning
+ + +	*MCK1*	YNL307C	Mitotic and meiotic chromosome segregation
+ + + +	*HCM1*	YCR065W	Transcription
+ + + + +	*STU2* truncated[c]	YLR045C	MT dynamics
+ + + + +	*SPC24*	YMR117C	Chromosome Segregation
+ + + + +	*SPC25*	YER018C	Chromosome Segregation

[a]growth of *spc24-9* mutant carrying rescue clone struck on .05M HU plates at 30^{o}C from weak (+) to strong (+++++) growth

[b]the *STU1* rescue clone is missing the N-terminal 97 amino acids

[c]the *STU2* rescue clone is missing the N-terminal 252 amino acids

[d]GO Annotation from *Saccharomyces* Genome Database

Table 2.2 List of Yeast Strains

Strain Number	Genotype	Source
CU1000	*MATa stu1-5 his3-Δ200 leu2-3,112 ura3-52*	(Yin *et al.*, 2002)
CUY1088	*MATa stu2-10::URA3 his3-Δ200 leu2-3,112 ura3-52*	(Kosco *et al.*, 2001)
TWY308	*MATα mec1-1 ura3 trp1*	(Weinert *et al.*, 1994)
YLM79	MATa *ura3-52, lys2-801, ade2-101, his3-Δ200, leu2-Δ1, trp1-Δ63 STU1-MYC::TRP1*	This study
YLM185	MATa *ura3-52, lys2-801, ade2-101, his3-Δ200, leu2-Δ1, trp1-Δ63 STU1-VFP::kanMX6 SPC29-CFP:: hphMX4*	This study
YLM187	MATa *ura3-52, lys2-801, ade2-101, his3-Δ200, leu2-Δ1, trp1-Δ63 STU2-VFP::kanMX6 SPC29-CFP:: hphMX4*	This study
YLM288	MATa *ura3-52, lys2-801, ade2-101, his3-Δ200, leu2-Δ1, trp1-Δ63 STU2-VFP::kanMX6 SPC29-CFP:: hphMX4 spc24-9::natMX4*	This study
YLM400	MATa *ura3-52, lys2-801, ade2-101, his3-Δ200, leu2-Δ1, trp1-Δ63 STU2-MYC::TRP1 spc24-9::natMX4*	This study
YLM451	MATa *ura3-52, lys2-801, ade2-101, his3-Δ200, leu2-Δ1, trp1-Δ63 STU1-MYC::TRP1 spc24-9::natMX4*	This study
YLM533	MATa *ura3-52, lys2-801, ade2-101, his3-Δ200, leu2-Δ1, trp1-Δ63 NDC80-VFP::kanMX6 SPC29-CFP:: hphMX4*	This study
YLM535	MATa *ura3-52, lys2-801, ade2-101, his3-Δ200, leu2-Δ1, trp1-Δ63 NDC80-VFP::kanMX6 SPC29-CFP:: hphMX4 spc24-9::natMX4*	This study
YLM542	MATa *ura3-52, lys2-801, ade2-101, his3-Δ200, leu2-Δ1, trp1-Δ63 NDC80-13MYC::His3MX6 SPC24::natMX4*	This study
YLM544	MATa *ura3-52, lys2-801, ade2-101, his3-Δ200, leu2 1, trp1-Δ63 NDC80-13MYC::His3MX6 spc24-9::natMX*	This study
YLM557	MATa *ura3-52, lys2-801, ade2-101, his3-Δ200, leu2-Δ1, trp1-Δ63 NDC10::13MYC::kanMX spc24-9::natMX4*	This study
YLM609	MATa *ura3-52, lys2-801, ade2-101, his3-Δ200, leu2-Δ1, trp1-Δ63 STU2-CFP:: hphMX4 pSTU2ΔN-VFP::kanMX*	

(To be continued)

Table 2. 2 List of Yeast Strains (continued)

Strain Number	Genotype	Source
YLM610	MATa *ura3-52, lys2-801, ade2-101, his3-Δ200, leu2-Δ1, trp1-Δ63 STU2-CFP:: hphMX4 spc24-9::natMX4 pSTU2 N-VFP::kanMX*	This study
YM234	MATa *ura3-52, lys2-801, ade2-101, his3-Δ200, leu2-Δ1, TRP1+ stu2-10::URA3 spc24-9::kanMX6*	This study
YM406	MATa *ura3-52, lys2-801, ade2-101, his3-Δ200, leu2-Δ1, trp1-Δ63 STU2-MYC::TRP1*	This study
YM480[a]	*MATa LacI-GFP::HIS3 LacO::URA3-CEN15(1.8) Spc29-CFP::kanMX6 SPC24::natMX4*	This study
YM482[a]	*MATa LacI-GFP::HIS3 LacO::URA3-CEN15(1.8) Spc29-CFP::kanMX6 spc24-9::natMX4*	This study
YM487[a]	*MATa LacI-GFP::HIS3 LacO::URA3-CEN15(1.8) Spc29-CFP::kanMX6 spc24-10::natMX4*	This study
YM836	MATa *ura3-52, lys2-801, ade2-101, his3-Δ200, leu2-Δ1, trp1-Δ63 bik1::kanMX6*	This study
YM903	MATa *ura3-52, lys2-801, ade2-101, his3-Δ200, leu2-Δ1, TRP1+ stu1-5 spc24-9::kanMX6*	This study
YM935	MATa *ura3-52, lys2-801, ade2-101, his3-Δ200, leu2-Δ1, trp1-Δ63 bik1::kanMX6 spc24-9::natMX4*	This study
YPH499	MATa *ura3-52, lys2-801, ade2-101, his3-Δ200, leu2-Δ1, trp1-Δ63*	P. Hieter
YPH1734	MATa *ura3-52, lys2-801, ade2-101, his3-Δ200, leu2-Δ1, trp1-Δ63 NDC10::13MYC::kanMX6*	(Measday *et al.*, 2002)
YVM1363	MATa *ura3-52, lys2-801, ade2-101, his3-Δ200, leu2-Δ1, trp1-Δ63 spc24-10::kanMX6*	(Montpetit *et al.*, 2005)
YVM1370	MATa *ura3-52, lys2-801, ade2-101, his3-Δ200, leu2-Δ1, trp1-Δ63 SPC24::kanMX6*	(Montpetit *et al.*, 2005)
YVM1380	MATa *ura3-52, lys2-801, ade2-101, his3-Δ200, leu2-Δ1, trp1-Δ63 spc24-9::kanMX6*	(Montpetit *et al.*, 2005)
YVM1448	MATa *ura3-52, lys2-801, ade2-101, his3-Δ200, leu2-Δ1, trp1-Δ63 spc24-8::kanMX6*	(Montpetit *et al.*, 2005)
YVM1591	MATa *ura3-52, lys2-801, ade2-101, his3-Δ200, leu2-Δ1, trp1-Δ63 spc24-9::natMX4*	This study

[a]These strains were created by mating a W303 strain derivative (Goshima and Yanagida, 2000) with an S288C strain derivative hence the precise genotype is not known.

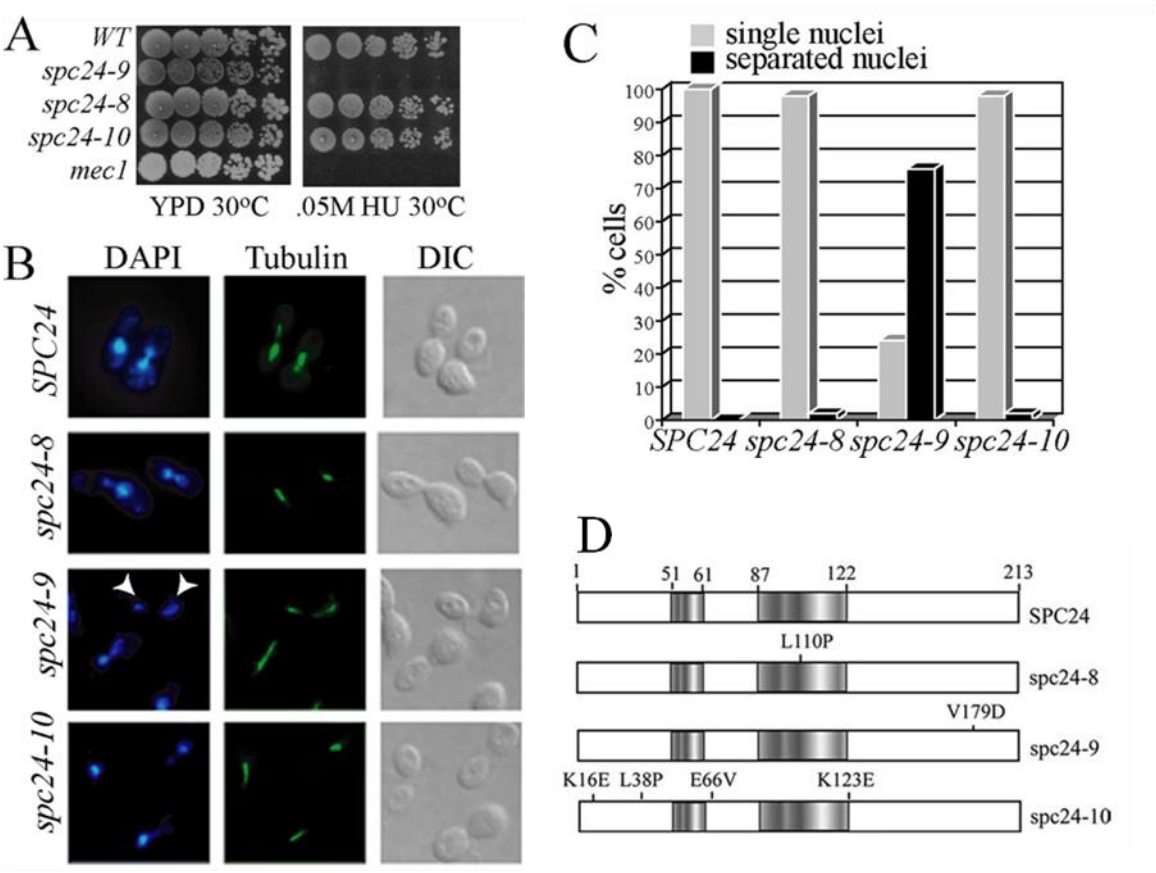

Figure 2.1 spc24-9 mutants are sensitive to HU due to inappropriate spindle expansion

(A) Cell dilution assay of indicated strains grown on YPD and .05M HU at 30°C for 3 days. (B) Immunofluorescence analysis of wild type (SPC24), spc24-8, spc24-9 and spc24-10 cells synchronized in G1 phase with α-factor, then released into 0.2M HU for 3 hours at 30°C. Shown are representative cells after 3 hours HU treatment imaged for DNA (DAPI), MTs (Tubulin) and cell morphology (DIC). White arrowheads point to separated nuclei in the spc24-9 mutant. (C) Percentage of cells (100 cells counted) described in (B) displaying single (grey bars) or separated (black bars) nuclei. (D) Schematic of point mutations in spc24 mutants. The predicted coiled-coil domain is shaded. The *spc24-9* V179D substitution is in the Spc24 C-terminal globular domain. (Cited from Montpetit *et al.*, Genetics 2005, by permission © Genetics Society of Amarica.)

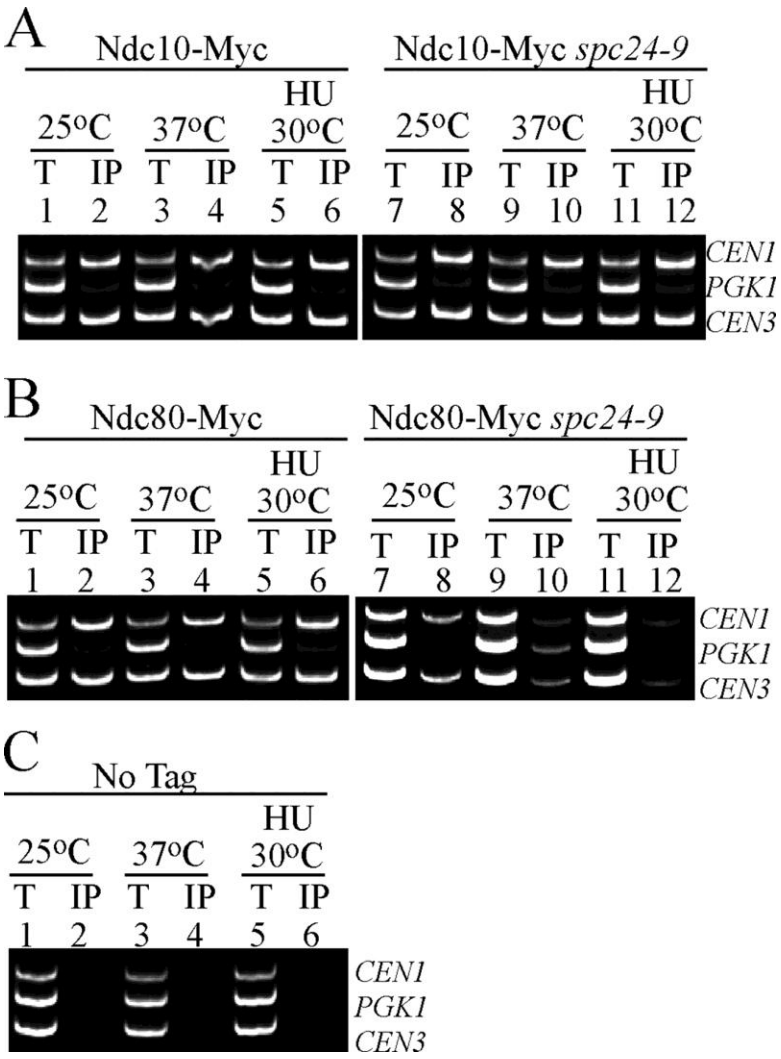

Figure 2.2 Ndc80 *CEN* association is disrupted in *spc24-9* mutants

Multiplex PCR analysis of *CEN1*, *PGK1* and *CEN3* loci was performed with total chromatin (T) or immunoprecipitate (IP) as PCR templates. Strains were grown at 25°C to log phase, then either shifted to 37°C for three hours, or incubated in 0.2M HU at 30°C for three hours. (A) Ndc10-Myc wild type (lanes 1-6) or *spc24-9* cells (lanes 7-12). (B) Ndc80-Myc wild type (lanes 1-6) or *spc24-9* cells (lanes 7-12). (C) Wild type strain carrying no epitope tag (No Tag, lanes 1-6) shown as a control. An untagged *spc24-9* mutant was also used as a control and showed similar results (data not shown).

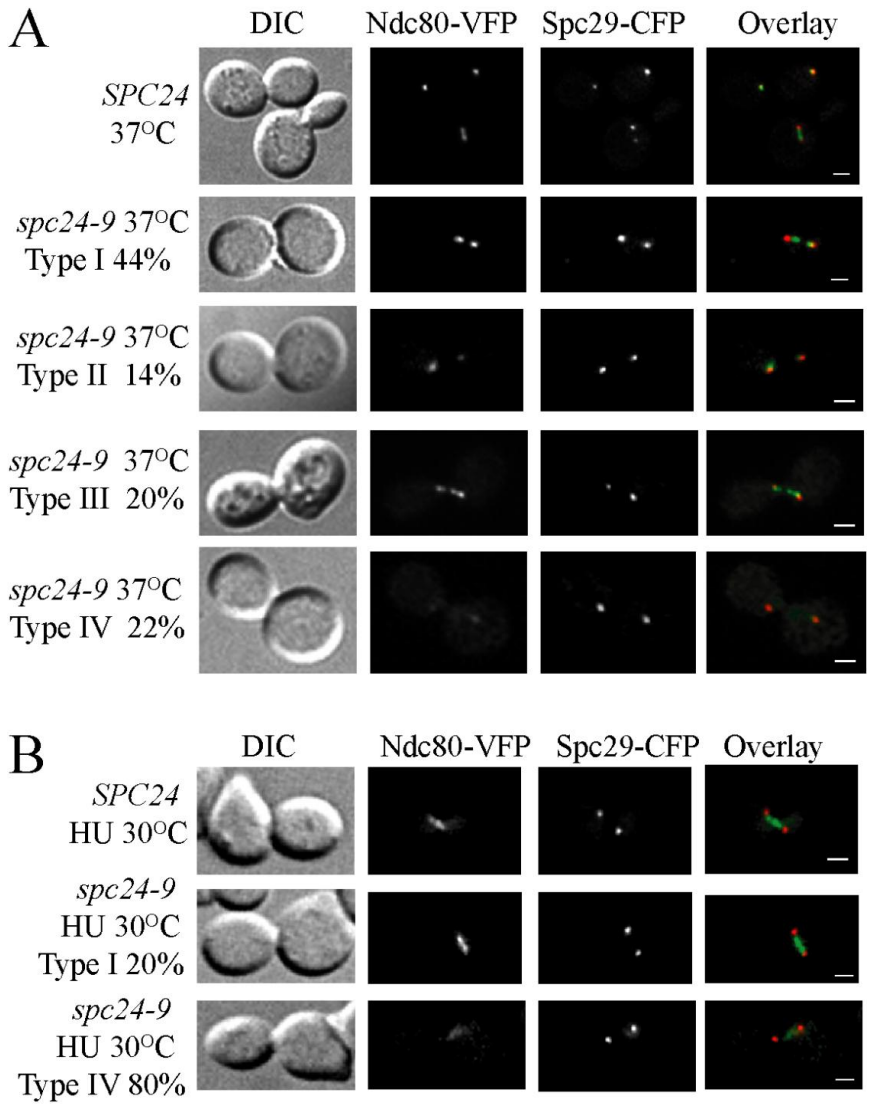

Figure 2.3 Ndc80 is mislocalized in *spc24-9* mutants

(A) Ndc80-VFP Spc29-CFP wild type (*SPC24*) and *spc24-9* cells were grown at 25°C to log phase, then incubated at 37°C for three hours, fixed in 70% ethanol and imaged. Four types of Ndc80 localization patterns were detected in *spc24-9* mutants: Type I: Wild type Ndc80, 44% of cells; Type II: Ndc80 localized to one SPB (14% of cells); Type III: Multiple Ndc80 foci (20% of cells); Type IV: Little or no Ndc80-VFP signal (22% of cells). (B) Ndc80-VFP Spc29-CFP wild type (*SPC24*) and *spc24-9* cells were grown at 25°C to log phase, then incubated at 30°C in 0.2M HU for three hours, fixed in 70% ethanol and imaged. In *spc24-9* cells, Ndc80-VFP localization either resembled wild type cells (20% of cells) or Ndc80-VFP levels were very low and barely detectable (80% of cells). In the overlay, green is VFP signal and red is CFP. Scale bar is 2μm for all images.

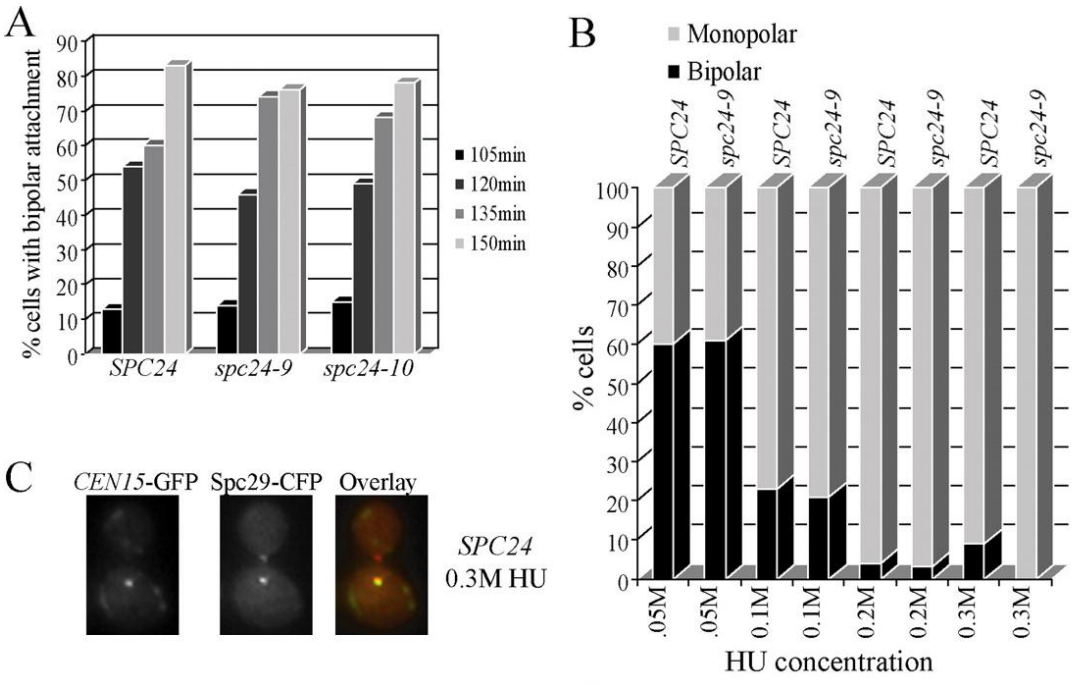

Figure 2.4 *spc24-9* mutants are capable of establishing bipolar attachment

(A) Wild type (*SPC24*), *spc24-9* and *spc24-10* strains carrying LacO repeats integrated 1.8kb from *CEN15*, LacI-GFP and Spc29-CFP were synchronized in G1 phase with α-factor and released at 30°C. Samples were taken every 15 min. and imaged using fluorescence microscopy for the presence of the *CEN15*-GFP and Spc29-CFP signal. Shown are the time points (105 min. onwards) at which the cells began to display bipolar attachment (separation of *CEN15*-GFP signals). Duplicate experiments were performed with similar results. Shown is the result of one experiment in which 100 cells containing a spindle of 0.5 μm or larger were counted for each time point. (B) Wild type (*SPC24*) and *spc24-9 CEN15*-GFP Spc29-CFP strains were synchronized in G1 phase with α-factor, split into four cultures and indicated concentrations of HU were added for 3 hours at 30°C. Similar results were seen with duplicate experiments thus data from one experiment is shown (100 cells counted). (C) Example of a wild type (*SPC24*) cell from (B) after 3 hours of 0.3M HU treatment that displays monopolar *CEN15* attachment. In the overlay, *CEN15*-GFP is green and Spc29-CFP is red.

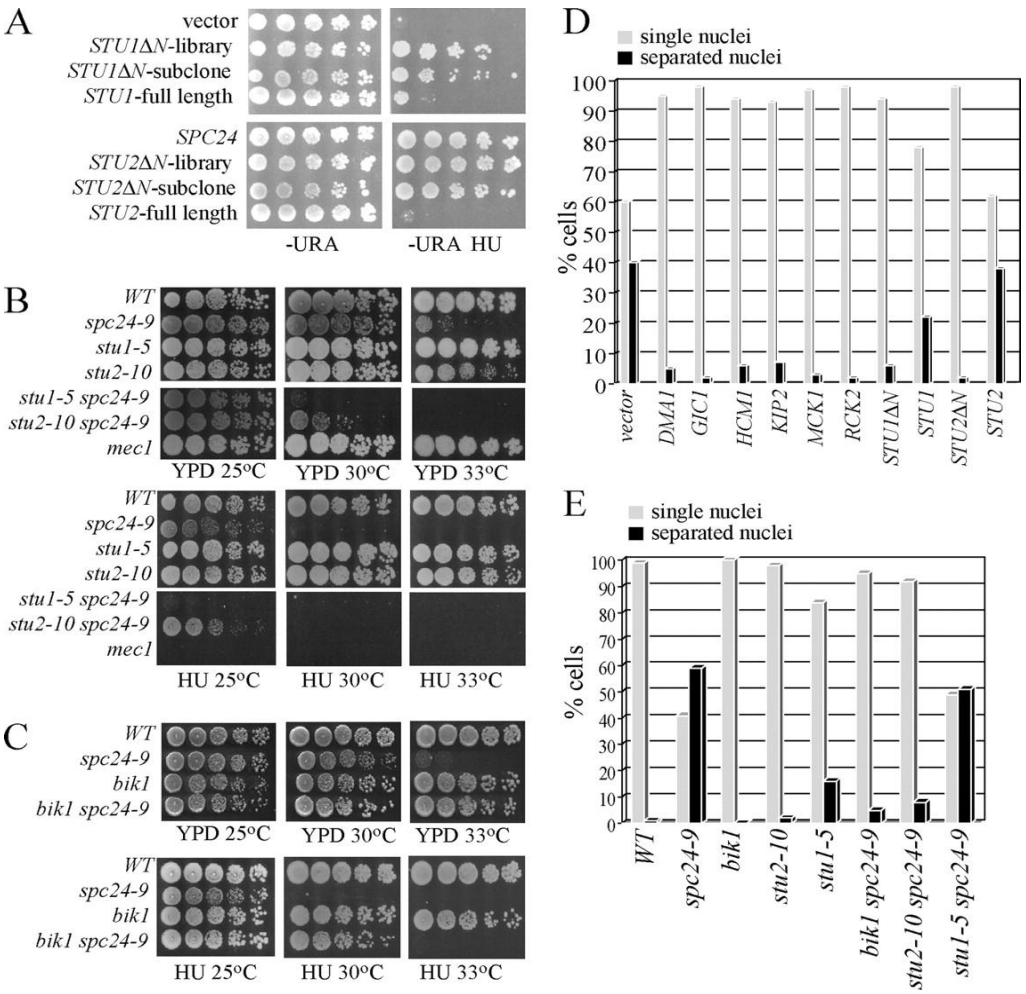

Figure 2.5 Spindle expansion in *spc24-9* mutants depends on active Stu2

(A) Cell dilution assay of *spc24-9* mutants carrying the following 2μ plasmids: vector (pRS202), *STU1*Δ*N*-library (HCS clone identified in screen), *STU1*Δ*N*-subclone (subclone of *STU1*Δ*N*-library containing only the *STU1* gene), *STU1* full length (gift of T. Huffaker), full length *SPC24*, *STU2*Δ*N*-library (HCS clone identified in screen), *STU2*Δ*N*-subclone (subclone of *STU2*Δ*N*-library containing only the *STU2* gene), *STU2* full length (gift of T. Huffaker) were grown on -URA plates at 30°C for 4 days or –URA .05M HU at 30°C for 5 days. (B) and (C) Cell dilution assay of indicated strains grown on YPD at 25°C (2 days), 30°C and 33°C (3 days) and .05M HU at 25°C, 30°C and 33°C (3 days). (D) Immunofluorescence analysis of *spc24-9* mutants carrying the indicated HCS plasmids synchronized in G1 phase with α-factor, then released into 0.2M HU for three hours at 30°C. Cells were counted (100 per sample) for single nuclei (grey bars) or separated nuclei (black bars) by DAPI staining. Duplicate experiments were performed with similar data and shown is the result of one experiment. (E) Immunofluorescence analysis of indicated strains treated and analyzed as described in (D).

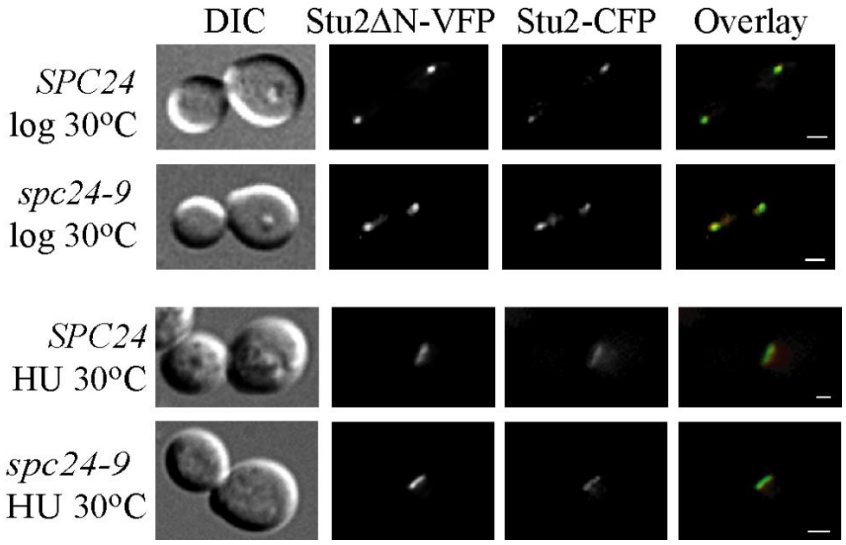

Figure 2.6 Stu2ΔN-VFP localization overlaps with endogenous Stu2-CFP

Wild type (*SPC24*) and *spc24-9* strains carrying Stu2ΔN-VFP on a 2μ plasmid and endogenous Stu2-CFP were either grown at 30°C to log phase or incubated in 0.2M HU for three hours, fixed in 70% ethanol and imaged. In the overlay, green is VFP signal and red is CFP. Scale bar is 2μm for all images.

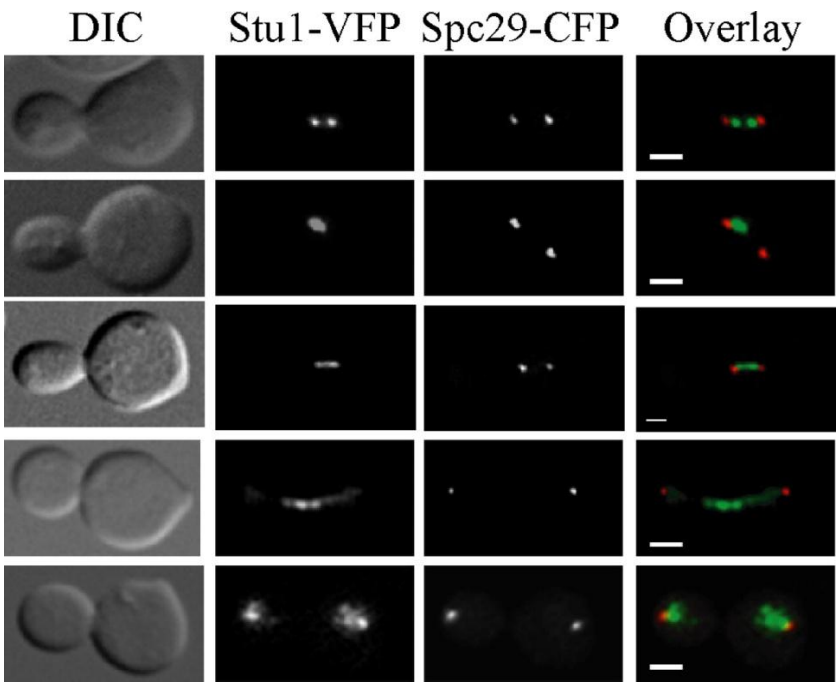

Figure 2.7 Stu1 localizes to kinetochores and the spindle midzone

Wild type Stu1-VFP Spc29-CFP cells were synchronized in G1 phase with α-factor and released into the cell cycle at 30°C. Cells were fixed in 70% ethanol every 15 min. for 90 min. and imaged as described in the Material and Methods. In the overlay, green is VFP signal and red is CFP. Scale bar is 2μm for all images.

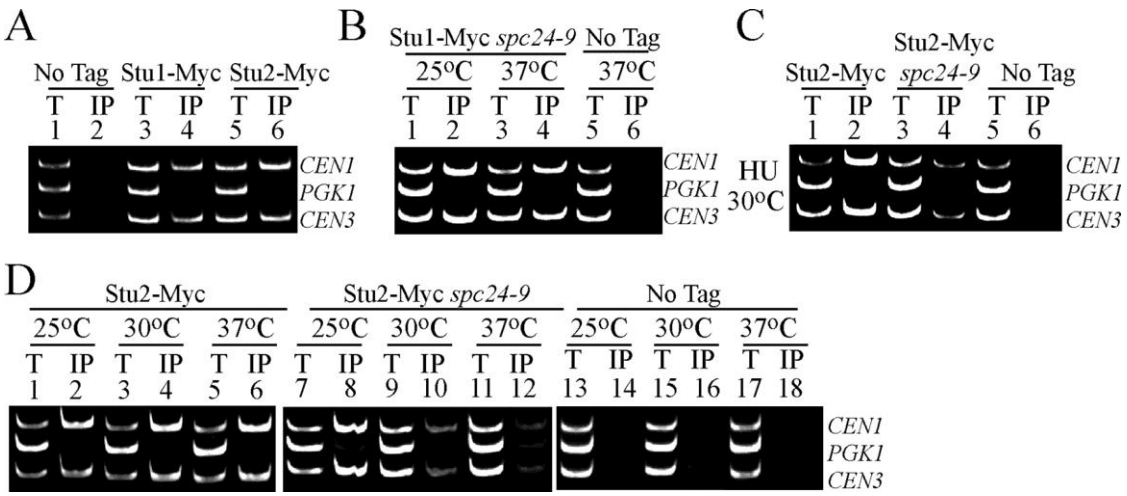

Figure 2.8 Stu2 *CEN* binding is abolished in *spc24-9* mutants whereas Stu1 is still able to associate with *CEN* DNA

Multiplex PCR analysis of *CEN1*, *PGK1* and *CEN3* loci was performed with total chromatin (T) or immunoprecipitate (IP) as PCR templates. Strains were grown at 25°C to log phase, then either kept at 25°C or incubated at 30°C or 37°C for three hours. (A) Wild type log phase cells grown at 30°C and carrying no epitope tag (No Tag), (lanes 1-2), Stu1-Myc (lanes 3-4) and Stu2-Myc (lanes 5-6). (B) *spc24-9* mutants carrying Stu1-Myc (lanes 1-4) and a wild type strain with no tag at 37°C (lanes 5-6). (C) Stu2-Myc in a wild type (lanes 1-2), *spc24-9* (lanes 3-4) and an untagged wild type strain (NoTag, lanes 5-6). Strains were grown to log phase at 25°C, HU was added to a final concentration of 0.2M HU and cells were shifted to 30°C for three hours. (D) Stu2-Myc in a wild type (lanes 1-6) and *spc24-9* (lanes 7-12) strains. No Tag strain (lanes 13-18) is an untagged wild type strain. For all ChIP assays where the *spc24-9* mutant was used, I included both a wild type and *spc24-9* untagged control and saw similar results thus only the wild type untagged control is presented.

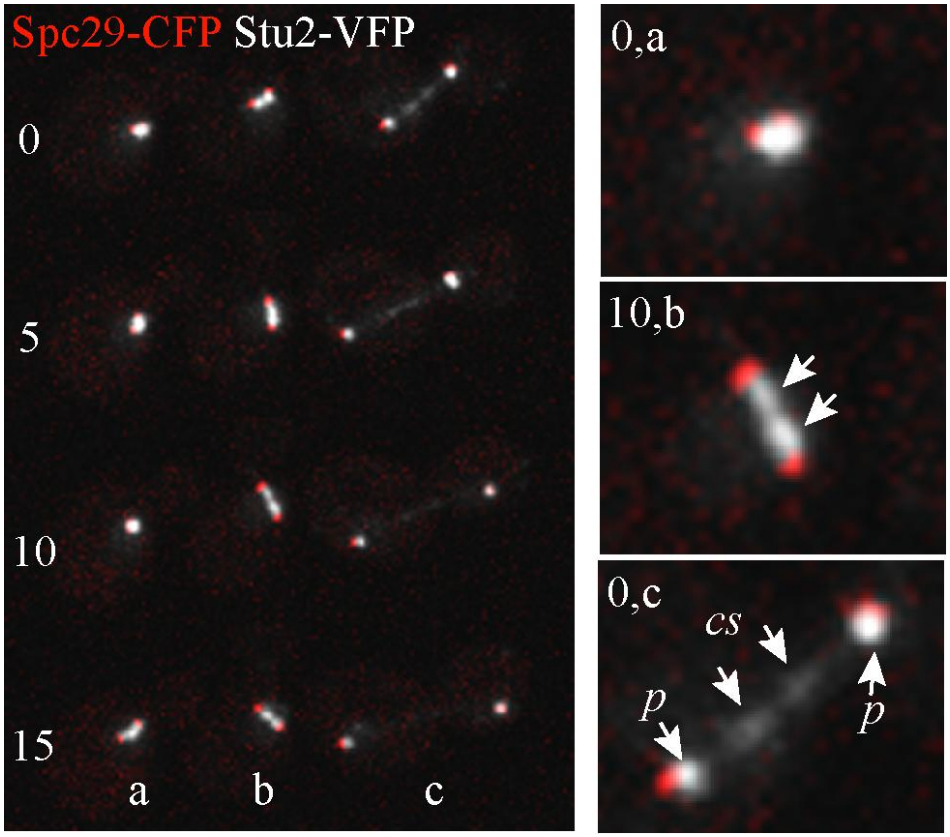

Figure 2.9 Time-lapse analysis of Stu2-VFP

Stu2-VFP Spc29-CFP cells were imaged using time-lapse microscopy at 30^{o}C as described in the Materials and Methods. Stu2-VFP is represented in greyscale and Spc29-CFP in red. Arrows in Image 10,b point to Stu2-VFP bilobed foci on the nuclear side Spc29-CFP. Arrows in Image 0,c point to Stu2-VFP localization on the central spindle (cs) and poles (p).

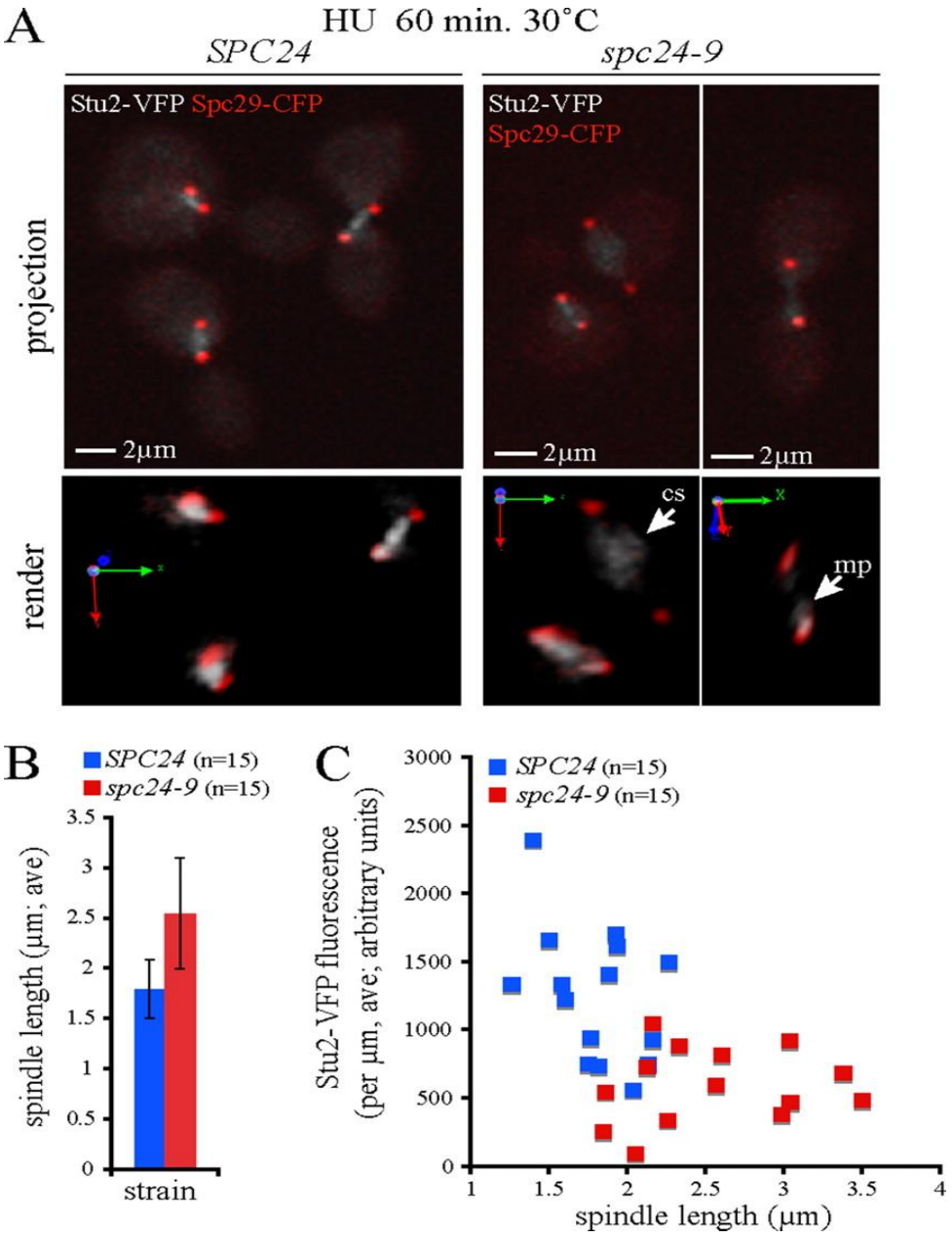

Figure 2.10 Increased spindle length correlates with Stu2 mislocalization and reduction

Wild type (*SPC24*) and *spc24-9* cells expressing Stu2-VFP Spc29-CFP were synchronized in G1 phase with pheromone, released into 0.2M HU at 25°C for 1.5h and shifted to 30°C in HU for 60 min., then fixed. (A) Representative images (extended focus and 3-dimensional render) of Stu2-VFP (greyscale) and Spc29-CFP (red) fluorescence in wild type and *spc24-9* cells at 60 min. after shift to 30°C are shown; mp indicates monopolar localization (near the SPB), whereas cs indicates localization to the central spindle. (B) Average (ave) spindle length of wild type (*SPC24*) and *spc24-9* cells after a 60 min. incubation in 0.2M HU at 30°C (n=15). (C) Quantitative analysis of Stu2-VFP fluorescence plotted as a function of spindle length.

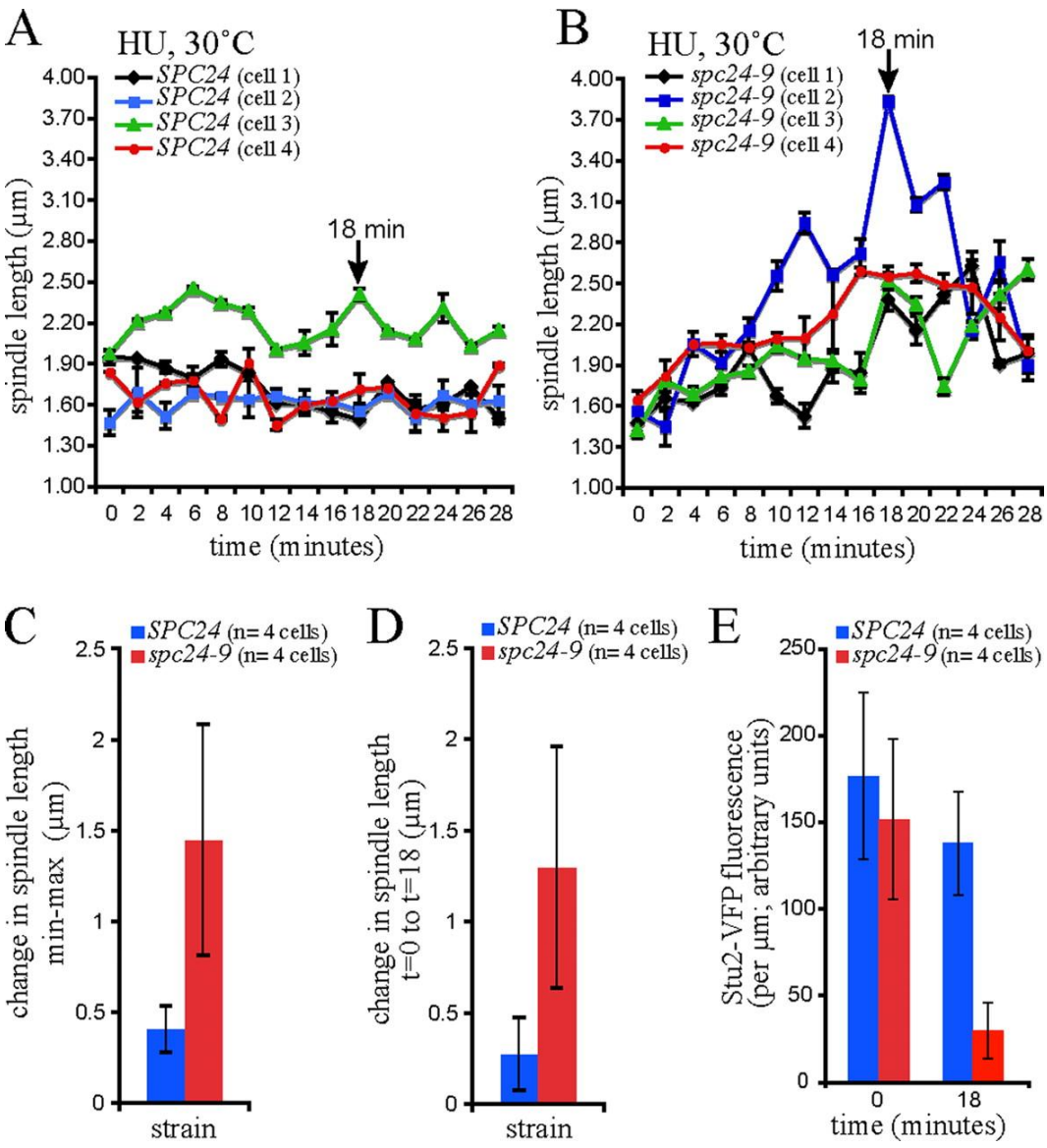

Figure 2.11 Decreased Stu2 in the *spc24-9* mutant results in oscillation of spindle length

Wild type (*SPC24*) and *spc24-9* cells carrying Stu2-VFP Spc29-CFP were synchronized in G1 phase with pheromone, released into 0.2M HU at 25°C for 1.5h, mounted in FP supplemented with HU, shifted to 30°C on a heated stage and time-lapse microscopy performed. Time zero is time in HU at 30°C after equilibration on the stage at 30°C for 15 min. Spindle length is plotted for four cells of each strain (A, *SPC24*; B, *spc24-9*) as a function of time, each depicted with a different colour, and shows oscillation with a net increase in length observed in all four *spc24-9* cells at 18 min. (C) In contrast with wild-type cells, spindle length increases in *spc24-9* cells. (D) Spindle length is significantly increased in all four *spc24-9* cells at 18 min. relative to length at t=0. (E) At 18 min., Stu2-VFP fluorescence on the spindle is significantly decreased in all *spc24-9* mutant cells relative to wild-type cells.

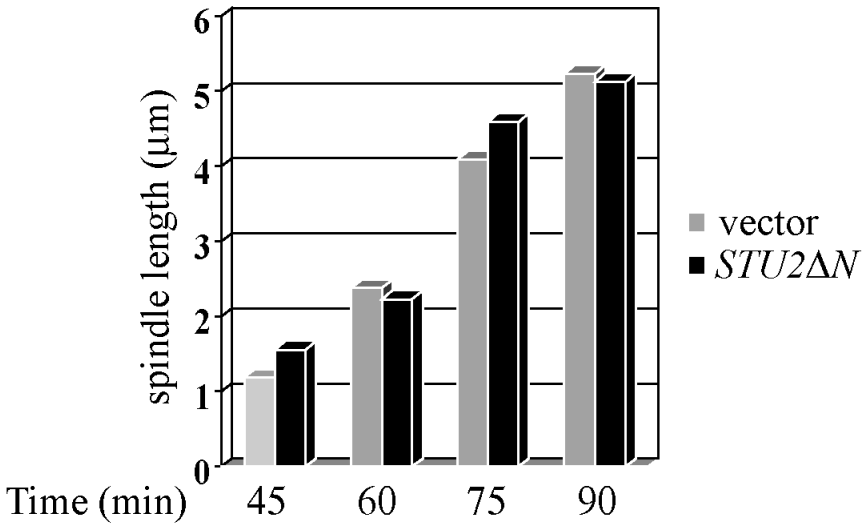

Figure 2.12 Overexpression of *STU2*Δ*N* does not affect wild type spindle length in an unperturbed cell cycle

Vector control (pRS326) and *STU2*Δ*N* were expressed in cells carrying Stu2VFP Spc29CFP. Cells were grown to log phase at 30^{o}C, arrested with α-factor for 1.5hours at 30^{o}C, released to 30^{o}C and time points taken every 15min. Spindle length was calculated as described in the Materials and Methods. Thirty cells were counted for each time point.

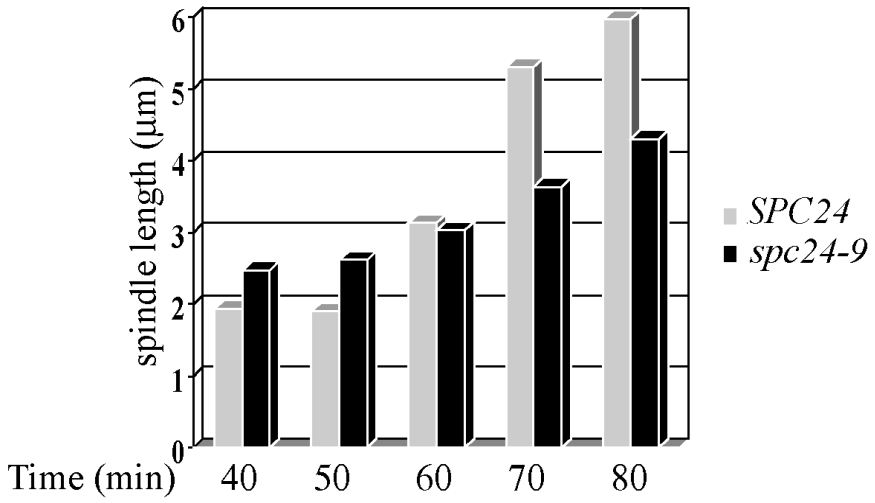

Figure 2.13 *spc24-9* mutants display spindle expansion early in the cell cycle but a delay in anaphase

Wild type (*SPC24*) and *spc24-9* cells carrying Stu2VFP Spc29CFP were grown at 25°C to log phase, incubated with α-factor for 1hour at 25°C, resuspended in prewarmed 37°C media with new α-factor and incubated for 2 hours at 37°C. Cells were then released from the G1 arrest into 37°C and time points taken every 10min. Spindle length was measured by calculating the distance from Spc29-CFP foci to Spc29-CFP foci. Fifty cells were counted per time point.

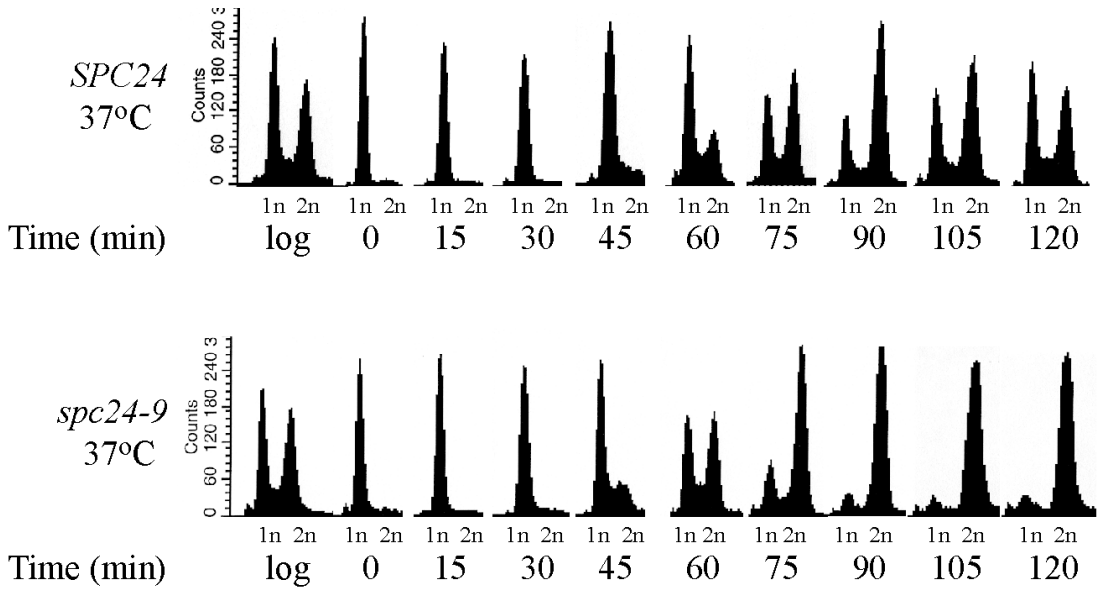

Figure 2.14 ***spc24-9*** **mutants accelerate through S phase and delay at anaphase at restrictive temperature**

Wild type (*SPC24*) and *spc24-9* cells were grown at 25°C to early log phase, arrested in G1 phase with pheromone, released to 37°C and time points taken every 15 min. DNA content was measured by flow cytometry as described in the Materials and Methods.

Chapter 3 Determination of a Novel Role for the Ndc80 Kinetochore Complex in the Ras2/cAMP/PKA Pathway

3.1 Introduction

Budding yeast *Saccharomyces cerevisiae* is able to use various carbon sources but prefers glucose. High concentrations of glucose represses the transcription of a large set of genes involved in utilization of alternate carbon sources, respiration and peroxisomal functions resulting in cells switching from respiratory growth to fermentative growth (Perlman & Mahler, 1974; Gancedo & Serrano, 1989; Ronne, 1995; De Winde, *et al.*, 1997). Glucose repression is derepressed when cells are carbon starved or grown on a non-fermentable carbon source like glycerol or ethanol. The addition of glucose or other rapidly fermentable sugars to derepressed cells triggers rapid activation of transcription and translation to enable cells to adapt to the fermentative carbon source. One of the best understood pathways mediating the glucose signaling cascade is the cyclic AMP (cAMP) /Protein Kinase A (PKA) pathway (Figure 3.1). Adenylate cyclase, Cyr1, which catalyzes the synthesis of cAMP from ATP, is a key component of the PKA signal transduction pathway. In budding yeast, the activity of adenylate cyclase is stimulated by the small G proteins Ras1 and Ras2, and a G protein coupled receptor (GPCR) system. The GPCR system includes the membrane glucose receptor Gpr1 and Gα protein Gpa2, and glucose activation by the GPCR system is strictly dependent on glucose phosphorylation

(Rolland, *et al*., 2000; Rolland, *et al*., 2001). Cdc25 and Sdc25 are two guanine nucleotide exchange factor proteins (GEF) for Ras that switch GDP-bound Ras to GTP-bound Ras, whereas Ira1 and Ira2 are redundant GTPase activating proteins (GAP) that inactivate Ras by hydrolysis of the bound GTP to GDP.

PKA, which is composed of the Tpk1, 2, 3 catalytic subunits and the inhibitory Bcy1 regulatory subunit, is the major target of cAMP. Once cAMP binds Bcy1, Tpk1, 2, 3 are released from Bcy1 and become active to phosphorylate multiple target proteins including the Msn2 and Msn4 transcription factors (Figure 3.1). High activity of the PKA pathway causes immobilization of storage carbohydrates (trehalose and glycogen), high sensitivity to heat and nutrient starvation, low expression of stress response genes and high expression of ribosomal protein genes. Low activity of the PKA pathway causes the opposite phenotype, such as high levels of trehalose and glycogen and high expression of stress response genes. cAMP accumulation in yeast is under strong feedback inhibition by PKA (Nikawa, *et al*., 1987; Mbonyi, *et al*., 1990). The Pde1 low-affinity cAMP phosphodiesterase, which hydrolyzes cAMP to AMP, is activated by PKA (Ma, *et al*., 1999). Ras2, Cdc25 and the Ira proteins have also been suggested as targets of the feedback-inhibition mechanism (Gross, *et al*., 1992; Tanaka, *et al*., 1989; Colombo, *et al*., 2004).

Two published articles have demonstrated a potential interaction between kinetochore proteins and the Ras2/cAMP/PKA pathway: 1) Sgt1, which is required for the assembly of the CBF3 inner kinetochore complex, physically interacts with Cyr1 and upregulates the activity of

the cAMP/PKA pathway (Dubacq, *et al*., 2002); 2) the function of the outer kinetochore Dam1 complex might be repressed by the Ras2/PKA pathway during a normal cell cycle (Li, *et al*., 2005). In this chapter, I extend these studies to demonstrate that the Ndc80 kinetochore complex might play a role in the cAMP/PKA pathway in addition to its well-known functions in chromosome segregation and the spindle checkpoint.

3.2 Materials and methods

3.2.1 Strains, plasmids and media

Yeast strains and plasmids used in this study are described in Table 3.1. The liquid media were rich medium (YPD) or supplemental minimal medium (SC) (Kaiser, *et al*., 1994). The solid plates for spot assays were YPD (2% glucose), YPR (2% raffinose), YPGal (2% galactose) and YPGly (2% glycerol).

3.2.2 Trehalose determination

The trehalose measurement was modified from a published trehalose quantitation method (Parrou & Francois, 1997). Cells were grown into stationary phase with 5-10ml YPD at 25℃ and collected by centrifugation (3min at 3500rpm). Cell pellets were washed once with distilled water, resuspended in 0.5ml of 0.25 M Na_2CO_3, and incubated at 95℃ for 1 h. The mixture was centrifuged (1min at 5000rpm) and the supernatant was removed into a new 1.5ml eppendorf tube. 50ul of supernatant was taken out and brought to pH5.2 with 30µl 1M acetic acid and 120µl

0.2M Na-acetate (pH5.2). The mixture was incubated overnight with 2.5µl trehalase (0.01unit) (Sigma, Cat.No. T8778) at 37℃ under constant agitation and glucose was determined with a glucose assay kit (Sigma GAGO20). Each sample was measured in triplicate.

3.2.3 Msn2 Western blot

spc24-8 (YVM1448), *spc24-9* (YVM1380) and *spc24-10* (YVM1363) cells were grown to mid-logarithmic phase in 50ml YPD at semi-permissive temperature for each strain (33℃, 30℃, 30℃, respectively). Wild type (YVM1370) cells were grown at both 33℃ and 30℃. One quarter of the culture was harvested and the pellet was washed once with cold dH_2O and kept on ice or at -80℃ for future use. The rest of the culture was washed once with prewarmed YP media, resuspended in prewarmed YP and kept shaking in the incubator at 33℃ or 30℃. 10ml culture was collected for each indicated time point. The cell pellet was lysed and 40µg protein was loaded per lane. Msn2 phosphorylation was detected with α-P-CREB (Görner, *et al*., 1998) (Cell Signaling No. 9196, Beverly, MA, USA) (1:1000), and with α-Msn2 (kind gift from Dr. Estruch, Valencia, Spain) (1:5000) as a loading control.

3.3 Results

3.3.1 The temperature sensitivity of spc24-9 is rescued by reducing cAMP/PKA activities

The Measday lab previously reported a synthetic genetic analysis (SGA) performed using

spc24-9 as the query strain (Montpetit, *et al*., 2005), which identified a synthetic lethal (SL) interaction with *ira2*Δ and a synthetic sick (SS) interaction with *pde2*Δ (Figure 3.2A). Consistently, I found that overexpressing *PDE2* rescues the temperature sensitivity (ts) of *spc24-9* at 33℃ (Figure 3.2B). Both Ira2 and Pde2 are negative regulators of Ras/cAMP/PKA pathway (Colombo, *et al*., 2004; Park, *et al*., 2005) (Figure 3.2C). I predicted that if the SS/SL interaction with *spc24-9* is due to hyperactivation of Ras/cAMP/PKA pathway, deletion of Ras1 or Ras2 would rescue the ts of *spc24-9*. I tested both *ras1*Δ *spc24-9* and *ras2*Δ *spc24-9* double mutants at a series of different temperatures. As shown in Figure 3.2D, *spc24-9* was fully rescued by *ras2*Δ at 33℃ and partially at 35℃ which is a semi-permissive temperature for *ras2*Δ, whereas *ras1*Δ partially rescued *spc24-9* at 33℃. Although Ras1 and Ras2 are two Ras homologs, there are several differences in their functions. For example, Ras2 activates adenylyl cyclase more efficiently than Ras1 (Broek, *et al*., 1985), *ras2*Δ cells have less cAMP levels compared to *ras1*Δ cells (Toda, *et al*., 1985), and Ras2 but not Ras1 activates the pseudohyphal pathway (Mösch & Fink, 1997; Mösch, *et al*., 1996). Since I did not observe pseudohyphal growth of *spc24-9* cells (data not shown), the different rescue ability of *ras1*Δ and *ras2*Δ probably relies on their effects on cAMP: *ras2*Δ cells have less cAMP levels than *ras1*Δ cells, therefore *ras2*Δ may rescue *spc24-9* ts lethality by reducing cAMP levels in *spc24-9* cells. Interestingly, I found that two other *spc24* ts alleles, *spc24-8* and *spc24-10*, were also rescued by *ras2*Δ (Figure 3.2 E), suggesting that compromising the function of the Ndc80 complex, by mutation of Spc24, might induce increased cAMP levels. Alternatively, the Ras cAMP pathway

may negatively regulate Ndc80 kinetochore complex function.

3.3.2 spc24-9 cells have less trehalose compared to wild type

The level of trehalose is a good marker for evaluating PKA activities because trehalose accumulation is downregulated by PKA via a combination of transcriptional repression of the genes encoding the trehalose synthase subunits and PKA-dependent phosphorylation of the neutral trehalase which degrades trehalose (Figure 3.1B). Accumulation of trehalose begins at the diauxic shift and continues until cells enter stationary phase. Degradation of trehalose begins once cells have entered stationary phase (Werner-Washburne, *et al*., 1996). Therefore, before testing trehalose levels in *spc24* alleles, it was important to analyze the growth curve of *spc24-8*, *spc24-9* and *spc24-10* strains at 25℃ and their semi-permissive temperature. At 25℃ all three *spc24* alleles have the same growth rate as wild-type cells (Figure 3.3A). At the semi-permissive temperature, *spc24-8* and *spc24-9* cells have a lower OD_{600} than the wild type in diauxic phase and sustain lower cell density during stationary phase (Figure 3.3B-C), but the growth curve of *spc24-10* is highly similar to wild type (Figure 3.3B). Subsequently, I tested the trehalose levels of *spc24* alleles grown in stationary phase. At 25℃ no dramatic difference is detected between *spc24* mutant cells and wild type cells (data not shown). At the semi-permissive temperature, the trehalose levels of *spc24-8* and *spc24-10* are both similar to the wild type, whereas *spc24-9* cells have lower trehalose levels compared to wild type (Figure 3.3D). Since PKA activity is associated with reduced trehalose levels, the *spc24-9* strain might have higher

PKA activity compared to the other two *spc24* alleles.

The addition of glucose to the stationary cells induces trehalase activity and trehalose mobilization (Thevelein, 1984). Therefore, I asked if *spc24* alleles have defects in glucose-induced trehalose mobilization. As showed in Figure 3.3E-F, all the three *spc24* mutant cells response to glucose in a similar manner to the wild type by reducing trehalose levels, but *spc24-8* and *spc24-9* cells have lower overall trehalose levels. Therefore, the glucose response machinery is not affected in stationary phase *spc24* mutant cells but the lower trehalose levels in *spc24-8* and *spc24-9* strains suggest that PKA activity may be higher in these mutants compared to the wild type.

3.3.3 Msn2 dephosphorylation is compromised in *spc24* upon glucose depletion

The Msn2 transcription factor is one of the targets of the PKA pathway. Activation of the PKA pathway causes phosphorylation of the Msn2 nuclear localization sequence on serine residues, prevention of Msn2 nuclear import and restoration of Msn2 to the cytoplasm (Görner, *et al*., 1998; Görner, *et al*., 2002; Jacquet, *et al*., 2003). In response to glucose starvation, the serine phosphorylation of Msn2 is acutely decreased due to PKA downregulation, however, this dephosphorylation is transient and is rapidly followed by re-phosphorylation in a PKA dependent manner (Görner, *et al*., 2002; Trott, *et al*., 2005). As shown in Figure 3.4, Msn2 phosphorylation was dramatically decreased in wild type cells within 10min (30^{o}C) or 5min (33^{o}C), and Msn2 rephosphorylation was established by 20min. Prior to glucose starvation, the phosphorylation

of Msn2 in *spc24-8, spc24*-9 and *spc24-10* was similar to the wild type (Figure 3.4). However, the dephosphorylation of Msn2 was attenuated in all the three *spc24* mutant cells: *spc24-9* and *spc24-10* cells had higher levels of phosphorylated Msn2 at 10min compared to wild type cells; *spc24-8* cells also had more phosphorylated Msn2 than wild type at both 5min and 10min. In addition, these mutant cells showed less phosphorylation compared to wild-type cells at 20min, suggesting that the reestablishment of Msn2 phosphorylation was delayed. The above alleviated, instead of acute, response to glucose starvation and the delay of Msn2 rephosphorylation implies defects in glucose sensing and PKA signaling in *spc24* mutant cells.

3.3.4 Non-glucose carbon sources rescue the ts of the mutants of Ndc80 complex components

Fermentable carbon sources increase PKA activity whereas non-fermentable carbon sources lower PKA activity (Thevelein, *et al*., 2008). Since our data suggest that PKA signaling is perturbed in *spc24* mutants, I asked if growth on non-fermentable carbon sources would rescue the ts of *spc24* mutants. I tested growth of *spc24-8, spc24-9* and *spc24-10* mutants by plate assay on a non-fermentable carbon source (glycerol) versus fermentable carbon sources (glucose, raffinose and galactose) as the sole carbon source. Interestingly, all the three *spc24* alleles were rescued by both the glycerol non-fermentable carbon source and the raffinose and galactose fermentable carbon sources (Figure 3.5B). Even though raffinose and galactose are both fermentable carbon sources, they are known as non-preferred carbon sources (NPCS) because

they cannot trigger a strong cAMP/PKA response (Rolland, *et al*., 2000; Rolland, *et al*., 2001). Therefore, raffinose, galactose and glycerol rescue the ts growth defect of *spc24* alleles possibly due to inability to fully activate the cAMP/PKA pathway, which further implies that *spc24* mutants have higher levels of PKA activity. Another possibility is that *spc24* alleles have growth defects on glucose media due to glucose repression of a gene important for kinetochore function. I tested this possibility by deleting *REG1*, which is the regulatory subunit of type I protein phosphatase complex and required for maintaining glucose repression (Dombek, *et al*., 2004). As shown in Figure 3.6, *reg1*Δ does not rescue the ts of *spc24-9*, on the contrary, the *reg1*Δ *spc24-9* double mutant grows slightly more slowly compared to *spc24-9* at 33 ^{o}C.

Next I asked if the glucose growth defect is unique to *spc24* alleles or universal to the ts alleles of other kinetochore components. All the tested kinetochore ts alleles are shown in Figure 3.5 (C-E). Dramatically, all the ts alleles of the components of Ndc80 complex, *spc24-1, spc24-12, spc24-13, spc25-1, ndc80-1* and *nuf2-61,* were rescued by NPCS (Figure 3.5 C). In contrast, growth of other kinetochore mutants on NPCS did not show such a consistent phenotype. Figure 3.5D demonstrates that the inner kinetochore mutants: *cse4-1, ctf13-30* and *ndc10-42* were mildly rescued by NPCS, whereas *ndc10-1* and *skp1-3* (not shown) had the same growth rate on different carbon sources. Notably the *ndc10-1* mutant, which eliminates kinetochore assembly and attachment of chromosomes to microtubules resulting in all chromosomes remaining in the mother cell (Goh, *et al*., 1993), did not show any growth difference on different carbon source. Therefore, the rescue by NPCS may require a partially

assembled kinetochore. *ame1-4* and *okp1-5*, two ts mutants of the COMA complex which bridges the inner and outer kinetochore, showed opposite sensitivity to NPCS (Figure 3.5 E). Three alleles of Spc34, a component of the Dam1 outer kinetochore complex that circles microtubules, were tested on NPCS. *spc34-5* was mildly rescued by NPCS, *spc34-6* did not show any difference on alternate carbon sources, and *spc34-7* was slow growing on NPCS. Taken together, the dramatic rescue by NPCS was only consistent within the mutants of Ndc80 complex but not other kinetochore complexes, suggesting that the Ndc80 complex might have a separate role in the PKA pathway or cellular response to glucose.

3.4 Discussion

spc24 alleles were rescued by decreasing PKA activity such as by deleting *ras2* or overproducing *PDE2* (Figure 3.2B, D and E). In addition, *spc24-9* is SS with *pde2* and SL with *ira2* (Figure 3.2A), suggesting that the cAMP/PKA pathway might antagonize the function of the Ndc80 complex, which is similar to the model predicted for the Dam/Dash kinetochore complex and Ras2/PKA pathway (Li, *et al*., 2005). Li *et al* proposed two models for why decreasing PKA activities rescued the ts of the *ask1* kinetochore mutant. The first model is based on the fact that newly replicated centromeres attach to the old SPB because the new SPB is not yet competent for kinetochore attachment, therefore the mono-polar attachments of both centromeres to one SPB must be corrected. A reduction of PKA activity may either delay the replication of centromeres or enable more rapid maturation of the SPB so that the number of mono-polar

attachments might be rescued. The second model suggests that PKA negatively regulates the kinetochore via phosphorylation of Dam/Dash components. To further characterize the relationship between the Ndc80 complex and the PKA pathway one approach could be to analyze the phosphorylation status of the Ndc80 complex in wild type versus PKA mutants using a mass spectrometry approach.

The rescue of *spc24*, *spc25*, *ndc80* and *nuf2* mutant growth by NPCS might occur because of at least two possibilities: 1) NPCS induce low PKA activities which diminish the increased PKA activities in the ts mutants of the Ndc80 complex; 2) the transcription of the genes essential for kinetochore function when the Ndc80 complex is compromised is repressed by glucose but derepressed on NPCS. My data suggest that the first possibility is more likely because compromising glucose depression by deleting *REG1* does not rescue the ts of *spc24-9* (Figure 3.6).

Unlike Li *et al*'s data where some, but not all the ts mutants of Dam/Dash complex were rescued by decreasing PKA activity, I found that all the ts mutants of the Ndc80 complex, but not the other kinetochore mutants, were dramatically rescued by NPCS (Figure 3.5). My data suggest that the Ndc80 complex might also have a role in regulation of the PKA pathway. *spc24* alleles demonstrate cellular phenotypes consistent with a hyperactivated cAMP/PKA pathway, such as decreased trehalose accumulation and alleviated Msn2 dephosphorylation in response to glucose depletion (Figure 3.3, 3.4). I therefore propose that *spc24* mutants have increased PKA activity and the Ndc80 complex may both be a target of the PKA pathway and

have a role in downregulation of the PKA pathway as well.

Since NPCSs rescue the glucose growth defects of ts alleles of Ndc80 complex components more dramatically than they do for other kinetochore complexes (Figure 3.5), I propose that the Ndc80 complex has a unique function in the PKA pathway or glucose response. Some mutants, such as *cse4-1, ctf13-30* and *ame1-4*, (Figure 3.5D) were mildly rescued by NPCS probably because the cell cycle is slowed down, which may help defects like monopolar attachment get repaired. On the other hand, the severe growth on NPCS of some mutants, like *spc34-7* (Figure 3.5E), might be due to the exacerbated defects induced by prolonged cell cycle. I did not analyze the *dam1* or *ask1* mutants from the Li *et al* paper by spot assays on NPCS, therefore, I cannot exclude the possibility that Dam1 and Ask1 might also play a role similar to the Ndc80 complex.

Mutants defective in the anaphase-promoting complex/cyclosome (APC/C) are also rescued by downregulation of the Ras2/PKA pathway or growth on non-glucose carbon sources (Irniger, *et al.*, 2000; Bolte, *et al.*, 2003). Activation of the spindle checkpoint results in inhibition of the APC, stabilization of securin (Pds1) and arrest at the metaphase to anaphase transition. Therefore, if *spc24* mutants activate the spindle checkpoint, the genetic interactions with the Ras2/PKA pathway could be due to APC inhibition. A previous researcher in the Measday lab, Harvey Su, tested Pds1 levels in *spc24* alleles throughout the cell cycle after releasing from a G1 block to the non-permissive temperature. Pds1 levels in s*pc24-8* were stabilized, suggesting that the spindle checkpoint is activated, whereas in *spc24-10* mutants Pds1

levels were quickly reduced and the spindle extended with an undivided nucleus remaining in the mother cell indicative of a defect in the spindle checkpoint (data not shown and Montpetit *et al.*, 2005). Since both *spc24-8* and *spc24-10* were rescued by *ras2*Δ or non-glucose carbon sources (Figure 3.1), activation of the spindle checkpoint cannot explain the genetic interaction detected between the Ndc80 complex and the PKA pathway.

In budding yeast, the PKA holoenzyme mostly localizes in the nucleus (Griffioen, *et al.*, 2000). The Bcy1 regulatory subunit almost specifically localizes in the nucleus in the presence of glucose, whereas the activated Tpk1 (and probably Tpk2, Tpk3 as well) is able to enter the cytoplasm presumably to phosphorylate cytoplasmic substrates. Upon depletion of glucose, Bcy1 has equal distribution in both nucleus and cytoplasm, probably for downregulating cytoplasmic PKA activities (reviewed in Griffioen, *et al*., 2002). At this point we do not know if the Ndc80 complex directly interacts with components of the PKA pathway.

Several questions remain: 1) Is Ndc80 one of the PKA targets? While the components of the Ndc80 complex were not listed as candidate PKA phosphorylation targets (Budovskaya, *et al*., 2005), we cannot exclude the possibility that Ndc80 components might be phosphorylated by PKA because Budovskaya *et al.* did not test Ndc80 in vivo. In addition, Ndc80 might be indirectly regulated through a chaperone protein like Sgt1 (Dubacq, *et al*., 2002). 2) How does the Ndc80 complex negatively regulate the PKA pathway? The Measday lab has identified Ndc80 complex-interacting proteins by mass spectrometry and detected some components of cAMP-PKA pathway including Gpa2, Asc1 and Sdc25. However, I did not successfully

confirm the physical interaction by co-IP between the PKA components (Gpa2, Asc1 and Sdc25) and Ndc80 components (Ndc80 and Spc24), possibly because Gpa2 and Sdc25 are localized at the cell cortex and Asc1 is in cytoplasm, whereas the majority of Ndc80 localizes to the nucleus. Thus any physical interaction between the Ndc80 cytoplasmic pool (see Appendix B) and cytoplasmic cAMP-PKA components will be challenging to detect by co-IP. One possibility is to overproduce Ndc80 in an effort to increase the amount of Ndc80 in the cytoplasm.

Table 3.1 List of strains

Strain	Genotype	Reference
YVM1370	MATa *ura3-52, lys2-801, ade2-101, his3Δ200, leu2Δ1,trp1Δ63 SPC24::kanMX6*	Montpetit *et al.* (2005)
YVM1380	MATa *ura3-52, lys2-801, ade2-101, his3Δ200, leu2Δ1,trp1Δ63 spc24-9::kanMX6*	Montpetit *et al.* (2005)
YVM1448	MATa *ura3-52, lys2-801, ade2-101, his3Δ200, leu2Δ1,trp1Δ63 spc24-8::kanMX6*	Montpetit *et al.* (2005)
YVM1363	MATa *ura3-52, lys2-801, ade2-101, his3Δ200, leu2Δ1,trp1Δ63 spc24-10::kanMX6*	Montpetit *et al.* (2005)
YLM1565	MATa *ura3-52, lys2-801, ade2-101, his3Δ200, leu2Δ1,trp1Δ63 ras1Δ::LEU2*	This study
YLM1562	MATa *ura3-52, lys2-801, ade2-101, his3Δ200, leu2Δ1,trp1Δ63 ras1Δ::LEU2 spc24-9::kanMX6*	This study
YLM1572	MATa *ura3-52, lys2-801, ade2-101, his3Δ200, leu2Δ1,trp1Δ63 ras2Δ::LEU2*	This study
YLM1568	MATa *ura3-52, lys2-801, ade2-101, his3Δ200, leu2Δ1,trp1Δ63 ras2Δ::LEU2 spc24-9::kanMX6*	This study
YLM1813	MATa *ura3-52, lys2-801, ade2-101, his3Δ200, leu2Δ1,trp1Δ63 ras2Δ::LEU2 spc24-8::kanMX6*	This study
YLM1815	MATa *ura3-52, lys2-801, ade2-101, his3Δ200, leu2Δ1,trp1Δ63ras2Δ::LEU2 spc24-10::kanMX6*	This study
YVM571	MATa *ura3-52, lys2-801, ade2-101, his3Δ200, leu2Δ1,trp1Δ63 ctf13-30*	P. Hieter
YVM567	MATa *ura3-52, lys2-801, ade2-101, his3Δ200, leu2Δ1,trp1Δ63 ctf14-42*	P. Hieter
SBD520-6C	MATa *ura3-52, leu2-3, ade2-101, trp1Δ901, his3-11,15, cse4-1::RSCL1-1H(HIS3) cse4-1*	Stoler *et al.* (1995)
YJL158	MATa *ade2-101, trp1-Δ63, leu2-Δ1, ura3-52, his3-Δ200, lys2-801, cyh2-r okp1::okp1-5::TRP1*	Ortiz *et al.* (1999)
YPH1175	MATa *ura3-52, lys2-801, ade2-101, his3Δ200, leu2Δ1,trp1Δ63 skp1-3::LEU2*	P.Hieter
YPH1160	MATa *ura3-52, lys2-801, ade2-101, his3Δ200, leu2Δ1,trp1Δ63* CFIII *(CEN3L) HIS3 SUP11 skp1-4::LEU2*	P.Hieter
YPH1338	MATa *ura3-52, lys2-801, ade2-101, his3Δ200, leu2Δ1,trp1Δ63* CFIII *(CEN3L) TRP1 SUP11 sgt1-3::LEU2*	P.Hieter

(To be continued)

Table 3.1 List of strains (continued)

Strain	Genotype	Reference
YPH1337	MATa *ura3-52, lys2-801, ade2-101, his3Δ200, leu2Δ1,trp1Δ63* CFIII *(CEN3L) TRP1 SUP11 sgt1-5::LEU2*	P.Hieter
YPH1676	MATa *ura3-52, lys2-801, ade2-101, his3Δ200, leu2Δ1,trp1Δ63 ame1-4::TRP1*	Pot *et al.* (2005)
YM40	MATa *ura3-52, lys2-801, ade2-101, his3Δ200, leu2Δ1,trp1Δ63 spc34-5::kanMX6*	V.Measday
YVM1864	MATa *ura3-52, lys2-801, ade2-101, his3Δ200, leu2Δ1,trp1Δ63 spc34-6::kanMX6*	Montpetit *et al.* (2005)
YM41	MATa *ura3-52, lys2-801, ade2-101, his3Δ200, leu2Δ1,trp1Δ63 spc34-7::kanMX6*	V.Measday
PWY473	MATa *ade2-1, can1-100, his3-11,15, leu2-3,112, trp1-1 spc24-1*	Wigge&Kilmartin (2001)
ILM126	MATa *ura3-52, lys2-801, ade2-101, his3Δ200, leu2Δ1,trp1Δ63 spc24-12*	Le Masson *et al.* (2002)
ILM127	MATa *ura3-52, lys2-801, ade2-101, his3Δ200, leu2Δ1,trp1Δ63 spc24-13*	Le Masson *et al.* (2002)
PWY754	MATa *ade2-1, can1-100, his3-11,15, leu2-3,112, trp1-1 spc25-1*	Wigge&Kilmartin (2001)
YKH628	MATa *ade2-1, can1-100, his3-11,15, leu2-3,112, trp1-1 ndc80-1*	Wigge&Kilmartin (2001)
PSY455	MATa *ura3-52 leu2-3,11 trp1-Δ1 nuf2-61*	P. Silver

A

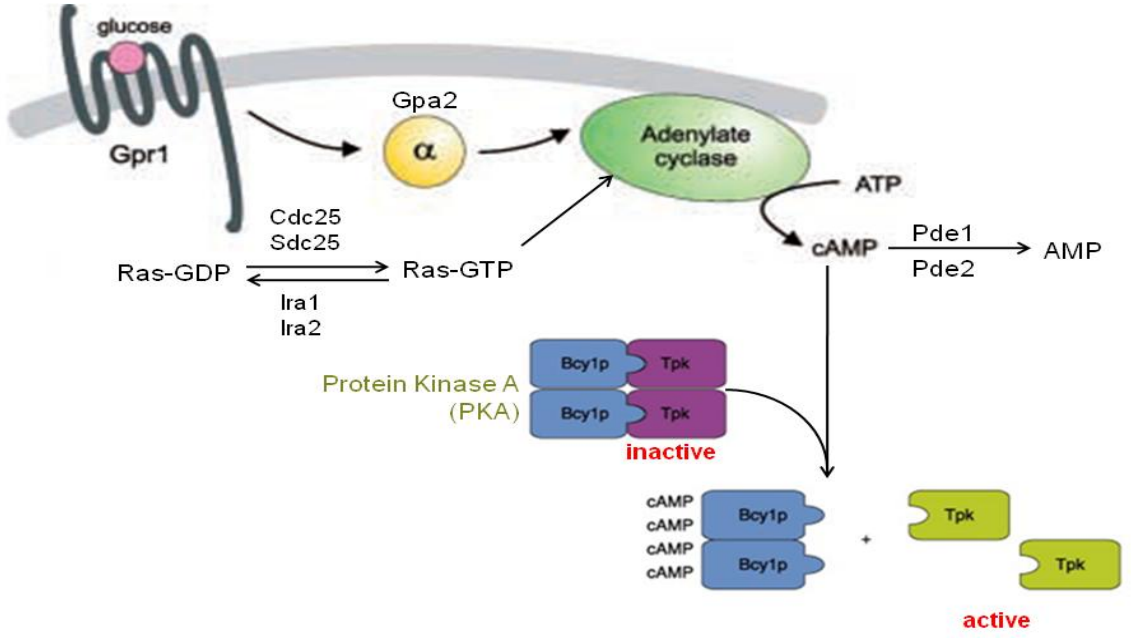

B

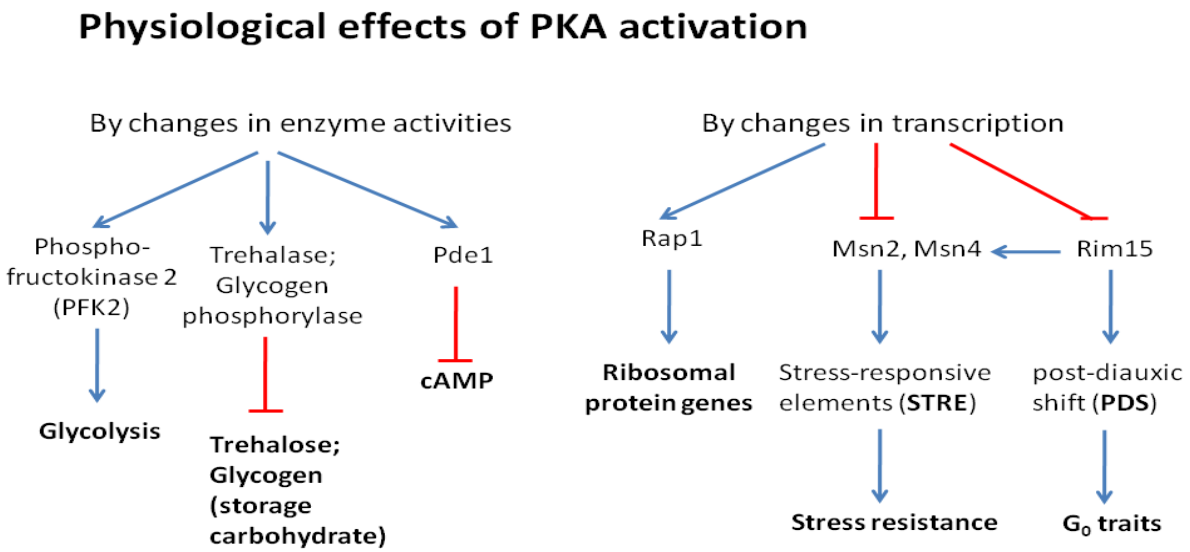

Figure 3.1 The cAMP-PKA pathway in yeast (A) and its physical effects (B)

(A) was modified from Peeters *et al.*, 2007, by permission © 2007 Elsevier Ltd All rights reserved.

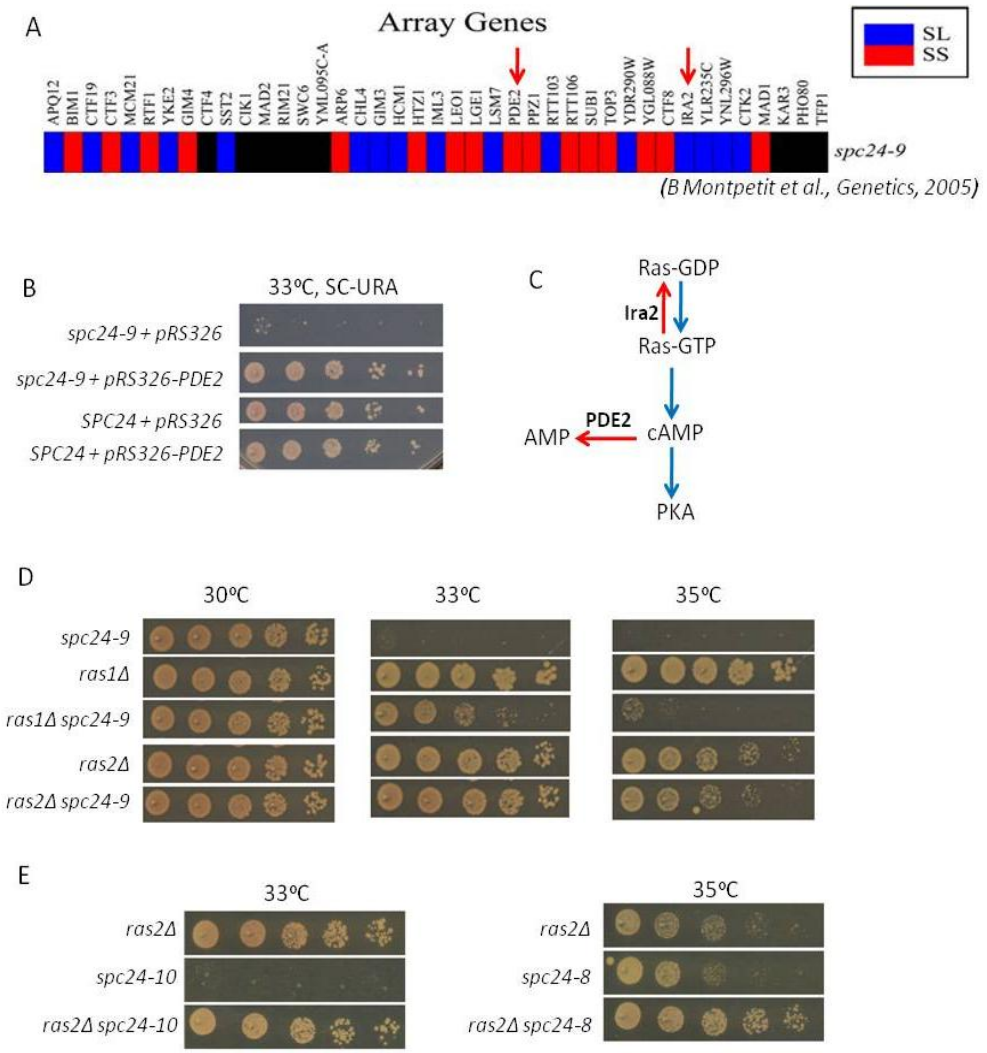

Figure 3.2 Genetic interactions between spc24-9 and the components of the Ras2/cAMP/PKA pathway

(A) SGA data was cited from Montpetit *et al*., Genetics 2005, by permission © Genetics Society of America.
(B) Cell dilution assay of wild type cells and *spc24-9* mutants carrying the plasmid vectors pRS326 and pRS326-PDE2.
(C) Genetic diagram of the Ras/PKA pathway. Blue arrows represent positive regulatory interactions and red arrows represent negative regulatory interactions.
(D) & (E) Cell dilution assay of indicated strains grown on YPD for 2 days.

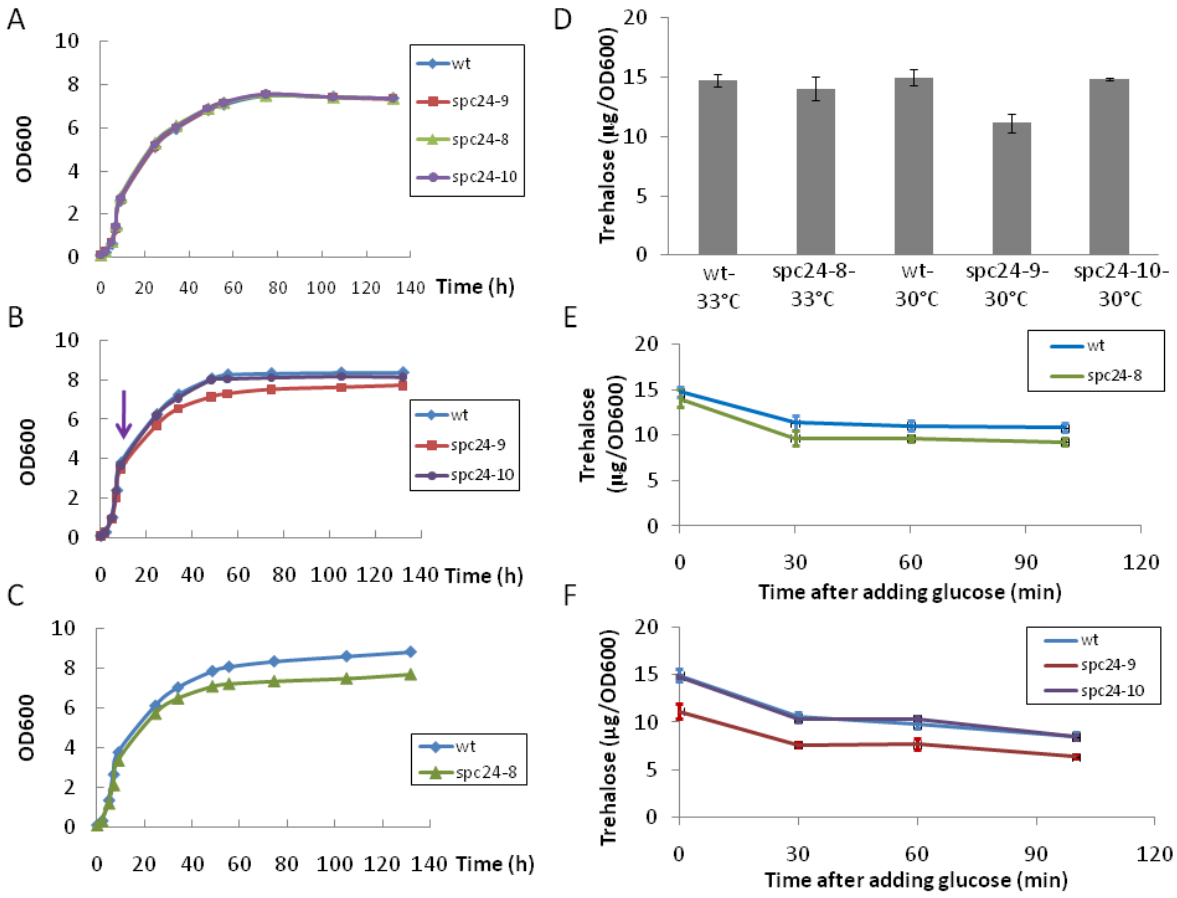

Figure 3.3 Growth curves (A-C) and trehlaose levels (D-F) in *spc24* cells

(A-C) *spc24-8*, *spc24-9*, *spc24-10* and wild type cells were grown to logarithmic phase at 25 ℃, diluted to OD_{600}=0.1, and incubated at 25 ℃ (all four strains), 30 ℃ (*spc24-9*, *spc24-10* and wild type) or 33 ℃ (*spc24-8* and wild type). Purple arrow in (B) points the start of the diauxic shift.
(D) Trehalose levels in stationary *spc24* cells at their semi-permissive temperatures (30 ℃ for *spc24-9* and *spc24-10*, 33 ℃ for *spc24-8*). wt-33 ℃ is the wild type control for *spc24-8* and wt-30 ℃ is the wild type control for *spc24-9* and *spc24-10*. Trehalose levels were measured enzymatically and normalized to total cell density (OD_{600}).
(E-F) Glucose induced trehalose mobilization. *spc24-8*, *spc24-9*, *spc24-10* and wild type cells were grown to stationary phase at 30 ℃ (*spc24-9*, *spc24-10* and wild type in E) or 33 ℃ (*spc24-8* and wild type in F). 100 mM glucose was added at time zero.

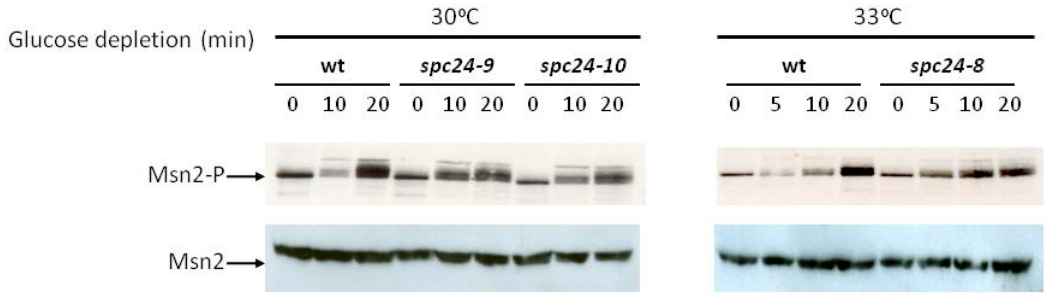

Figure 3.4 Kinetic analysis of Msn2 phosphorylation upon glucose starvation

Cells were grown to midlogarithmic phase at the semi-permissive temperature of *spc24* mutants (30 ℃ for *spc24-9* and *spc24-10*, 33 ℃ for *spc24-8*) in YPD medium and shifted to prewarmed YP medium lacking glucose. A timecourse was performed whereby samples were taken every 5 or 10min and equal amount of protein lysates were loaded on a 12% SDS-PAGE gel. Western blot were probed with antiphospho CREB for detecting the phosphorylation of Msn2 and anti-Msn2 as a loading control.

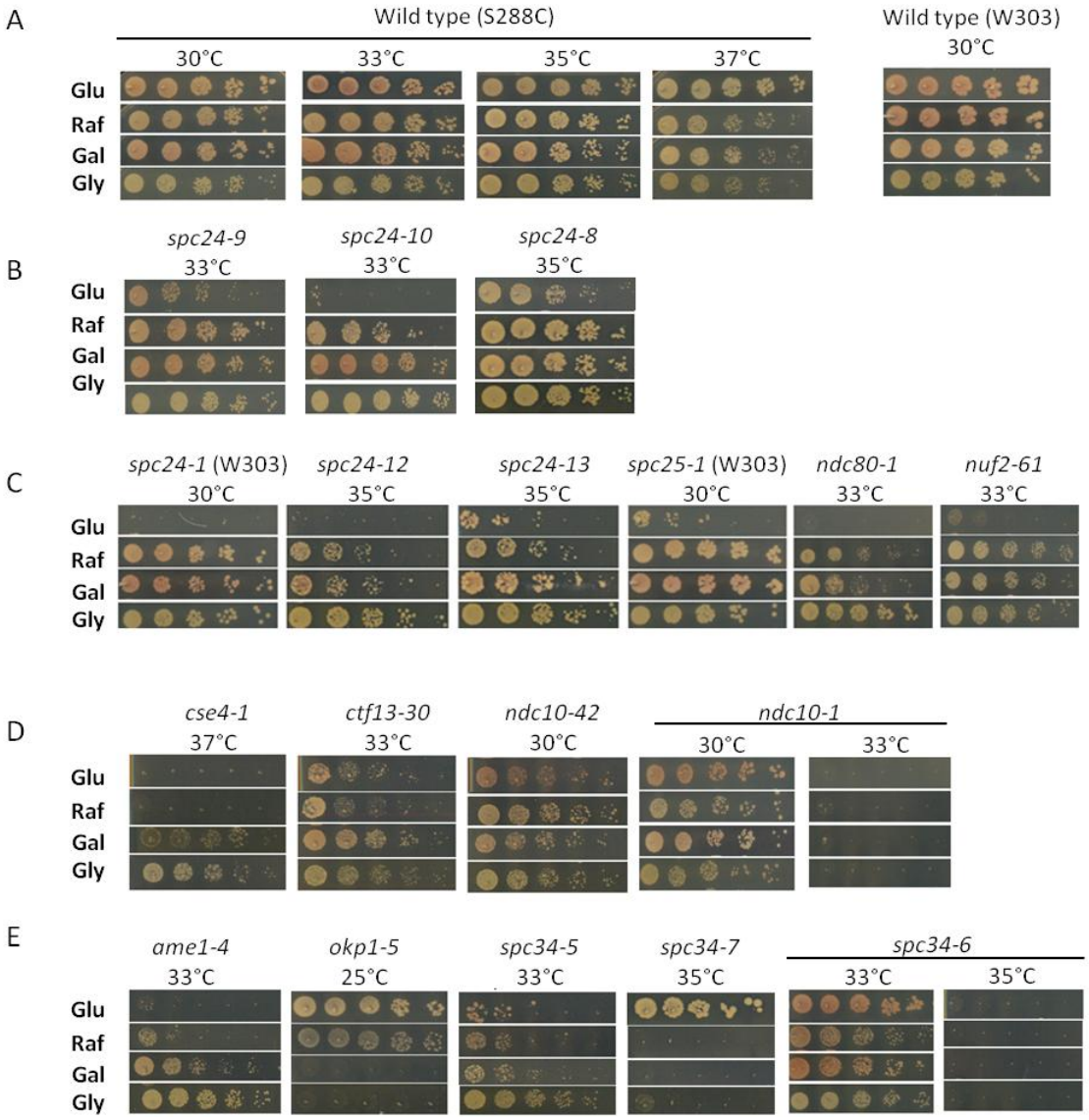

Figure 3.5 Cell dilution assay of kinetochore mutants on various carbon sources

Cell dilution assay of indicated strains on YP plus 2% of either glucose, raffinose, galactose or glycerol. Plates were incubated at the indicated temperature for 3 days.

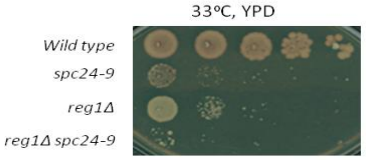

Figure 3.6 Cell dilution assay of indicated strains grown on YPD for 3 days

Chapter 4 Identification of Actin Defects in Kinetochore Mutants in the Budding Yeast *S. cerevisiae*

4.1 Introduction

The unicellular yeast *Saccharomyces cerevisiae* is a good model for the establishment of cell polarity. Yeast cells grow by budding, which requires recognizing a specific site of the mother cell cortex and polarizing many cellular components towards this site to promote bud growth. Figure 4.1 shows the establishment of the cell polarity throughout the cell cycle. Many proteins concentrate in the incipient bud site to form the polarity cap and facilitate bud emergence and growing. Actin patches concentrate around the polarity cap and actin cables align along the mother-bud axis towards the bud tip. Myosin motors (Myo2p and Myo4p) walk along the cables towards the polarity cap transporting various cargoes including secretory vesicles to support bud growth, the plus ends of cytoplasmic microtubules to position the nucleus for nuclear division, organelles for the daughter cell and RNA-protein complexes to provide daughter cell-specific proteins (Figure 4.2).

A cytoskeletal filament ring composed of septin proteins surrounds the polarity cap. The septins are a conserved family of GTP binding proteins that include Cdc3, Cdc10, Cdc11, Cdc12 and Shs1/Sep7 in the budding yeast. Septins assemble into filaments in a cell cycle regulated pattern (Figure 4.3). In G1 phase, septins are recruited to the incipient bud site and form a ring

in a fluid state. After bud emergence, septin rings are stabilized and expand like an hourglass at the bud neck. At the onset of cytokinesis, the hourglass shaped septin collar splits into two rings on mother and bud sides flanked by the actomyosin contractile ring. The septin ring is disassembled and degraded after cell separation. The filament ring/collar of septins at the bud neck is a scaffold that recruits various proteins important for cytokinesis, the morphogenesis checkpoint, the spindle assembly checkpoint and bud-site selection. Additionally, the septins act as diffusion barriers to compartmentalize the mother and daughter cells (see reviews in Kinoshita, 2006 and Douglas, *et al*., 2005).

Filamentous actin in budding yeast has three different structures: patches, cables and rings (Figure 4.4A). Actin patches undergo rapid turnover and mediate endocytosis and exocytosis, whereas actin cables function as polarized tracks that deliver cargo to build the daughter cell. Patches are formed by Arp2/3-dependent actin nucleation, whereas cables are assembled by the actin nucleating activity of the formins (Bnr1 and Bni1) and profilin. Prior to anaphase, actin cables are assembled at two locations, the bud tip (where Bni1 localizes) and the bud neck (where Bnr1 localizes). At anaphase, Bni1, Bud6 and other components of the polarity cap abruptly relocalize from the bud tip to the bud neck. Consequently, actin cables are reorganized to polarize towards the bud neck and direct all secretion to the division plane. The actomyosin contractile ring forms in cytokinesis and constricts in a Myo1-dependent manner to help close the neck (see review in Moseley, *et al*., 2006).

The Rho-family Cdc42 GTPase is essential for polarity establishment and plays a key

role in actin organization and septin assembly (see review in Park, *et al*., 2007). Cdc42 localizes to the plasma membrane and the sites of polarized growth, to the incipient bud site in G1 cells, the tips of growing buds in S/G2/M cells, and to the bud neck in anaphase and telophase cells (Figure 4.4B). The Cdc42 effectors Ste20p, Cla4p, Gic1p and Gic2p, and the scaffold proteins Bem1, Boi1 and Boi2 act together with Cdc42 and its GDP-GTP exchange factor (GEF) Cdc24 to establish polarity (Park, *et al*., 2007). The formins Bni1 and Bnr1 are another set of downstream effecters of Cdc42 for the assembly of actin cables (Evangelista, *et al*., 2002; Pruyne, *et al*., 2002; Sagot, *et al*., 2002a; Sagot, *et al*., 2002b) and the actomyosin ring (Tolliday, *et al*., 2002). The two formins partially overlap in their localization at the bud tip and the bud neck (Figure 4.4B), and in their functions in the assembly of actin cables and the actomyosin ring. Bni1 is one of the components of the 12S polarisome which is required for apical growth. The polarisome also includes Spa2, Pea2 and Bud6, which all localize in a similar manner to Bni1 (Tcheperegine, *et al*., 2005;van Drogen & Peter, 2002). Bud6 stimulates the activity of Bni1 to promote actin organization, and Bud6 and Bni1 are both suggested to have roles in spindle orientation and organization of the endoplasmic reticulum at the bud neck (Moseley & Goode, 2005).

Bud growth in budding yeast is divided into two phases, apical growth and isotropic growth. Apical bud growth occurs in G1 and is restricted to the tip of the bud. Upon entry into mitosis, buds switch to isotropic growth, in which the bud continues growing but growth is no longer restricted to the tip and instead growth occurs uniformly throughout the entire bud surface

(Lew & Reed, 1995). One checkpoint related to apical versus isotropic growth is the Swe1 dependent morphology checkpoint (Figure 4.5). In response to depolarization of the actin and/or a delay in bud emergence, the Swe1 kinase stalls the cell cycle in G2/M with an apical bud shape by inactivating the cyclin-dependent kinase (CDK) Cdc28 until the cell has recovered from the stress (see review in Keaton, *et al*., 2006). This morphogenesis checkpoint pathway starts with septin reorganization from a ring to an hourglass shaped collar during bud emergence. Subsequently, a septin-binding protein kinase, Hsl1, is activated to recruit an adaptor protein Hsl7, which brings Swe1 to the septins at the bud neck to undergo degradation. As a result of Swe1 degradation, Cdc28 is activated and cells enter mitosis with spindle elongation and isotropic bud growth (Lee, *et al*., 2005). Stresses that delay bud formation prevent Swe1 recruitment to the bud neck and block Swe1 degradation which results in mitotic delay. Even after a bud has formed and Hsl1 is active, a Swe1-dependent cell cycle arrest can be triggered by actin depolarization (McNulty & Lew, 2005).

The CBF3 inner kinetochore has been reported to have a novel role in regulating septin assembly and cell polarity (Gillis, *et al*., 2005) independently of its kinetochore function. Gillis *et al*. described a delay in septin ring separation and disassembly and a defect in actin polarization upon inhibiting CBF3 assembly. However, no septin defects were detected in central or outer kinetochore mutants. Interestingly, I have found that *spc24* mutant cells have actin defects. In addition, *spc24* alleles have multiple genetic interactions with actin, formin, and *cdc42* mutants and overexpression of the Cdc42 effector, *GIC1* rescues *spc24-9* temperature

sensitivity.

4.2 Materials and methods

4.2.1 Strains, plasmids and microbial techniques

Yeast strains and plasmids used in this study are described in Table 4.1. The *CEN* plasmid containing the *CDC3* promoter followed by the full length *CDC3* ORF was a gift from John Pringle's lab. The *CEN* plasmid containing the GFP tag followed by the full length *BUD6* ORF was a gift from Charlie Boone's lab. The 2μ plasmid containing the full length *GIC1* ORF and its own promoter was isolated from the work in Chapter 2 (Ma, *et al*., 2007). All the GFP tagging was performed by PCR-based homologous recombination (Longtine, *et al*., 1998). The liquid media used was either rich medium (YPD) or supplemental minimal medium (SC) (Kaiser, *et al*., 1994). For spot assays, fivefold serial dilutions were spotted on YPD (2% glucose) plates and grown at 30℃ for 2 days. To assay latrunculin A (Lat A) sensitivity, Lat A was added at the indicated concentration onto the paper discs that had been placed on the YPD plates. Dimethyl sulfoxide was used in the control spot (0 μg/ml Lat A). Flow cytometry analysis to monitor DNA content was performed as previously described (Haase, *et al*., 1997).

4.2.2 Timecourse and western blot

Cells were grown to early-logarithmic phase in 150 ml of liquid YPD at 25℃, arrested with 5ug/ml α-mating factor (BioVectra, Charlottetown, Prince Edward Island, Canada) for 2 hours at

25℃, resuspended with 37℃ prewarmed fresh liquid YPD and shifted to 37℃. 10ml of culture was collected for each indicated time point and the cell pellet was lysed using glass beads. Western blot analysis was performed using standard procedures. A mouse monoclonal antibody specific for the MYC epitope (anti-c-MYC) was purchased from Roche Diagnostics Canada (Laval, QB) and used at a 1:5000 dilution.

4.2.3 Fluorescence Microscopy

For actin staining, cells were fixed with SC containing 4% formaldehyde for 1 hour, washed with PBS three times, resuspended in 100ul PBS plus 10ul Rhodamine Phalloidin (6.6μM in MeOH) (Molecular Probes Inc.), incubated in the dark at 4°C overnight, washed and resuspended with PBS, and 1-2μl placed on slides for imaging. Cells were imaged at room temperature using a fluorescence microscope (Axioplan 2; Carl Zeiss MicroImaging, Inc.) with a plan-Apochromat 63× NA 1.4 differential interference contrast oil immersion objective (Carl Zeiss MicroImaging, Inc.) with filter sets 38 for GFP and filter set 45 for Rhodamine Phalloidin (Carl Zeiss MicroImaging, Inc.). 3D images (0.2-μm steps) were acquired with a camera (CoolSNAP HQ; Roper Scientific) and analyzed using MetaMorph software (Invitrogen). Images are presented as maximum intensity 2D projections.

4.3 Results

4.3.1 Morphology defects of *spc24-9*

spc24-9 arrests with 2N DNA content (Figure 4.6D) and large budded G2 cells at the non-permissive temperature of 37℃ and ~12% of mutant cells have elongated buds when incubated at 37℃ for 4hrs (Figure 4.6A). Bud elongation is a characteristic morphological phenotype of cells with stabilized Swe1. Upon the activation of the Swe1-dependent morphology checkpoint, Swe1 is stabilized and the switch from apical to isotropic growth is blocked, resulting in bud elongation. Therefore, I tested if the Swe1 dependent morphology checkpoint is activated in *spc24-9* by performing a time course with synchronized cells. Wild type and *spc24-9* cells were arrested in G1 phase at 25^{o}C with mating pheromone, then released from the arrest into 37^{o}C and samples taken every 10 min for a total of 150 min. Western blot analysis was performed to compare the protein expression levels of Swe1-MYC in wild type versus *spc24-9* cells. As shown in Figure 4.6B, after G1 release, Swe1 levels in wild type cells peak at 60~70min followed by Swe1 degradation and the second peak of Swe1 expression occurs at 100 min followed by degradation at 130min (Figure 4.6B). However, in *spc24-9* cells Swe1 levels first peaked at 100min, a 30min-delay compared to the wild type, and Swe1 was stabilized with high levels after 100min, indicative of activation of the morphology checkpoint (Figure 4.6B).

Next, I tested whether Swe1 accumulation is the consequence of the morphology defects of *spc24-9* with *spc24-9 swe1*Δ double mutants. Even though the elongated bud morphology is

partially rescued by the absence of Swe1 (Figure 4.6C), cells still accumulate with a 2N content of DNA in *spc24-9 swe1*Δ strains at 37^{o}C (Figure 4.6D), and the temperature sensitivity (ts) of *spc24-9* is not suppressed by *swe1*Δ at 33^{o}C (Figure 4.6E). The above observations indicate that the poor viability of *spc24-9* at the restrictive temperature is not solely due to a Swe1-dependent G2 block.

4.3.2 *spc24* mutants have actin defects

Actin defects might contribute to the unsuccessful apical/isotropic switch in the *spc24-9* mutant that leads to the elongated bud morphology. Therefore, I studied actin in *spc24-9* versus wild type cells by staining with rhodamine phalloidin after growing cells at 37 ℃ for 3 hrs (Figure 4.7). In the wild type cells with medium to large buds, the actin patches are concentrated in the daughter cell, whereas in *spc24-9* cells with similar bud sizes, more actin patches are present in the mother cell (Figure 4.7A, yellow arrows). The distribution of actin patches to the *spc24-9* mother cell might suggest a defect of the septin diffusion barrier at the bud neck (see Figure 4.4). Additionally, the actin patches fail to accumulate at the bud neck and no actin rings are visible in *spc24-9* cells with large buds (Figure 4.7A, light blue arrows, compare wild type to *spc24-9*). The actin localization analysis suggests that *spc24-9* mutants might have defects in actin ring formation, formin and/or Bud6 function since all of these factors are required for the assembly of the actin cables and rings at the bud neck. To address these possibilities, I studied the localization of Bni1, Bnr1 and Bud6 fused to a C-terminal GFP tag in

spc24-9 versus wild type cells. While no dramatic localization defects were detected for Bni1 and Bnr1 in *spc24-9* (data not shown), Bud6 is mislocalized in the mutant upon shifting to 37℃ (Figure 4.7B). During a normal cell cycle in wild type cells, Bud6 localizes to the prebud site at START, to the bud cortex while the bud is growing and accumulates at the bud neck upon entry into mitosis where it remains for the rest of the cell cycle (Segal, *et al*., 2000) (Figure 4.7B, upper panel). When *spc24-9* cells were incubated at 37℃ for 3 hrs, Bud6 is either randomly scattered within the cell or does not form the rings at the mother-bud neck in large budded cells (24% in *spc24-9* versus 6% in wild type) (Figure 4.7 B, C). Additionally, *bud6*Δ has synthetic growth defect with *spc24-9* (Figure 4.7D), indicative of a genetic interaction between *BUD6* and *SPC24*. To determine if there is any interaction between the Ndc80 complex and Bud6, I performed a co-immunoprecipitation with a Ndc80-13MYC Bud6-GFP strain, but no direct interaction was detected (data not shown). Therefore, the mislocalization of Bud6 in *spc24-9* might be induced by the defects of the cytoskeleton or septin scaffold in *spc24-9* cells but not due to defects in physical interaction with the Ndc80 complex.

The lack of visible actin rings in *spc24-9* cells compared to the wild type cells may be because the *spc24-9* cells arrest prior to actin ring formation. Actin ring formation occurs when Cyk1, a protein playing an essential and specific role in cytokinesis, is recruited to the bud neck during late anaphase (Lippincott, *et al*., 1998). To distinguish between defects in actin ring formation and *spc24-9* cell cycle arrest, I blocked cell entry into mitosis by repressing expression of Cdc20. Cdc20 is an activator of the anaphase-promoting complex/cyclosome (APC/C) and

mediates the proteolysis of securin (Pds1). Degradation of Pds1 allows the Esp1 separase (Esp1) to cleave the Scc1 cohesin subunit and initiate sister chromatid separation. Inhibition of Cdc20 leads to cell cycle arrest in metaphase due to stabilization of Pds1. In order to regulate *CDC20* expression, a *GAL1-CDC20* strain was created whereby growth on galactose enables expression of *CDC20* and growth on glucose turns off *CDC20* expression (Hwang, *et al*., 1998). I mated the *GAL1-CDC20* strain with *spc24*-9, *spc24-8* and *spc24-10* mutants and isolated meiotic recombinants that contained both the *spc24* mutation and *GAL1-CDC20*. The strains were grown in galactose, arrested in metaphase with glucose treatment and released into mitosis with galactose at 37^{o}C. As shown in Figure 4.8 when released from a metaphase block to restrictive temperature, none of the three *spc24* alleles have defects in actin ring formation. Therefore, the lack of actin rings in *spc24-9* cells (Figure 4.7A) is likely due to the stage of the cell cycle arrest and not due to a specific defect in actin ring assembly.

4.3.3 Septin localization in mutants of the Ndc80 complex

Septins are a family of conserved proteins that assemble into filaments at the site of bud growth and are membrane associated scaffolds important for separating the mother/bud compartments and cytokinesis. Gillis *et al*. studied the *ndc80-1*, *spc25-7* and *dam1-1* outer kinetochore mutants and found that none of them had septin defects (Gillis, *et al*., 2005). Since *ndc80-1* and *spc25-7* might have different defects than our *spc24* mutants, and I have shown that *spc24-9* has more actin patches in the mother cell and mislocalized Bud6 (see 4.3.2), I analyzed

septin localization in our *spc24* mutants. I constructed both Cdc10-GFP and Cdc12-GFP endogenously tagged strains but the Cdc12-GFP strain grew slowly at 33℃ and both strains had a filamentous phenotype suggesting that the C-terminal GFP tag interfered with septin function. Therefore, I transformed the *GFP-CDC3* plasmid (gift from Brenda Andrews) into the *spc24-8, spc24-9, spc24-10* mutants plus another two alleles of the Ndc80 complex, *spc25-1* and *nuf2-61*, to study septin localization. I found that none of these mutants have septin defects upon shifting to 37℃ (data not shown). However, when I looked at *spc25-1* mutants in another strain background (W303) , 70% of *spc25-1* cells were not able to form septin rings after incubation at restrictive temperature for 3 hours, suggesting that defects in kinetochore function dramatically affect septin localization in the W303 strain background but not our lab strain background (S288C) (Figure 4.9). Interestingly, *spc24-9* is synthetically lethal when combined with the septin mutant *cdc12-1* at 30℃ (Figure 4.9D), suggesting that *spc24-9* might have subtle septin defects. I did not analyze dynamic septin defects in *spc24* mutants because the cells were fixed before imaging. Therefore, septin defects may be revealed in *spc24-9* cells by performing live imaging.

4.3.4 *spc24* alleles might have more actin patches

During the analysis of actin ring formation using a *GAL-CDC20* block/release method (described in 4.3.2), I also analyzed actin by staining large budded cells with Rhodamine Phalloidin. As shown in Figure 4.10B, 40min after release from arrest due to Cdc20 depletion,

wild type cells have actin patches mostly around the cell cortex, but *spc24-8* and *spc24-9* cells have more actin patches throughout the cell, which is consistent with the scattered actin patches in *spc24-9* shown in Figure 4.7A. Since brighter or even chunky actin patches are associated with defects of actin turnover (Lappalainen, *et al*., 1997), I speculated that the actin patches in *spc24* cells might not undergo rapid turnover.

Studying the cell sensitivity to Latrunculin A (Lat A), an actin sequestering drug (Ayscough, *et al*., 1997), is a method for evaluating the stability of the actin cytoskeleton. The double mutant *tpm1-2 tpm2*Δ, which has mutations in two isoforms of the tropomyosin (Tpm) actin cable components (Pruyne, *et al.*, 1998), is sensitive to Lat A due to the defects in actin polymerization (Figure 4.10C). Since *spc24-8, spc24-9* and *spc24-10* mutants may have stabilized actin structures, I expected the Lat A halo to be reduced in size compared to the wild type. However, no dramatic difference was detected between the halo size of *spc24 mutants* and the wild type (Figure 4.10D), probably because the actin defects in *spc24* cells at 33℃ are not as dramatic as 37℃, or the Lat A concentration is too high to visualize the difference.

4.3.5 Genetic interactions between *spc24* alleles and actin mutants

To further confirm the interaction between *spc24* alleles and actin, I crossed *spc24-8* and *spc24-9* strains into a series of actin mutants, generated double mutants and analyzed their growth by spot assay (Figure 4.11). The actin mutants used for these genetic interaction studies are *pfy1-111*, a ts allele of the *PFY1* profilin gene (Haarer, *et al*., 1993), *cof1-5* and *cof1-22*, both

ts alleles of the *COF1* cofilin gene, and a null mutation of the *TWF1* twinfilin gene. Cof1 and Twf1 are both actin filament severing proteins and facilitate actin cable turnover (Moseley, *et al*., 2006). Although the activity of profilin remains unclear, it is proposed to have a function in accelerating actin turnover (Moseley, *et al*., 2006). As shown in Figure 4.11A, *cof1-5* and *cof1-22*, which both have more actin patches compared to wild type (Lappalainen, *et al*., 1997), have a severe synthetic growth phenotype when combined with *spc24-9* or *spc24-8* mutants. Additionally, *spc24* mutants are synthetic sick with *pfy1-111* (impaired in binding actin (Haarer, *et al*., 1996)). The genetic interactions between *cof1, pfy1-111* and *spc24* are consistent with the hypothesis that *spc24* mutants have actin turnover defects (described in 4.3.4). Surprisingly, *twf1*Δ, which causes reduced rates of actin patch turnover (Moseley, *et al*., 2006), suppresses the ts of *spc24-9* at 33 ℃ and *spc24-8* at 35 ℃ (Figure 4.11B).

4.3.6 Formin mutants rescue the ts of *spc24* alleles

In budding yeast, formins are required for actin cable nucleation. Since *spc24* mutants have more actin patches, I was curious to determine if there are also actin cable defects in these mutants. If *spc24* mutants have more stabilized actin cables, they might be rescued by compromising the nucleation function of formins. *bni1-11* has two amino acid mutations (D1511G, K1601R) in the second formin-homology domain (FH2) which is thought to have an essential role in actin cable nucleation (Figure 4.12A) (Evangelista, *et al*., 2002). I crossed *spc24* alleles with *bnr1*Δ, *bni1*Δ and the *bni1-11* ts allele and generated double mutant strains.

spc24-10 does not have a dramatic growth phenotype when combined with any of the three formin alleles, however both *spc24-8* and *spc24-9* were rescued by *bnr1*Δ and *bni1-11* (Figure 4.12B), suggesting *spc24* mutants might have excess actin filaments. Interestingly, the ts of *spc24* mutants were not rescued by *bni1*Δ (Figue 4.12B). Since Bni1 but not Bnr1 plays an additional role in microtubule dependent nuclear migration through its Rho-binding domain (RBD) (Fujiwara, *et al*., 1999), I speculate that *bni1*Δ does not rescue *spc24* due to the defects of the Bni1 in nuclear migration.

4.3.7 Hyperactivation of Cdc42 pathway might rescue the ts of *spc24-9*

The Cdc42 GTPase is the key component in polarity establishment. Since *spc24-9* is rescued by formin mutants and the formins are major targets of Cdc42 in actin cable nucleation, I determined the phenotype of combining a *cdc42* mutant with the *spc24-9* mutant. *cdc42-117* has mutations in the GTPase activation protein (GAP) binding domain (Figure 4.13A), suggesting that *cdc42-117* may fail to interact with one of its GAPs and thus be in a hyperactivated state (Kozminski, *et al*., 2000). I found that *cdc42-117* is synthetic lethal with *spc24-9* (Figure 4.13B), suggesting that the actin defects of *spc24-9* might be induced by hyperactivation of the cellular polarization signal transduction pathway.

Gic1 and Gic2, two effectors of Cdc42, were first identified as homologs with redundant functions in cell polarization (Brown, *et al*., 1997), septin recruitment (Iwase, *et al*., 2006) and mitotic exit (Höfken, *et al*., 2004). Even though no distinct function of Gic1 or Gic2 has been

reported, Gic1 is well-known to be stable throughout the cell cycle (Chen, *et al*., 1997), whereas Gic2 is partially degraded upon bud emergence probably to restrict cytoskeleton polarization and thereby contribute to efficient bud emergence (Jaquenoud, *et al*., 1998). Since Gic1 and Gic2 play positive roles in Cdc42 signal transduction pathway (Chan, *et al*., 1997) and the hyperactive allele *cdc42-117* is synthetic sick with *spc24-9*, I tested if deletion of Gic proteins would rescue the ts of *spc24-9* mutants. As showed in Figure 4.13C, *gic2*Δ and *gic1*Δ *gic2*Δ double mutant, but not *gic1*Δ, rescues *spc24-9* at 33℃. Since Gic2 is involved in recruiting Bud6 and Bni1 to activated Cdc42 to facilitate actin polarization (Jaquenoud, *et al*., 2000), the rescue of *spc24-9* mutants by deletion of *GIC2* perhaps occurs due to the downregulation Cdc42 signaling or a decrease in efficiency of actin nucleation. *gic1*Δ does not rescue *spc24-9* mutants probably because the adapter function linking Cdc42 and actin nucleation is specific to Gic2 but not Gic1. Interestingly, overexpressing *GIC1* suppresses the ts of *spc24-9* at 33℃ (Figure 4.13D), suggesting overproducing *GIC1* might antagonize the adapter function of Gic2.

4.4 Discussion

Swe1 protein accumulation is periodic during the cell cycle, rising at the time of bud emergence and declining before nuclear division (McMillan, *et al*., 1998), so that Clb2-Cdc28 can be activated to initiate mitosis. When *spc24*-9 cells are synchronized in G1 phase with mating pheromone and released to restrictive temperature of 37℃, cells are arrested in G2 with 2N DNA content and Swe1 is not degraded after its appearance at 100min, (Figure 4. 6B),

suggesting that the Swe1-dependent morphology checkpoint is activated. The activation of the morphology checkpoint, and subsequence defects in Swe1 degradation, inhibits isotropic bud growth and induces an abnormal elongated bud morphology. However, elongated bud growth is not a major defect in *spc24-9* mutants (only ~12% cells), possibly because our S288C strain background does not tend to display highly elongated buds compared to other *S. cerevisiae* strain backgrounds (Enserink, *et al.,* 2006). Nevertheless, the minor defects in morphology of bud elongation in *spc24-9* is suppressed by *swe1*Δ (Figure 4.6C). However, *swe1*Δ does not suppress either the G2 arrest or the ts of *spc24-9* (Figure 4.6D, E), suggesting the activation of the morphology checkpoint is not the only reason for the inviability of *spc24-9* at the non-permissive temperature. Interestingly, before 90min in Figure 4.6D, the cell cycle progression in *spc24-9* is similar to the wild type, as indicated by the DNA content, but the abundance of Swe1 is lower in *spc24-9* than the wild type for all the indicated timepoints (0~90min) (Figure 4.6B), suggesting a delay of Swe1 expression in *spc24-9*. One possibility is that *SWE1* is transcribed during S-phase, and *spc24-9* cells have defects at S-phase (see Chapter 2), which compromises the transcription of *SWE1*. Alternatively, Spc24 or Ndc80 complex might be required for the expression of Swe1 during normal cell cycle.

The following data presented in this chapter suggest that *spc24* cells might have defects in actin turnover: (1) *spc24* cells have brighter, or bigger actin patches thoughout the cell; (2) *spc24* mutants are synthetic sick with *cof1* mutants which have more stable actin structures; (3) the ts of *spc24* cells is suppressed by compromising the actin nucleation functions of formins.

However, the fact that *spc24-9* ts growth is suppressed by *twf1*Δ (Figure 4.10B) conflicts with the above conclusion. As stated above, Twf1 is an actin filament severing protein that facilitates actin cable turnover (Goode, *et al*., 1998; Moseley, *et al*., 2006). The defects in actin turnover in *twf1*Δ mutants are not nearly as severe as *cof1-22* mutants (Moseley, *et al*., 2006). Perhaps having highly stabilized actin structures is lethal for *spc24* mutants as suggested by the synthetic lethality of *spc24 cof1-22* double mutants, however slightly stabilized actin is beneficial for *spc24*, as suggested by the *twf1 spc24* rescue. The lack of LatA sensitivity suggests that *spc24* mutants do not have a deficiency in the organization of actin cytoskeleton.

Activation of Cdc42 by its exchange factor Cdc24 is required to organize the actin cytoskeleton and establish cell polarity. Since the viability of *spc24-9* is severely compromised when combined with the *cdc42-117* dominant allele (Kozminski, *et al*., 2000), *spc24-9* might have a highly activated Cdc42 signaling cascade, which is consistent with the data that depleting the downstream effectors of Cdc42, such as *bni1-11*, *bnr1*Δ and *gic2*Δ, suppresses the ts of *spc24-9*.

Why a nuclear kinetochore protein has genetic interactions with the actin cytoskeleton and cytoplasmic/cell cortex elements is still mysterious. I have detected a minor pool of Ndc80 in the cytoplasm, likely at the plus end of cytoplasmic microtubules or in the vicinity of cell cortex (see Appendix 2). Therefore, the cytoplasmic pool of Ndc80 might be able to mediate the crosstalk between kinetochore and the cell cortex, possibly at the polarity cap. Alternatively, mutation of the nuclear Ndc80 complex might affect a transcription factor and cause defects in

expression of genes involved in polarity establishment or actin dynamics. Future work will distinguish between a direct role for the Ndc80 complex in regulating actin dynamics versus an indirect role in regulating transcription of polarity genes.

Table 4.1 List of strains

Strain	Genotype	Reference
YVM1370	*MATa ura3-52, lys2-801, ade2-101, his3Δ200, leu2Δ1,trp1Δ63 SPC24::kanMX6*	Montpetit *et al*. (2005)
YVM1380	*MATa ura3-52, lys2-801, ade2-101, his3Δ200, leu2Δ1,trp1Δ63 spc24-9::kanMX6*	Montpetit *et al*. (2005)
YVM1448	*MATa ura3-52, lys2-801, ade2-101, his3Δ200, leu2Δ1,trp1Δ63 spc24-8::kanMX6*	Montpetit *et al*. (2005)
YVM1363	*MATa ura3-52, lys2-801, ade2-101, his3Δ200, leu2Δ1,trp1Δ63 spc24-10::kanMX6*	Montpetit *et al*. (2005)
YLM1165	*MATa ura3-52, lys2-801, ade2-101, his3Δ200, leu2Δ1,trp1Δ63 SWE1-13MYC::HIS3*	This study
YLM1166	*MATa ura3-52, lys2-801, ade2-101, his3Δ200, leu2Δ1,trp1Δ63 SWE1-13MYC::HIS3 spc24-9::kanMX6*	This study
YJM125	*MATa ura3-52, lys2-801, ade2-101, his3Δ200, leu2Δ1,trp1Δ63 swe1Δ::LEU2*	Measday lab
YLM1133	*MATa ura3-52, lys2-801, ade2-101, his3Δ200, leu2Δ1,trp1Δ63 swe1Δ::LEU2 spc24-9::kanMX6*	This study
YJM79	*MATa ura3-52, lys2-801, ade2-101, his3Δ200, leu2Δ1,trp1Δ63 hsl1Δ::HIS3*	Measday lab
YJM121	*MATa ura3-52, lys2-801, ade2-101, his3Δ200, leu2Δ1,trp1Δ63 hsl1Δ::HIS3 swe1Δ::LEU2*	Measday lab
YLM1131	*MATa ura3-52, lys2-801, ade2-101, his3Δ200, leu2Δ1,trp1Δ63 hsl1Δ::HIS3 spc24-9::kanMX6*	This study
YLM1129	*MATa ura3-52, lys2-801, ade2-101, his3Δ200, leu2Δ1,trp1Δ63 swe1Δ::LEU2 hsl1Δ::HIS3 spc24-9::kanMX6*	This study
YJM87	*MATa ura3-52, lys2-801, ade2-101, his3Δ200, leu2Δ1,trp1Δ63 hsl7Δ::HIS3*	Measday lab
YJM134	*MATα ura3-52, lys2-801, ade2-101, his3Δ200, leu2Δ1,trp1Δ63 hsl7Δ::HIS3 swe1Δ::LEU2*	Measday lab
YLM1135	*MATa ura3-52, lys2-801, ade2-101, his3Δ200, leu2Δ1,trp1Δ63 hsl7Δ::HIS3 spc24-9::kanMX6*	This study
YLM1137	*MATa ura3-52, lys2-801, ade2-101, his3Δ200, leu2Δ1,trp1Δ63 swe1Δ::LEU2hsl7Δ::HIS3 spc24-9::kanMX6*	This study

(To be continued)

Table 4.1 List of strains (Continued)

Strain	Genotype	Reference
ABY944	*MATa his3Δ-200 leu2-3,112 lys2-801 trp1-1 ura3-52 tpm1-2::LEU2 tpm2::HIS3*	This study
BHY46	*MATa ura3 his3 leu2 ade2 ade3 pfy1-111::LEU2*	Haarer *et al.* (1993)
YLM1424	*MATa ura3 his3 leu2 ade2 ade3/ura3-52, lys2-801, ade2-101, his3Δ200, leu2Δ1,trp1Δ63 pfy1-111::LEU2spc24-8::KanMX6*	This study
YLM1414	*MATa ura3 his3 leu2 ade2 ade3/ura3-52, lys2-801, ade2-101, his3Δ200, leu2Δ1,trp1Δ63 pfy1-111::LEU2spc24-9::KanMX6*	This study
DDY1254	*MATα ura3-52, his3Δ200, leu2-3,112, lys2-801 cof1-5::LEU2*	Lappalainen *et al*. (1997)
DDY1266	*MATα ura3-52, his3Δ200, leu2-3,112, lys2-801 cof1-22:LEU2*	Lappalainen *et al*. (1997)
YLM1485	*MATa ura3-52, his3Δ200, leu2-3,112, lys2-801/his3-Δ200 ade2-101 ura3-52 lys2-801 leu2-Δ1 trp1-Δ63 cof1-5::LEU2 spc24-9::KanMX6*	This study
YLM1481	*MATa ura3-52, his3Δ200, leu2-3,112, lys2-801/his3-Δ200 ade2-101 ura3-52 lys2-801 leu2-Δ1 trp1-Δ63 cof1-5::LEU2 spc24-8::KanMX6*	This study
YLM1497	*MATa ura3-52, his3Δ200, leu2-3,112, lys2-801/his3-Δ200 ade2-101 ura3-52 lys2-801 leu2-Δ1 trp1-Δ63 cof1-22::LEU2 spc24-9::KanMX6*	This study
YLM1493	*MATa ura3-52, his3Δ200, leu2-3,112, lys2-801/his3-Δ200 ade2-101 ura3-52 lys2-801 leu2-Δ1 trp1-Δ63 cof1-22::LEU2 spc24-8::KanMX6*	This study
DDY1434	*MATa ade2-1, his3200, leu2-3,112, ura3-52 twf1::URA3*	Goode *et al*. (1998)
YLM1473	*MATa ade2-1, his3-Δ200, leu2-3,112, ura3-52/his3-Δ200 ade2-101 ura3-52 lys2-801 leu2-Δ1 trp1-Δ63 twf1::URA3 spc24-8::KanMX6*	This study
YLM1475	*MATa ade2-1, his3-Δ200, leu2-3,112, ura3-52/his3-Δ200 ade2-101 ura3-52 lys2-801 leu2-Δ1 trp1-Δ63 twf1::URA3 spc24-9::KanMX6*	This study
YLM1285	*MATa his3Δ1 met15Δ0 leu2Δ0 ura3Δ0/his3-Δ200 ade2-101 ura3-52 lys2-801 leu2-Δ1 trp1-Δ63 bni1::KanMX6*	This study

(To be continued)

Table 4.1 List of strains (Continued)

Strain	Genotype	Reference
YLM1289	*MATa his3Δ1 met15Δ0 leu2Δ0 ura3Δ0/his3-Δ200 ade2-101 ura3-52 lys2-801 leu2-Δ1 trp1-Δ63 bni1::KanMX6 spc24-8::KanMX6*	This study
YLM1314	*MATa his3Δ1 met15Δ0 leu2Δ0 ura3Δ0/his3-Δ200 ade2-101 ura3-52 lys2-801 leu2-Δ1 trp1-Δ63 bni1::KanMX6 spc24-9::KanMX6*	This study
YLM1217	*MATa his3Δ1 met15Δ0 leu2Δ0 ura3Δ0/his3-Δ200 ade2-101 ura3-52 lys2-801 leu2-Δ1 trp1-Δ63 bnr1::KanMX6*	This study
YLM1266	*MATa his3Δ1 met15Δ0 leu2Δ0 ura3Δ0/his3-Δ200 ade2-101 ura3-52 lys2-801 leu2-Δ1 trp1-Δ63 bnr1::KanMX6 spc24-8::KanMX6*	This study
YLM1268	*MATa his3Δ1 met15Δ0 leu2Δ0 ura3Δ0/his3-Δ200 ade2-101 ura3-52 lys2-801 leu2-Δ1 trp1-Δ63 bnr1::KanMX6 spc24-9::KanMX6*	This study
YLM1188	*MATa his3Δ1 met15Δ0 leu2Δ0 ura3Δ0/his3-Δ200 ade2-101 ura3-52 lys2-801 leu2-Δ1 trp1-Δ63 bni1-11::URA3*	This study
YLM1276	*MATa his3Δ1 met15Δ0 leu2Δ0 ura3Δ0/his3-Δ200 ade2-101 ura3-52 lys2-801 leu2-Δ1 trp1-Δ63 bni1-11::URA3 spc24-9::KanMX6*	This study
YLM1274	*MATa his3Δ1 met15Δ0 leu2Δ0 ura3Δ0/his3-Δ200 ade2-101 ura3-52 lys2-801 leu2-Δ1 trp1-Δ63 bni1-11::URA3 spc24-8::KanMX6*	This study
YLM1404	*MATa ura3-52, lys2-801, ade2-101, his3Δ200, leu2Δ1,trp1Δ63 gic2::ClonNAT*	This study
YLM1406	*MATa ura3-52, lys2-801, ade2-101, his3Δ200, leu2Δ1,trp1Δ63 gic1::TRP spc24-9::KanMX6*	This study
YLM1402	*MATa ura3-52, lys2-801, ade2-101, his3Δ200, leu2Δ1,trp1Δ63 gic2::ClonNAT spc24-9::KanMX6*	This study
YLM125	*MATa ura3-52, lys2-801, ade2-101, his3Δ200, leu2Δ1,trp1Δ63 gic1::TRP*	This study
YLM1408	*MATa ura3-52, lys2-801, ade2-101, his3Δ200, leu2Δ1,trp1Δ63 gic1::TRP gic2::ClonNAT*	This study
YLM1400	*MATa ura3-52, lys2-801, ade2-101, his3Δ200, leu2Δ1,trp1Δ63 gic1::TRP gic2::ClonNAT spc24-9::KanMX6*	This study

(To be continued)

Table 4.1 List of strains (Continued)

Strain	Genotype	Reference
DDY1324	*MATa his3-Δ200 ura3-52 lys2-801 leu2-Δ1 trp1-Δ63/ura3-52 leu2-3,112 his3Δ200 lys2-801am cdc42-117::LEU2*	Kozminski *et al*. (2000)
YLM1347	*MATa his3-Δ200 ura3-52 lys2-801 leu2-Δ1 trp1-Δ63/ura3-52 leu2-3,112 his3Δ200 lys2-801am cdc42-117::LEU2 spc24-9::KanMX6*	This study
YLM56	*MATa ade2-1 can1-100 his3-3-11,15 leu2-3,112 trp1-1 spc25-1*	Measday lab
YLM1381	*MATa his3-Δ200 ura3-52 lys2-801 leu2-Δ1 trp1-Δ63 ade2-101 spc25-1*	This study
YLM1424	*MATa ura3 his3 leu2 ade2 ade3/ura3-52, lys2-801, ade2-101, his3Δ200, leu2Δ1,trp1Δ63 pfy1-111::LEU2 spc24-8::KanMX6*	This study
YLM1414	*MATa ura3 his3 leu2 ade2 ade3/ura3-52, lys2-801, ade2-101, his3Δ200, leu2Δ1,trp1Δ63 pfy1-111::LEU2 spc24-9::KanMX6*	This study
YLM860	*MATa his3-Δ200 ura3-52 lys2-801 leu2-Δ1 trp1-Δ63 ade2-101 bud6::TRP1*	This study
YLM921	*MATa his3-Δ200 ura3-52 lys2-801 leu2-Δ1 trp1-Δ63 ade2-101 bud6::TRP1 spc24-9::KanMX6*	This study

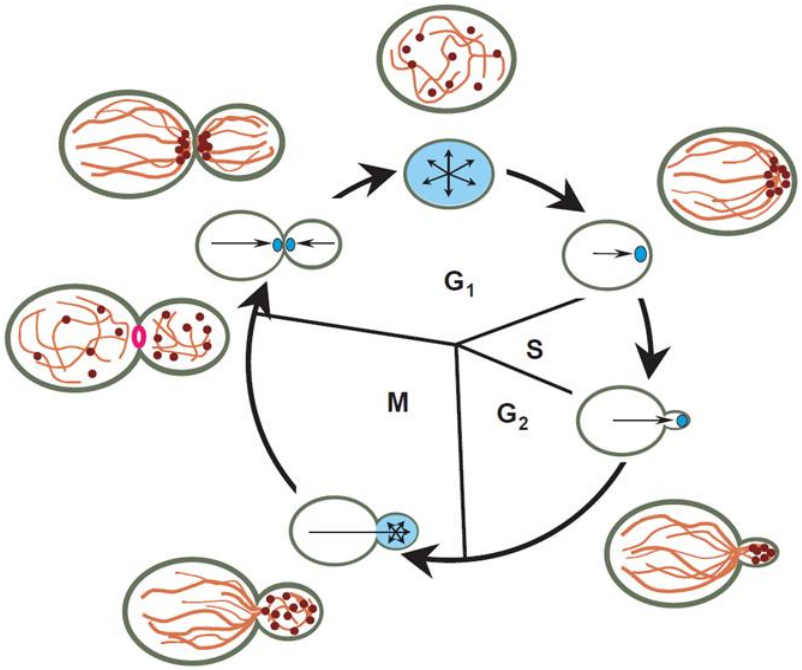

Figure 4.1 Cell polarity in budding yeast is established by a polarized actin cytoskeleton throughout the cell cycle

Cell polarity (arrows) is established by a cluster of regulatory and cytoskeletal proteins (blue). Brown: actin cables and actin patches. Pink: actin ring. (Cited from Pruyne D & Bretscher A. *J Cell Sci*. 2000, 113 (Pt 4):571-85, reproduced with permission of the Company of Biologists©)

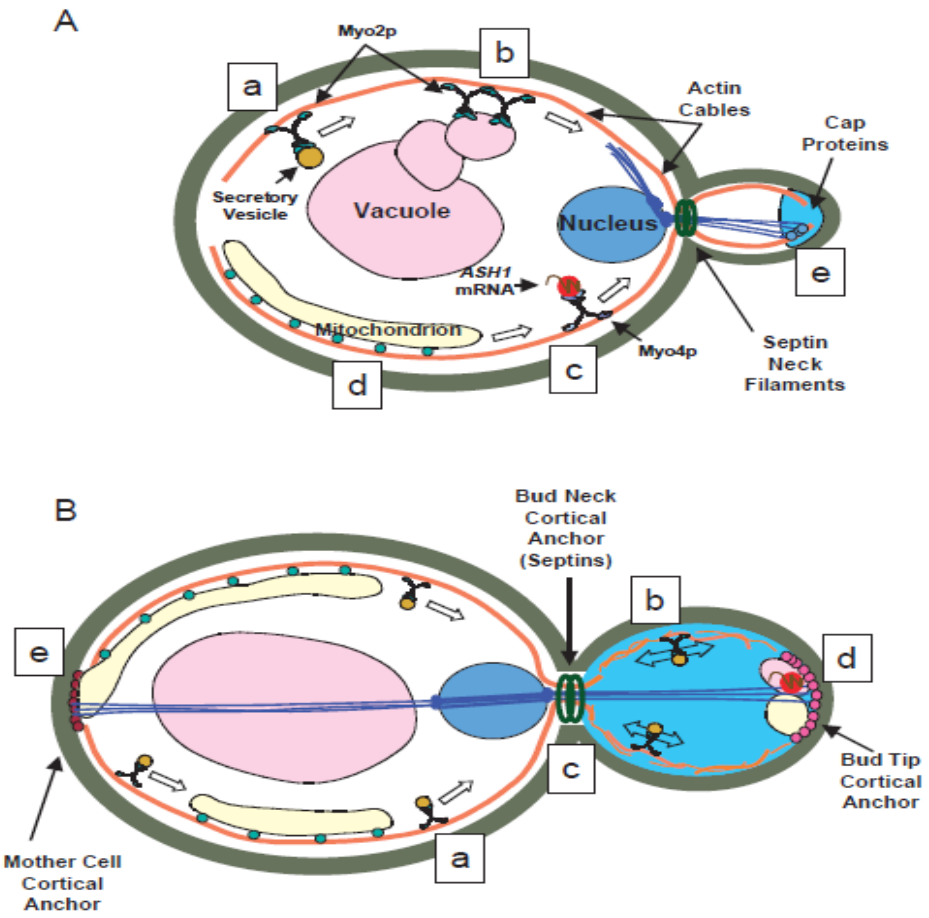

Figure 4.2 A variety of cellular components are polarized through interactions with actin cables and the cell cortex

(A) During early bud growth, Myo2p transports secretory vesicles (a) and vacuolar membranes (b) from the mother cell to the bud tip along actin cables. (c) Myo4p delivers mRNA encoding the transcriptional repressor Ash1p along cables. (d) Mitochondria migrate along actin cables by an unknown mechanism. (e) Cytoplasmic microtubules emanating from one spindle pole enter the bud and attach to the bud tip.

(B) During later bud growth, (a) Myo2p continues to deliver secretory vesicles into the bud along actin cables in the mother cell, but (b) in the bud actin cables form a meshwork that randomizes Myo2p motions, which permits isotropic bud growth. (c) Proteins secreted at the start of bud emergence remain anchored to the bud neck by a scaffold of septin neck. (d) A cortical anchor that was established at the bud tip during earlier apical bud growth immobilizes *ASH1* mRNA, mitochondrial membranes and cytoplasmic microtubules at the bud tip. (e) Cortical anchors in the mother retain mitochondria within the mother and anchor cytoplasmic microtubules emanating from the other spindle pole.

(Cited from Pruyne D & Bretscher A. *J Cell Sci*. 2000 Feb;113 (Pt 4):571-85, reproduced with permission of the Company of Biologists©)

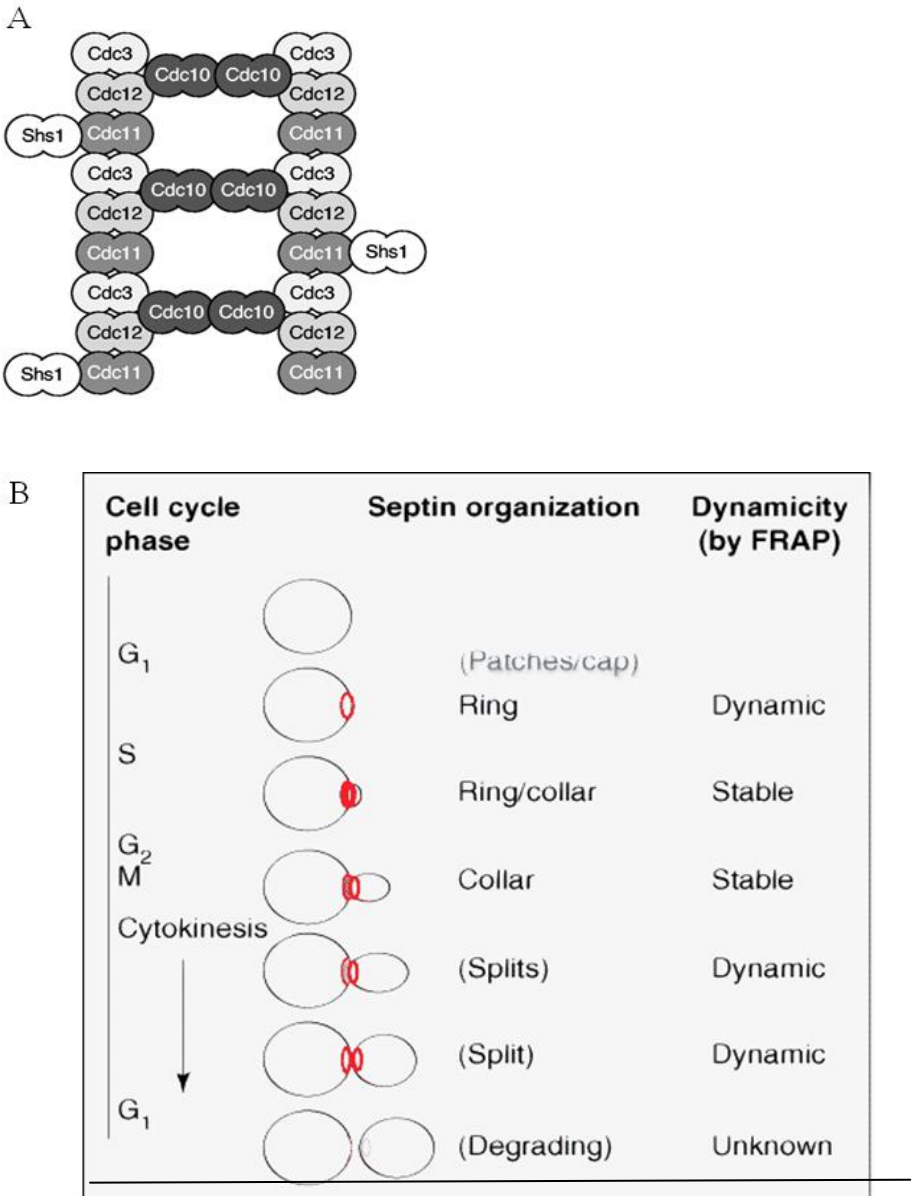

Figure 4.3 Septins in budding yeast

(A) Model for septin filament assembly. (Cited from Douglas LM, *et al*., *Eukaryot Cell. 2005 September; 4(9): 1503–1512,* by permission © American Society for Microbiology)
(B) A scheme showing the dynamicity of the septin organization during the cell cycle. (Cited from Kinoshita M. *Curr Opin Cell Biol. 2006 Feb;18(1):54-60,* by permission © Elsevier Ltd. All rights reserved.)

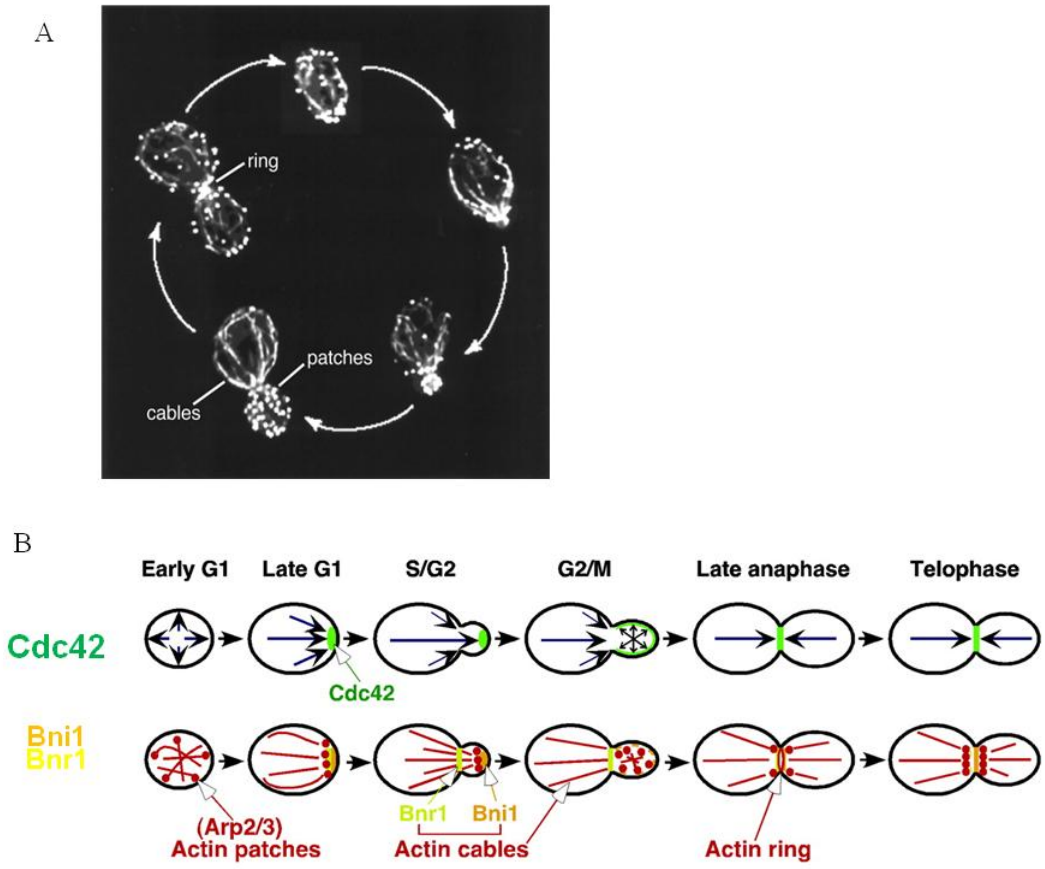

Figure 4.4 Cell cycle-regulated organization of actin cytoskeleton and Cdc42 localization in budding yeast

(A) Cell cycle-regulated organization of the budding yeast actin cytoskeleton (Cited from . Moseley JB and Goode BL. *Microbiol Mol Biol Rev. 2006 Sep;70(3):605-45,* by permission © American Society for Microbiology)

(B) Localization of Cdc42 (green) and Cdc42-controlled actin (red) and septin organization. (Actin cables are nucleated by the formins Bni1 (brown) and Bnr1 (yellow). (Cited from HO Park and E Bi, *Micro Mol Bio Reviews. 2007 71(1):48-96,* by permission © American Society for Microbiology)

A

B

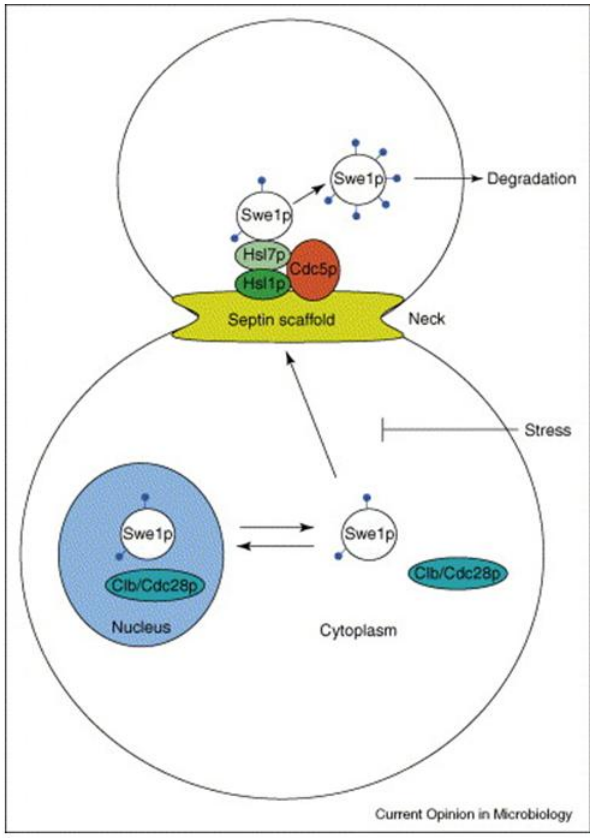

Figure 4.5 Swe1-dependent morphology checkpoint in budding yeast

(A) A scheme showing transition from apical to isotropic growth of the bud.
(B) Swe1 localization and degradation in yeast. Swe1 is firstly accumulated and phosphorylated by Cdc28 in the nucleus in unbudded cells. Upon bud growth, Hsl1 is activated and recruits Hsl7, which recruits Swe1 and Cdc5 to the septin. Cdc5 phosphorylates Swe1 leading to Swe1 degradation. Stresses that delay bud emergence prevent activation of Hsl1 and degradation of Swe1. (Cited from Keaton MA & Lew DJ. *Curr Opin Microbiol. 2006 Dec;9(6):540-6,* by permission)

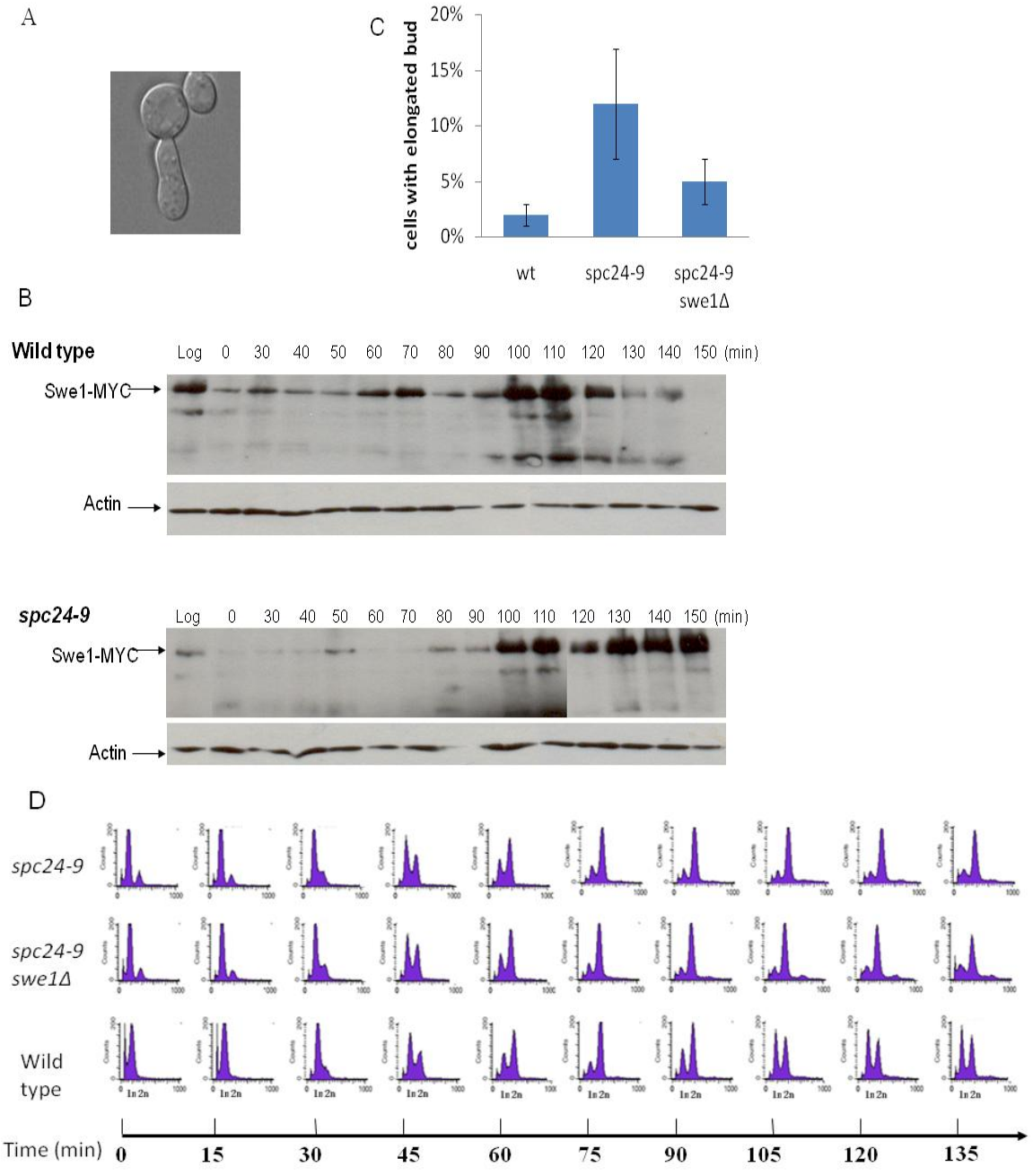
A
C
20%
15%
10%
5%
0%
cells with elongated bud
wt
spc24-9
spc24-9 swe1Δ
B
Wild type
Log 0 30 40 50 60 70 80 90 100 110 120 130 140 150 (min)
Swe1-MYC
Actin
spc24-9
Log 0 30 40 50 60 70 80 90 100 110 120 130 140 150 (min)
Swe1-MYC
Actin
D
spc24-9
spc24-9 swe1Δ
Wild type
1n 2n
Time (min)
0 15 30 45 60 75 90 105 120 135
E
YPD 25 °C
YPD 33 °C
Wild type
spc24-9 swe1Δ
spc24-9 swe1Δ
swe1Δ
spc24-9

Figure 4.6 The Swe1 dependent morphology checkpoint is activated in *spc24-9*

(A) Example of the bud elongation morphology in *spc24-9* mutants
(B) Periodic Swe1 accumulation during the cell cycle. Wild type cells and *spc24-9* cells containing an integrated SWE1-13MYC were synchronized in G1 with mating pheromone at 25℃ and released to 37℃. Time points were taken at 0min, 30min and every 10min thereafter for 2.5 hours. Lysates were separated by SDS-PAGE and immunoblotted with the monoclonal anti-myc antibody, or monoclonal anti-ACT1 antibody as a loading control.
(C) Bud elongation in *spc24-9* is suppressed by *swe1*Δ. Asynchronous wild type cells, *spc24-9* cells and *spc24-9 swe1*Δ double mutant cells were grown at 37℃ for 4 hours. The percentage of the cells with elongated buds is shown.
(D) Cells were grown in YPD at 25^{o}C, synchronized in G1 with mating pheromone at 25℃ and released to 37℃. Time points were taken at 0min, and every 15min for 135min. FACs data is shown at indicated times.
(E) (F) Spot assays of the indicated mutants and wild type. Plates were incubated at the indicated temperatures for 2 days.

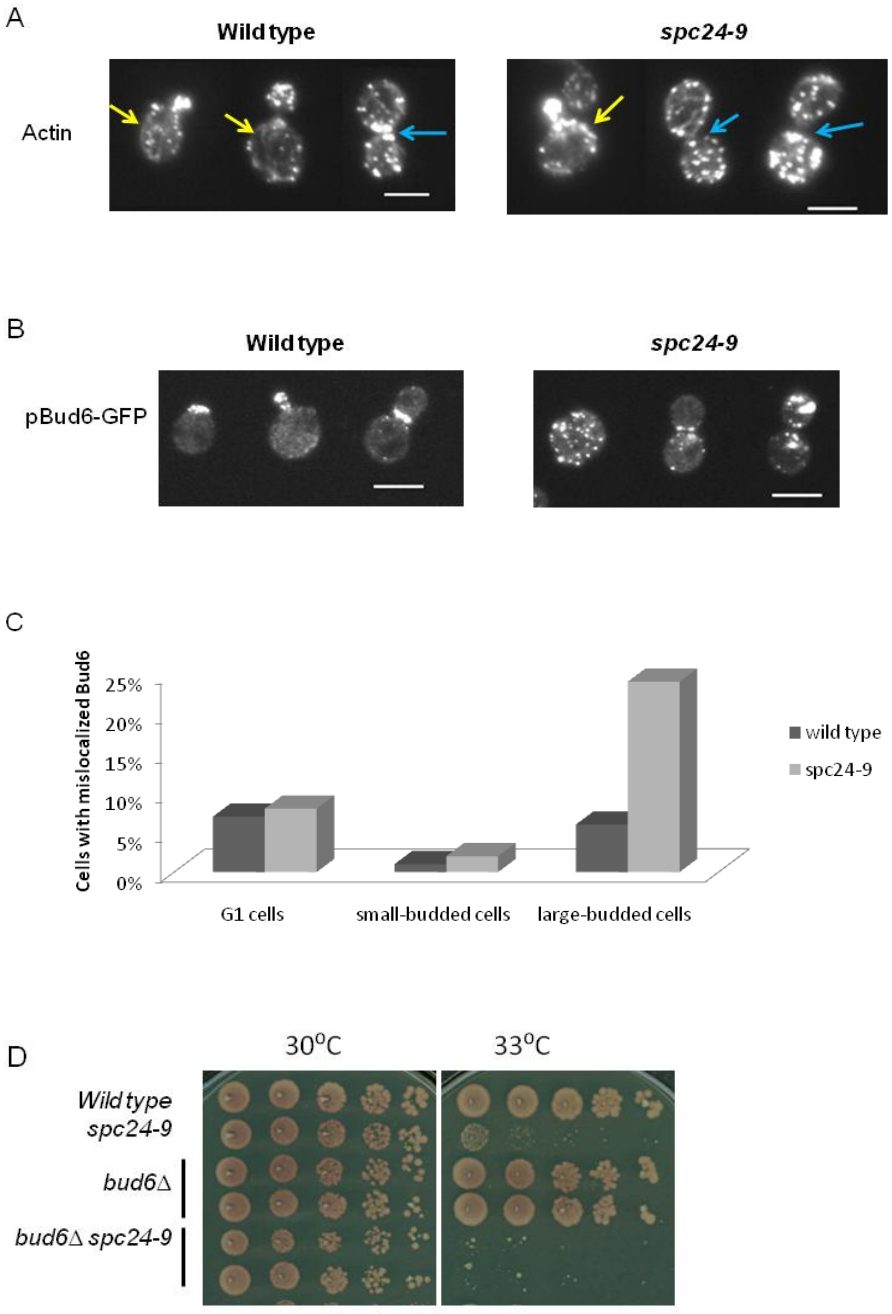

Figure 4.7 Actin defects and Bud6 mislocalization in *spc24-9* mutants

Log phase wild type and *spc24-9* cells were incubated at 37°C for 3 hours and then fixed with formaldehyde. (A) Cells were stained with Rhodamine Phalloidin to visualize actin (B)(C) Cells carrying the pBud6-GFP plasmid were imaged (B) and percentage of the cells with mislocalized Bud6 is shown (C). Scale bar, 2μm. (D) Spot assay of the indicated mutants and wild type. Plates were incubated at the indicated temperature for 2 days.

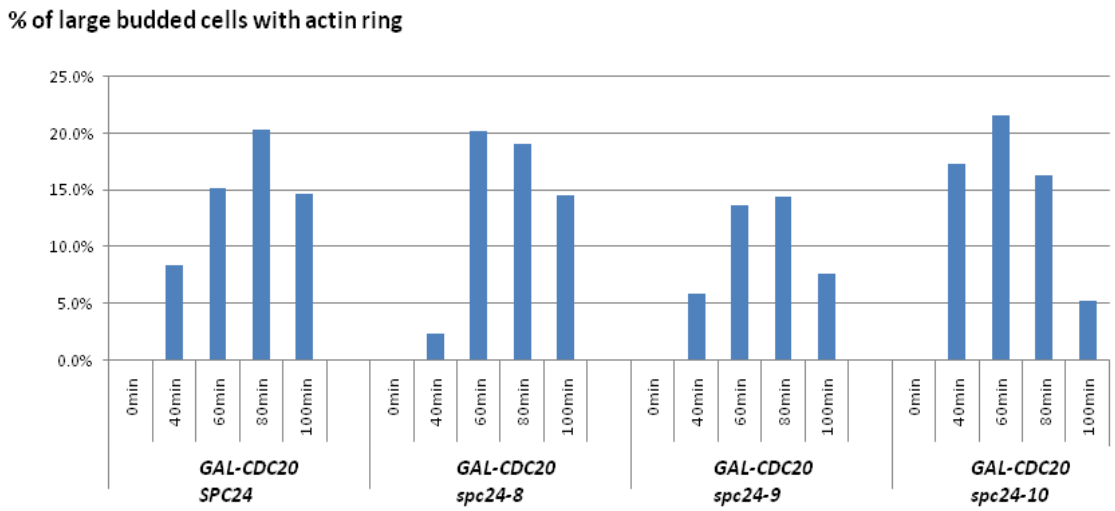

Figure 4.8 *spc24* mutants have normal actin ring formation

GAL-CDC20 cells were grown in galactose at 25°C, arrested in metaphase with 2% glucose (YPD) for 2hrs at 25 ℃, washed and resuspended with YPG and released to 37 ℃. Time points were taken at indicated time. Actin was stained with Rhodamine Phalloidin to enable visualization of actin ring formation.

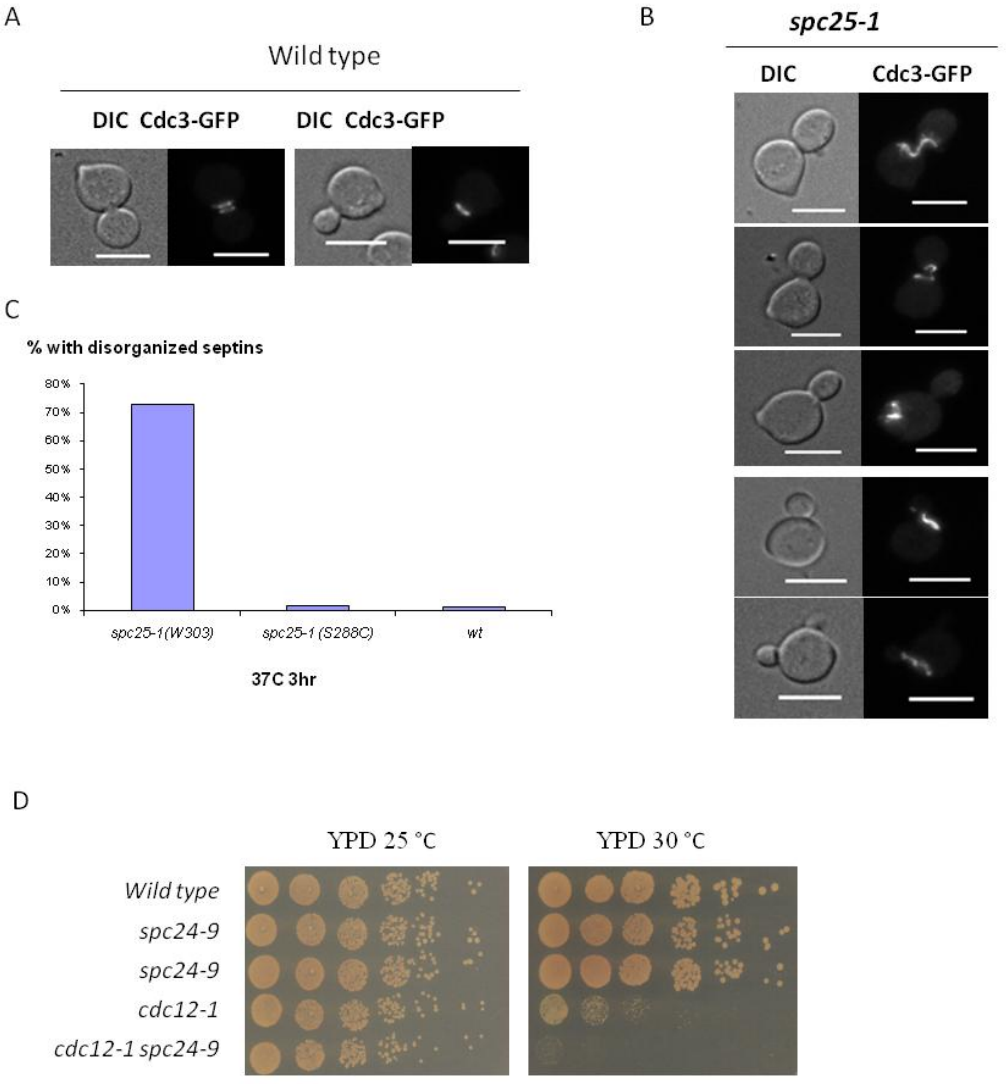

Figure 4.9 Analysis of septin function in *spc24* mutants

(A) -(C) Cells harboring the pCDC3-GFP plasmid were fixed with formaldehyde after an asynchronous block at 37ºC for 3 hrs. scale bar, 2µm. (A) Septin localization in wild type cells. (B) Septin disorganization in *spc25-1* (W303 background) (C) Comparison of septin defects in *spc25-1* with two different strain backgrounds, W303 and S288C.
(D) Spot assays of the indicated mutants and wild type. Plates were incubated at the indicated temperatures for 2 days.

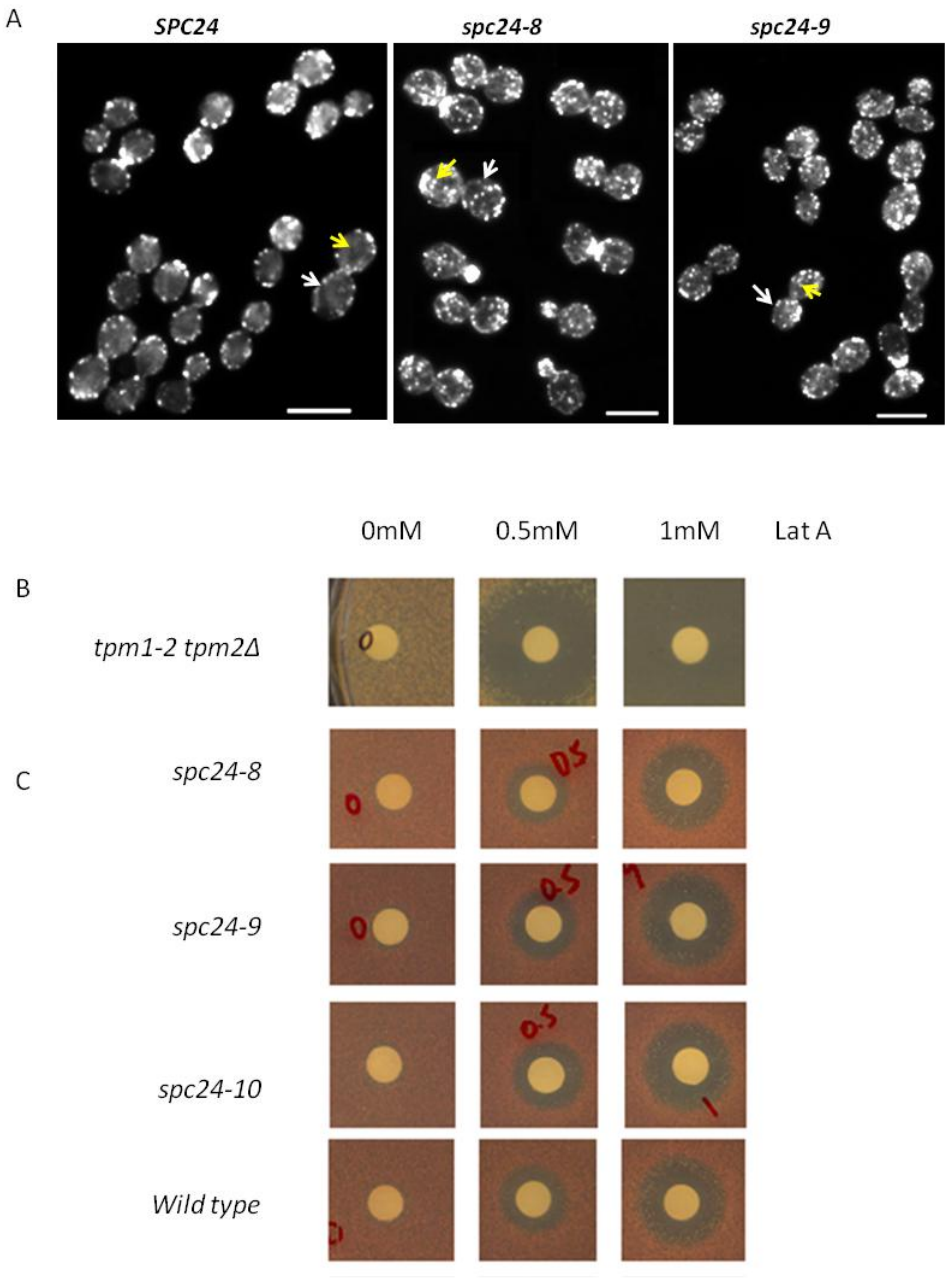

Figure 4.10 *spc24* mutants have increased numbers of actin patches

(A) *GAL-CDC20* cells were grown in galactose at 25°C, arrested in metaphase with 2% glucose (YPD) for 2 at 25℃, washed and resuspended with YPG and released to 37℃ for 40min. Actin was stained with Rhodamine phalloidin. Scale bar, 2μm.
(B) (C) Lat-A halo sensitivity assay was carried out as described in the Materials and Methods. Round white filter paper with Lat-A (with indicated concentration) is in the center of each image. Grown colonies are pink or white and the dark halos are due to the absence of cell growth. Plates were incubated at 30°C for 2 days.

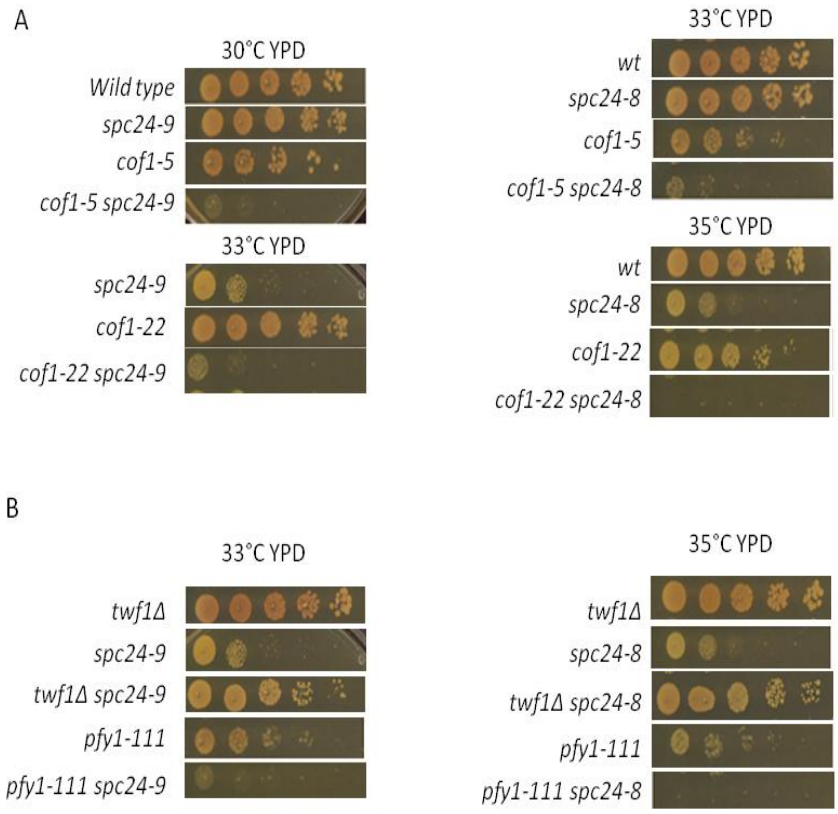

Figure 4.11 Genetic interactions between *spc24* and actin mutants

Spot assays of the indicated mutants and wild type. *spc24-8* and *spc24-9* are synthetic sick with *cof1* mutants (*cof1-5* and *cof1-22*) (A) and *pfy1-111* (B), whereas *spc24-8* and *spc24-* are rescued by *twf1*Δ (B) at the indicated temperature. Plates were incubated at the indicated temperatures for 2 days.

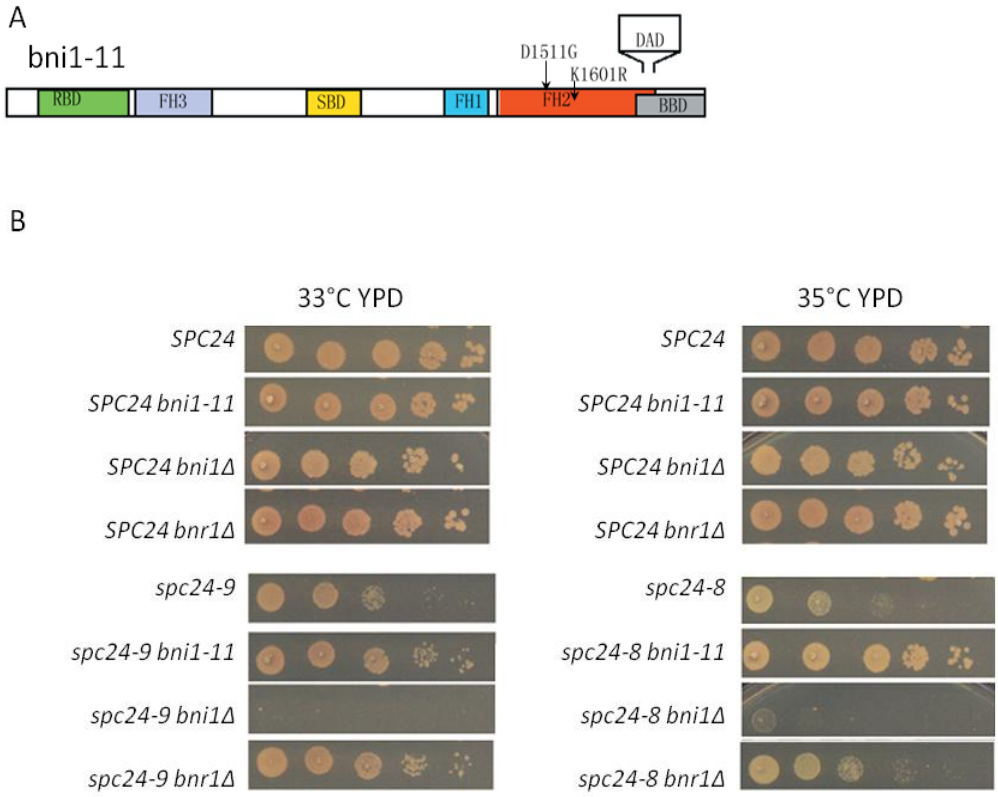

Figure 4.12 Suppression of *spc24* mutant growth defect by formin mutants

(A) Schematic representation of the primary structures of the yeast formin homologue Bni1. Domains include Rho-binding domain (RBD), formin-homology domains (FH1, FH2 and FH3), Dia-autoregulatory domain (DAD), Spa2-binding domain (SBD) and Bud6-binding domain (BBD). Percentage identities between related domains are indicated. (Cited from Evangelista M *et al*., *Nat Cell Biol. 2002 Mar;4(3):260-9*.)
(B) Spot assays of the indicated mutants and wild type. Plates were incubated at the indicated temperatures for 2 days.

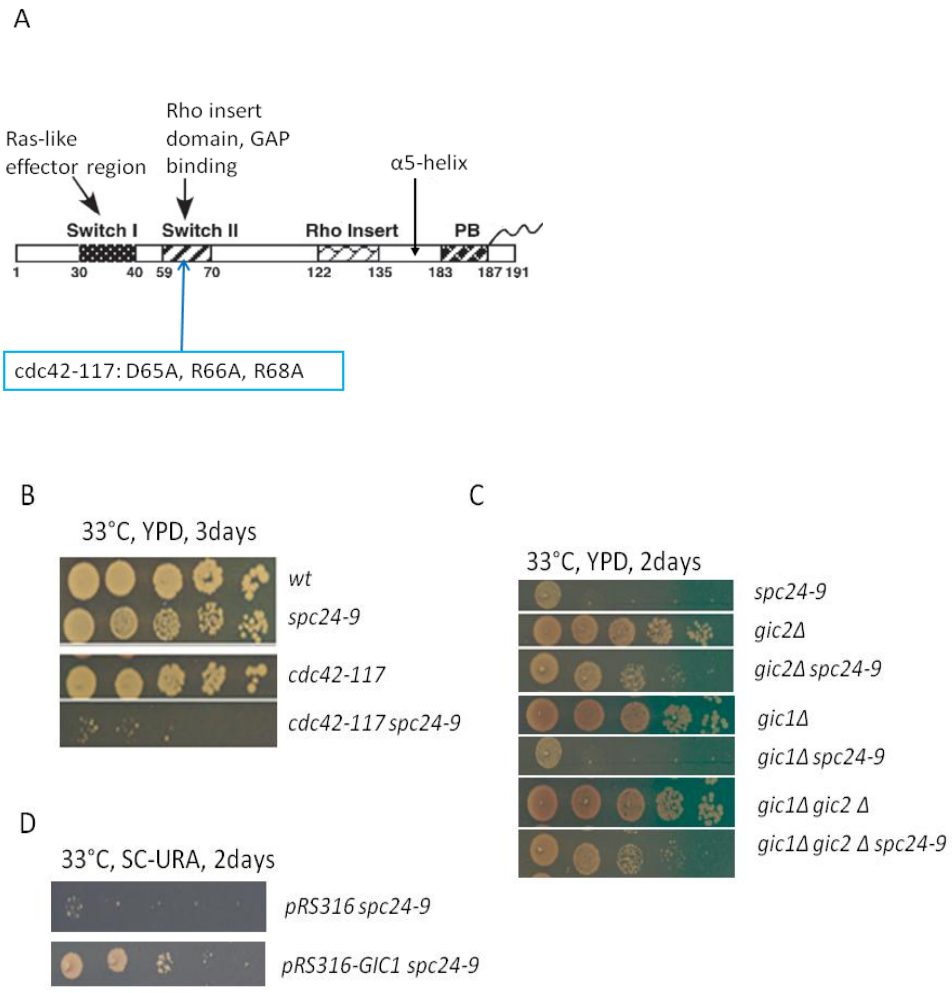

Figure 4.13 Genetic interaction between *spc24* and *cdc42-117* and *gic* mutants

(A) Schematic representation of Cdc42 structure. Mutations of *cdc42-117* are in the GAP binding domain as indicated. (Modified from HO Park and E Bi, *Micro Mol Bio Reviews. 2007, 71(1):48-96*)

(B)-(D) Spot assays of the indicated mutants and wild type. Plates were incubated at the indicated temperatures for 2 days.

Chapter 5 Summary and Perspectives

In this thesis, I have dissected the cellular function of the Ndc80 kinetochore complex in spindle integrity, the cAMP/PKA pathway and the regulation of polarity. Firstly, our laboratory demonstrated that a mutation of Spc24 (*spc24-9*), a component of the conserved Ndc80 kinetochore complex, causes lethality when cells are exposed to the DNA replication inhibitor hydroxyurea (HU) due to premature spindle expansion and segregation of incompletely replicated DNA. Consequently, I performed a high copy suppressor (HCS) screen and identified 10 genes that when overexpressed rescue the HU sensitivity and spindle expansion defect of the *spc24-9* mutant strain (Ma *et al.*, 2007). Overexpression of Stu1, a CLASP-related MT-associated protein or a truncated form of the XMAP215 orthologue Stu2 rescues *spc24-9* HU lethality and prevents spindle expansion. Truncated Stu2 likely acts in a dominant-negative manner, because overexpression of full-length *STU2* does not rescue *spc24-9* HU lethality, and spindle expansion in *spc24-9* HU-treated cells requires active Stu2. I have shown that Stu1 and Stu2 localize to the kinetochore early in the cell cycle and Stu2 kinetochore localization depends on Spc24. Therefore I propose that mislocalization of Stu2 results in premature spindle expansion in S phase stalled *spc24-9* mutants, and anticipate that identifying factors that restrain spindle expansion upon inhibition of DNA replication is likely applicable to the mechanism by which spindle elongation is regulated during a normal cell cycle. Secondly, the Measday lab

previously reported a synthetic lethal screen performed using *spc24-9* as the query strain and identified a genetic interaction with two mutants (*ira2*, *pde2*) that display increased activation of the cAMP/PKA pathway. I extended this study and have shown that the ts of three *spc24* mutants, *spc24-8*, *spc24-9* and *spc24-10*, is suppressed by *ras1*Δ and *ras2*Δ, which have reduced activation of the cAMP/PKA pathway. Therefore, my data suggest that *spc24* mutants do not tolerate increased cAMP/PKA activity and are rescued by reduction of cAMP/PKA activity. In wild type cells, the transcription factor Msn2 is rapidly dephosphorylated in response to glucose, however *spc24* mutants have defects in Msn2 dephosphorylation in response to glucose depletion. Non-preferred carbon sources like galactose, raffinose and glycerol dramatically rescue the glucose growth defects of all mutant alleles of the Ndc80 complex and specific alleles of other kinetochore complexes. I therefore propose that *spc24* mutants have increased PKA activity and the Ndc80 complex may both be a target of the PKA pathway and have a role in downregulation of the PKA pathway as well. Thirdly, I identified actin defects in *spc24* mutants and genetic interactions with mutants defective in actin cable nucleation, actin patch formation, and upstream regulators of cell polarity. I found that the Swe1-dependent morphology checkpoint is activated in *spc24-9* mutants probably due to actin disorganization, but the checkpoint activation is not the only reason for *spc24-9* G2 arrest and inviability at the non-permissive temperature. Since a dominant allele of Cdc42 reduces the restrictive temperature of *spc24-9* whereas depletion of downstream targets of Cdc42 suppresses the ts of *spc24-9*, I speculate that the actin defects in *spc24* mutants might be due to hyper activated Cdc42. Below, I discuss new questions raised by

my findings and future directions for research on the cellular function of the Ndc80 complex.

What is the specific role of Ndc80 in cAMP/PKA pathway? I have shown evidence that the Ndc80 complex might have a role in the cAMP/PKA pathway but it is still unclear whether the Ndc80 complex is negatively regulated by the PKA pathway or whether the Ndc80 complex is a negative regulator of the PKA pathway. Firstly, I could test if the Ndc80 complex is phosphorylated by PKA (Tpk1,2,3) using in vitro kinase assays and to use a mass spectrometry approach to identify any PKA phosphorylation sites on the components of Ndc80 complex. If PKA phosphorylation sites are identified on Spc24, Spc25, Nuf2 or Ndc80, I would next proceed by using site-directed mutagenesis to abolish or mimic phosphorylation sites. The phenotypes of the mutant alleles would be studied by comparing growth conditions under different carbon source, analyzing Msn2 phosphoryation levels and trehalose levels as described in Chapter 3. Secondly, if the PKA pathway negatively regulates kinetochore function, hyperactivation of the PKA pathway, for example by using dominant alleles of the PKA pathway such as *ras2val19* or *bcy1*Δ, would promote detachment of kinetochores from MTs which could be detected by GFP-tagged tetracycline operator (tetO) system or monitoring kinetochore proteins fused to fluorescent tags (Michaelis *et al.*, 1997; Fuchs *et al.*, 2002). On the other hand, if the Ndc80 complex negatively regulates the PKA pathway, overproducing Ndc80 may decrease the viability of *ras2*Δ or rescue *ras2val19* or affect intracellular cAMP levels. One intriguing data from recent quantitive mass spectrometry analysis performed by Angel Chang (MSc student in

the Measday lab) in collaboration with Dr. Thibault Mayor at UBC is that Ndc80 may interact with Gcr1 which is a transcriptional activator of genes involved in glycolysis, suggesting that the Ndc80 complex might regulate the PKA pathway at the transcription level. Therefore, we propose to confirm the Gcr1-Ndc80 interaction by co-IP and to determine if expression levels of Gcr1 regulated genes, such as *ENO1,2* or *GAPDH* are affected in *spc24-9* mutants (Holland, *et al.*, 1987). Next I propose to perform follow up studies such as ChIP assays to determine if Ndc80 binds to Gcr1 binding sites (Huie, *et al.*, 1992) or if Gcr1 binds to the centromere.

Does Ndc80 accumulate to the plus end of cMT? In Appendix B, I show that Ndc80-GFP, in addition to its well established kinetochore localization, also localizes to a punctate focus in the cytoplasm. I speculate that the cytoplasmic localization of Ndc80-GFP is the plus end of cMT, but the co-localization need to be further confirmed. Thereafter, I am interested to know if Ndc80 itself, the Ndc80-Nuf2 dimer, or the entire Ndc80 complex accumulates at the plus end of cMTs. It is reported that Ndc80 components interact by the two-hybrid assay with the dynein-dynactin complex (Jnm1 and Nip100) (Wong, *et al.*, 2007). The dynein-dynactic complex anchors at the cell cortex and walks along the cMTs towards SPBs, which might provide a mechanism of communication between the cytoplasm and nucleus. Thus it would be interesting to study if Ndc80 is transported by these motor proteins to the plus ends of cMT and if the cMT pool of Ndc80 is translocalized from the kinetochore or from a separate cytoplasmic pool of Ndc80.

Next, what are the functions of Ndc80 at the cMT? Since the dynein/dynactin complex

facilities spindle orientation and nuclear migration, it is possible that Ndc80 at cMTs are also involved in this process. To address this further, I propose to determine if *spc24* mutants have any defects in spindle orientation or nuclear migration. The second possibility is that the pool of Ndc80 at cMT reaches the cell cortex and therefore interacts with the components in the PKA pathway (see discussion in Chapter 3), responds to environmental stress (see below), or, as described in Chapter 4, interacts with proteins that function in regulation of actin dynamics (see below).

Why do cells recruit Ndc80 to the cytoplasm? I have some preliminary data with overproduced pNDC80-GFP suggesting that more Ndc80 may accumulate in the cytoplasm at higher temperature (37^{o}C) versus normal temperature (25^{o}C) in glucose but less in the cytoplasm at 25^{o}C in NPCS such as galactose compared to glucose media (25^{o}C) (data not shown). Different carbon sources might address the role of the Ndc80 complex in the PKA pathway or other nutrient pathway, whereas 37^{o}C is a mild heat stress belonging to the environmental stress response (ESR). Yeast is a unicellular cell, unlike mammalian cells that have multiple organs to retain a relatively stable internal environment, therefore yeast has evolved autonomous programs for adapting to changes in environmental conditions. Consequently, the yeast Ndc80 complex might have additional functions compared with its vertebrate homologue. Gasch (2000) and others have reported that the PKA pathway may govern the entire ESR in response to nutritional signals, and both the positive and negative regulators of the PKA pathway are induced by the

ESR, presumably to allow sensitive posttranslational control through the pathway. Therefore, I am planning to confirm and study the localization of Ndc80, especially at the cMT, in response to different ESR, such as glucose depletion, switching the media from NPCS to glucose, or mild heat shock. Notably, we need to repeat the experiment with endogenous GFP tagged Ndc80 strains using a better camera or confocal microscope in order to confirm that the phenotypes observed upon different carbon sources or mild heat are not due to the overexpression of Ndc80. The Measday lab is currently setting up a sensitive system on the microscope for these experiments.

What the role of Spc24 in G1? The cellular function of Spc24 in G1 has never been carefully studied. In Appendix 1, I show that when *spc24-9* cells are blocked in metaphase and released to restrictive temperature, the cells arrest as unbudded cells with a 1N DNA content, suggesting that Spc24 might have a role in G1. However, since this experiment involves a carbon source shift (from glucose to galactose), the G1 arrest could be occurring because of defects with the *spc24-9* strain in adapting to the different carbon source.. Therefore, I propose to repeat this experiment using a different approach such as a *MET-CDC20* or telophase ts alleles (e.g. *cdc15-2, cdc5-1, cdc14-1*) to block the cells in anaphase prior to release. If the G1 arrest is confirmed, I could characterize the arrest further by analyzing G1 cyclin levels, the position of polarity determinants, and the SPB attachment state of the kinetochore to determine the cause of G1 arrest.

What are the cytoplasm interaction partners of Ndc80? The data presented in Chapter 3, Chapter 4 and Appendix 2 all indicate that the Ndc80 complex has a cytoplasmic cellular function - either in the PKA pathway or regulation of actin dynamics. Thus an important question is "What are the cytoplasmic targets of the Ndc80 complex?" A graduate student in Dr. Measday's lab, Angel Chang, is currently performing quantitative Mass-spectrometry in collaboration with Dr. Thibault Mayor by immunoprecipitating a GFP-tagged version of Ndc80. One caveat to this approach is that the majority of Ndc80 is localized to the nucleus and thus it will be difficult to detect interactions with the minor pool of Ndc80 that is localized to the cytoplasm. One possibility is to use a kinetochore mutant (such as *ndc10-1*) to disrupt kinetochore function and possibly increase the chances of detecting an interaction between Ndc80 and its cytoplasmic targets. One interesting candidate to mention here is Srv2, which binds to adenylyl cyclase complex to activate the cAMP/PKA pathway, and also binds to actin monomers to play a central role in regulation of actin dynamics (Gerst, *et al.*, 1991; Kawamukai, *et al.*, 1992; Freeman, *et al.*, 1995; Yu, *et al.*, 1999; Mattila, *et al.*, 2004). At the pointed end of an actin filament, Srv2 accelerates the cofilin-dependent severing and depolymerization by displacing cofilin from binding to actin monomers (Quintero-Monzon, *et al.*, 2009), whereas at the barbed end, Srv2 binds actin monomers and profilin simultaneously and facilitates actin filament polymerization (Bertling, *et al.*, 2007). Since I have found defects in both cAMP/PKA pathway and actin dynamics in *spc24* mutants, it would be interesting to test for a potential interaction between Srv2 and the Ndc80 complex.

Bibliography

Adams, I.R., and Kilmartin, J.V. (1999). Localization of core spindle pole body (SPB) components during SPB duplication in Saccharomyces cerevisiae. *J Cell Biol., 145*, 809-823.

Al-Bassam, J., Larsen, N.A., Hyman, A.A., and Harrison, S.C. (2007). Crystal Structure of a TOG Domain: Conserved Features of XMAP215/Dis1-Family TOG Domains and Implications for Tubulin Binding. *Structure, 15*, 355-362.

Al-Bassam, J., van Breugel, M., Harrison, S.C., and Hyman, A. (2006). Stu2p binds tubulin and undergoes an open-to-closed conformational change. *J Cell Biol., 172*, 1009-1022.

Allen, J.B., Zhou, Z., Siede, W., Friedberg, E.C., and Elledge, S.J. (1994). The SAD1/RAD53 protein kinase controls multiple checkpoints and DNA damage-induced transcription in yeast. *Genes Dev., 8*, 2401-2415.

Akiyoshi, B., Nelson, C.R., Ranish, J.A. and Biggins, S. (2009). Analysis of Ipl1-mediated phosphorylation of the Ndc80 kinetochore protein in Saccharomyces cerevisiae. *Genetics*, 183,1591-1595.

Ault, J., and Rieder, C. (1992). Chromosome mal-orientation and reorientation during mitosis. *Cell Motil Cytoskeleton. , 22*, 155-159.

Ault, J., DeMarco, A., Salmon, E., and Rieder, C. (1991). Studies on the ejection properties of asters: astral microtubule turnover influences the oscillatory behavior and positioning of mono-oriented chromosomes. *J Cell Sci. , 99*, 701-710.

Ayscough, K., Stryker, J., Pokala, N., Sanders, M., Crews, P., and Drubin, D. (1997). High rates of actin filament turnover in budding yeast and roles for actin in establishment and maintenance of cell polarity revealed using the actin inhibitor latrunculin-A. *J Cell Biol. , 137*, 399-416.

Bachant, J., Jessen, S.R., Kavanaugh, S.E., and Fielding, C.S. (2005). The yeast S phase checkpoint enables replicating chromosomes to bi-orient and restrain spindle extension during S phase distress. *J Cell Biol 168*, 999-1012.

Baroni, M., Monti, P., and Alberghina, L. (1994). Repression of growth-regulated Gl cyclin expression by cyclic AMP in budding yeast. *Nature , 371*, 339-342.

Berlin, V., Styles, C. A., and Fink, G. R. (1990). BIK1, a protein required for microtubule function during mating and mitosis in Saccharomyces cerevisiae, colocalizes with tubulin. *J. Cell Biol 111*, 2573–2586

Bertling, E., Quintero-Monzon, O., Mattila, P., Goode, B., and Lappalainen, P. (2007). Mechanism and biological role of profilin-Srv2/CAP interaction. *J Cell Sci. , 120*, 1225-1234.

Bharadwaj, R., Qi, W., and Yu, H. (2004). Identification of two novel components of the human NDC80 kinetochore complex. *J Biol Chem. , 279* (13), 13076-13085.

Biggins, S., and Murray A.W. (2001). The budding yeast protein kinase Ipl1/Aurora allows the absence of tension to activate the spindle checkpoint. *Genes Dev.*, 15, 3118–3129.

Bilsland-Marchesan, E., Arino, J., Saito, H., Sunnerhagen, P., and Posas, F. (2000). Rck2 kinase is a substrate for the osmotic stress-activated mitogen-activated protein kinase Hog1. *Mol Cell Biol., 20*, 3887-3895.

Blake-Hodek, K.A., Cassimeris, L. and Huffaker, T.C. (2010). Regulation of Microtubule Dynamics by Bim1 and Bik1, the Budding Yeast Members of the EB1 and CLIP-170 Families of Plus-End Tracking Proteins. *Mol Biol Cell. 21*, 2013-2023

Bloom, K., and Joglekar, A. (2010). Towards building a chromosome segregation machine. *Nature. , 463*, 446-456.

Bolte M, Dieckhoff P, Krause C, Braus GH, Irniger S. (2003). Synergistic inhibition of APC/C by glucose and activated Ras proteins can be mediated by each of the Tpk1-3 proteins in Saccharomyces cerevisiae. *Microbiology. 149(Pt 5)*,1205-1216.

Bouck, D., and Bloom, K. (2005). The role of centromere-binding factor 3 (CBF3) in spindle stability, cytokinesis, and kinetochore attachment. *Biochem Cell Biol., 83*, 696-702.

Broek, D., Samiy, N., Fasano, O., Fujiyama, A., and Tamanoi, F. (1985). Differential activation of yeast adenylate cyclase by wild-type and mutant RAS proteins. *Cell , 41*, 763-769.

Brown, J., Jaquenoud, M., Gulli, M., Chant, J., and Peter, M. (1997). Novel Cdc42-binding proteins Gic1 and Gic2 control cell polarity in yeast. *Genes Dev. , 11*, 2972-2982.

Budovskaya, Y., Stephan, J., Deminoff, S., and Herman, P. (2005). An evolutionary proteomics approach identifies substrates of the cAMP-dependent protein kinase. *Proc Natl Acad Sci , 102*, 13933-13938.

Canman, C.E. (2001). Replication checkpoint: preventing mitotic catastrophe. *Curr Biol., 11*, R121-124.

Cheeseman, I., and Desai, A. (2008). Molecular architecture of the kinetochore-microtubule interface. *Nat Rev Mol Cell Biol. , 9*, 33-46.

Cheeseman, I., Brew, C., Wolyniak, M., Desai, A., Anderson, S., Muster, N., *et al*. (2001). Implication of a novel multiprotein Dam1p complex in outer kinetochore function. *J Cell Biol. , 155*, 1137-1145.

Cheeseman, I., Anderson, S., Jwa, M., Green, E.M., Kang, J., Yates, J.R., *et al.* (2002). Phospho-regulation of kinetochore-microtubule attachments by the Aurora kinase Ipl1p, *Cell*, *111*, 163–172.

Cheeseman, I., Chappie, J., Wilson-Kubalek, E., and Desai, A. (2006). The conserved KMN network constitutes the core microtubule-binding site of the kinetochore. *Cell., 127*, 983-97.

Chen, G., Kim, Y., and Chan, C. (1997). The Cdc42 GTPase-associated proteins Gic1 and Gic2 are required for polarized cell growth in Saccharomyces cerevisiae. *Genes Dev. , 11*, 2958-2971.

Chen, X.P., Yin, H., and Huffaker, T.C. (1998). The yeast spindle pole body component Spc72p interacts with Stu2p and is required for proper microtubule assembly. *J Cell Biol*., *141*, 1169-1179.

Ciferri, C., De Luca, J., Monzani, S., Ferrari, K., Ristic, D., Wyman, C., *et al*. (2005). Architecture of the human ndc80-hec1 complex, a critical constituent of the outer kinetochore. *J Biol Chem. , 280*, 29088-29095.

Ciferri, C., Pasqualato, S., Screpanti, E., Varetti, G., Santaguida, S., Dos Reis, G., *et al*. (2008). Implications for kinetochore-microtubule attachment from the structure of an engineered Ndc80 complex. *Cell. , 133*, 427-439.

Cimini, D., Wan, X., Hirel, C., and Salmon, E. (2006). Aurora kinase promotes turnover of kinetochore microtubules to reduce chromosome segregation errors. *Curr Biol.,16*, 1711-1178.

Clarke, D.J., Segal, M., Jensen, S., and Reed, S.I. (2001). Mec1p regulates Pds1p levels in S phase: complex coordination of DNA replication and mitosis. *Nat Cell Biol*., *3*, 619-627.

Colombo, S., Ma, P., Cauwenberg, L., Winderickx, J., Crauwels, M., Teunissen, A., *et al*. (1998).

Involvement of distinct G-proteins, Gpa2 and Ras, in glucose- and intracellular acidification-induced cAMP signalling in the yeast Saccharomyces cerevisiae. *EMBO J. , 17*, 3326-3341.

Colombo, S., Ronchetti, D., Thevelein, J., Winderickx, J., and Martegani, E. (2004). Activation state of the Ras2 protein and glucose-induced signaling in Saccharomyces cerevisiae. *J Biol Chem. , 279*, 46715-46722.

Connelly, C., and Hieter, P. (1996). Budding yeast SKP1 encodes an evolutionarily conserved kinetochore protein required for cell cycle progression. *Cell, 86*, 275-285.

Cuschieri, L., Miller, R., and Vogel, J. (2006). {gamma}-Tubulin Is Required for Proper Recruitment and Assembly of Kar9-Bim1 Complexes in Budding Yeast. *Mol Biol Cell.,17*, 4420-4434.

Daniel, J.A., Keyes, B.E., Ng, Y.P., Freeman, C.O., and Burke, D.J. (2006). Diverse functions of spindle assembly checkpoint genes in Saccharomyces cerevisiae. *Genetics 172*, 53-65.

DeLuca, J., Gall, W., Ciferri, C., Cimini, D., Musacchio, A., and Salmon, E. (2006). Kinetochore microtubule dynamics and attachment stability are regulated by Hec1. *Cell. , 127*, 969-82.

DeLuca, J., Howell, B., Canman, J., Hickey, J., Fang, G., and Salmon, E. (2003). Nuf2 and Hec1 are required for retention of the checkpoint proteins Mad1 and Mad2 to kinetochores. *Curr Biol. , 13*, 2103–2109.

DeLuca, J., Moree, B., Hickey, J., Kilmartin, J., and Salmon, E. (2002). hNuf2 inhibition blocks stable kinetochore-microtubule attachment and induces mitotic cell death in HeLa cells. *J Cell Biol. , 159*, 549-555.

De Winde, J. H., Thevelein, J. M., and Windercrix, J. (1997). In: Yeast Stress Responses (Hohmann, S., and Mager, W. H., eds). Springer, Berlin, 7–52,

De Wulf, P. , McAinsh, A.D. and Sorger, P.K. (2003) Hierarchical assembly of the budding yeast kinetochore from multiple subcomplexes, *Genes Dev. 17*, 2902–2921

Dewar, H., Tanaka, K., Nasmyth, K., and Tanaka, T.U. (2004). Tension between two kinetochores suffices for their bi-orientation on the mitotic spindle. *Nature, 428*, 93-97.

Diaz-Rodr ́guez, E., Sotillo, R., chvartzman, J., and Benezra, R. (2008). Hec1 overexpression hyperactivates the mitotic checkpoint and induces tumor formation in vivo. *Proc Natl Acad Sci. ,*

105, 16719-16724.

Doheny, K., Sorger, P., Hyman, A., Tugendreich, S., Spencer, F., and Hieter, P. (1993). Identification of essential components of the S. cerevisiae kinetochore. *Cell. ,73*, 761-774.

Dombek, K., Kacherovsky, N., and Young, E. (2004). The Reg1-interacting proteins, Bmh1, Bmh2, Ssb1, and Ssb2, have roles in maintaining glucose repression in Saccharomyces cerevisiae. *J Biol Chem. , 279*, 39165-39174.

Douglas, L., Alvarez, F., McCreary, C., and Konopka, J. (2005). Septin function in yeast model systems and pathogenic fungi. *Eukaryot Cell. , 4*, 1503-1512.

Dubacq, C., Guerois, R., Courbeyrette, R., Kitagawa, K., and Mann, C. (2002). Sgt1p contributes to cyclic AMP pathway activity and physically interacts with the adenylyl cyclase Cyr1p/Cdc35p in budding yeast. *Eukaryot Cell. , 1*, 568-582.

Enquist-Newman, M., Cheeseman, I.M., Van Goor, D., Drubin, D.G., Meluh, P. and Barnes, G. (2001). Dad1p, third component of the Duo1p/Dam1p complex involved in kinetochore function and mitotic spindle integrity, *Mol. Biol. Cell, 12*, 2601–2613.

Enserink, J., Smolka, M., Zhou, H., and Kolodner, R. (2006). Checkpoint proteins control morphogenetic events during DNA replication stress in Saccharomyces cerevisiae. *J. Cell. Biol. 175*, 729-741.

Erickson, J., Wu, J., Goddard, J., Tigyi, G., Kawanishi, K., Tomei, L., *et al*. (1998). Edg-2/Vzg-1 couples to the yeast pheromone response pathway selectively in response to lysophosphatidic acid. *J Biol Chem. , 273*, 1506-1510.

Espelin, C., Simons, K., Harrison, S., and Sorger, P. (2003). Binding of the essential Saccharomyces cerevisiae kinetochore protein Ndc10p to CDEII. *Mol Biol Cell. , 14*, 4557-4568.

Euskirchen, G.M. (2002). Nnf1p, Dsn1p, Mtw1p, and Nsl1p: a new group of proteins important for chromosome segregation in Saccharomyces cerevisiae. *Eukaryot Cell, 1*, 229-40

Evangelista, M., Pruyne, D., Amberg, D., Boone, C., and Bretscher, A. (2002). Formins direct Arp2/3-independent actin filament assembly to polarize cell growth in yeast. *Nat Cell Biol. , 4*, 32-41.

Feng, W., Collingwood, D., Boeck, M.E., Fox, L.A., Alvino, G.M., Fangman, W.L., Raghuraman, M.K., and Brewer, B.J. (2006). Genomic mapping of single-stranded DNA in

hydroxyurea-challenged yeasts identifies origins of replication. *Nat Cell Biol., 8,* 148-155.

Fraschini, R., Bilotta, D., Lucchini, G., and Piatti, S. (2004). Functional characterization of Dma1 and Dma2, the budding yeast homologues of Schizosaccharomyces pombe Dma1 and human Chfr. *Mol Biol Cell., 15,* 3796-3810.

Freeman, N., Chen, Z., Horenstein, J., Weber, A., and Field, J. (1995). An actin monomer binding activity localizes to the carboxyl-terminal half of the Saccharomyces cerevisiae cyclase-associated protein. *J. Biol. Chem. , 270,* 5680-5685.

Fujiwara, T., Tanaka, K., Inoue, E., Kikyo, M., and Takai, Y. (1999). Bni1p regulates microtubule-dependent nuclear migration through the actin cytoskeleton in Saccharomyces cerevisiae. *Mol Cell Biol. , 19,* 8016-8027.

Gancedo, C., and Serrano, R. (1989). In: The Yeast (Harrison, J. S., and Rose, A. H., eds). Academic Press, London, 205–259.

Gard, D.L., Becker, B.E., and Josh Romney, S. (2004). MAPping the eukaryotic tree of life: structure, function, and evolution of the MAP215/Dis1 family of microtubule-associated proteins. *Int Rev Cytol., 239,* 179-272.

Gardner, M., Haase, J., Mythreye, K., Molk, J., Anderson, M., Joglekar, A., *et al.* (2008). The microtubule-based motor Kar3 and plus end-binding protein Bim1 provide structural support for the anaphase spindle. *J Cell Biol. , 180 ,* 91-100.

Gardner, R., Poddar, A., Yellman, C., Tavormina, P., Monteagudo, M., and Burke, D. (2001). The spindle checkpoint of the yeast Saccharomyces cerevisiae requires kinetochore function and maps to the CBF3 domain. *Genetics. , 157* , 1493-1502.

Gasch, A., Spellman, P., Kao, C., Carmel-Harel, O., Eisen, M., Storz, G., *et al.* (2001). Genomic expression programs in the response of yeast cells to environmental changes. *Mol Biol Cell. , 11* , 4241-4257.

Gerst, J., Ferguson, K., Vojtek, A., Wigler, M., and Field, J. (1991). CAP is a bifunctional component of the Saccharomyces cerevisiae adenylyl cyclase complex. *Mol. Cell. Biol. , 11,* 1248-1257.

Gillett, E., and Sorger, P. (2001). Tracing the pathway of spindle assembly checkpoint signaling. *Dev Cell. , 1* (2), 162-164.

Gillett, E., Espelin, C., and Sorger, P. (2004). Spindle checkpoint proteins and chromosome-microtubule attachment in budding yeast. *J Cell Biol. , 164* (4), 535-546.

Gillis, A., Thomas, S., Hansen, S., and Kaplan, K. (2005). A novel role for the CBF3 kinetochore-scaffold complex in regulating septin dynamics and cytokinesis. *J Cell Biol. , 171*, 773-784.

Goh, P., and Kilmartin, J. (1993). NDC10: a gene involved in chromosome segregation in Saccharomyces cerevisiae. *J Cell Biol. , 121*, 503-512.

Goode, B., Drubin, D., and Lappalainen, P. (1998). Regulation of the cortical actin cytoskeleton in budding yeast by twinfilin, a ubiquitous actin monomer-sequestering protein. *J Cell Biol. , 142*, 723-33.

Görner, W., Durchschlag, E., Martinez-Pastor, M., Estruch, F., Ammerer, G., Hamilton, B., *et al*. (1998). Nuclear localization of the C2H2 zinc finger protein Msn2p is regulated by stress and protein kinase A activity. *Genes Dev. , 12* , 586-97.

Görner, W., Durchschlag, E., Wolf, J., Brown, E., Ammerer, G., Ruis, H., *et al*. (2002). Acute glucose starvation activates the nuclear localization signal of a stress-specific yeast transcription factor. *EMBO , 21*, 135-144.

Goshima, G., and Yanagida, M. (2000). Establishing biorientation occurs with precocious separation of the sister kinetochores, but not the arms, in the early spindle of budding yeast. *Cell*., *100*, 619-633.

Griffioen, G., and Thevelein, J. (2002). Molecular mechanisms controlling the localisation of protein kinase A. *Curr Genet. , 41*, 199-207.

Griffioen, G., Anghileri, P., Imre, E., Baroni, M., and Ruis, H. (2000). Nutritional control of nucleocytoplasmic localization of cAMP-dependent protein kinase catalytic and regulatory subunits in Saccharomyces cerevisiae. *J Biol Chem. , 275*, 1449-1456.

Grishchuk, E.L., Efremov, A.K., Volkov, V.A., Spiridonov, I.S., Gudimchuk, N., Westermann, S, *et al.* (2008). The Dam1 ring binds microtubules strongly enough to be a processive as well as energy-efficient coupler for chromosome motion. *Proc Natl Acad Sci, 105*, 15423-15428.

Gross, E., Goldberg, D., and Levitzki, A. (1992). Phosphorylation of the S. cerevisiae Cdc25 in response to glucose results in its dissociation from Ras. *Nature , 360*, 762-765.

Guimaraes, G., Dong, Y., McEwen, B., and Deluca, J. (2008). Kinetochore-microtubule attachment relies on the disordered N-terminal tail domain of Hec1. *Curr Biol. , 18*, 1778-1784.

Guthrie, C., and Fink, G.R. (1991). Guide to Yeast Genetics and Molecular Biology. Academic Press: New York.

Haarer, B., Corbett, A., Kweon, Y., Petzold, A., Silver, P., and Brown, S. (1996). SEC3 mutations are synthetically lethal with profilin mutations and cause defects in diploid-specific bud-site selection. *Genetics. , 144* , 495-510.

Haarer, B., Petzold, A., and Brown, S. (1993). Mutational analysis of yeast profilin. *Mol Cell Biol. , 13*, 7864-7873.

Haase, S., and Lew, D. (1997). Flow cytometric analysis of DNA content in budding yeast. *Methods Enzymol. , 283*, 322-332.

Hartwell, L. (1994). cAMPing out. *Nature , 371*, 286-286.

He, X., Asthana, S., and Sorger, P.K. (2000). Transient sister chromatid separation and elastic deformation of chromosomes during mitosis in budding yeast. *Cell 101*, 763-775

He, X., Rines, D., Espelin, C., and Sorger PK., (2001). Molecular analysis of kinetochore-microtubule attachment in budding yeast. *Cell. , 106*, 195-206.

Höfken, T., and Schiebel, E. (2004). Novel regulation of mitotic exit by the Cdc42 effectors Gic1 and Gic2. *J Cell Biol. , 164*, 219-231.

Hofmann, C., Cheeseman, I.M., Goode, B.L., McDonald, K.L., Barnes ,G. and Drubin D.G., (1998). Saccharomyces cerevisiae Duo1p and Dam1p, novel proteins involved in mitotic spindle function, *J. Cell Biol.*, 143, 1029–1040.

Holland, M.J., Yokoi, T., Holland, J.P., Myambo, K. and Innis, MA. (1987). The GCR1 gene encodes a positive transcriptional regulator of the enolase and glyceraldehyde-3-phosphate dehydrogenase gene families in Saccharomyces cerevisiae. *Mol Cell Biol. 7,* 813-820.

Horak, C.E., Luscombe, N.M., Qian, J., Bertone, P., Piccirrillo, S., Gerstein, M., and Snyder, M. (2002). Complex transcriptional circuitry at the G1/S transition in Saccharomyces cerevisiae. *Genes Dev., 16*, 3017-3033.

Hori, T., Haraguchi, T., Hiraoka, Y., Kimura, H., and Fukagawa, T. (2003). Dynamic behavior of

Nuf2-Hec1 complex that localizes to the centrosome and centromere and is essential for mitotic progression in vertebrate cells. *J Cell Sci. , 116*, 3347-62.

Howe, M., McDonald, K., Albertson, D., and Meyer BJ., B. (2001). HIM-10 is required for kinetochore structure and function on Caenorhabditis elegans holocentric chromosomes. *J Cell Biol. , 153*, 1227-38.

Hoyt, M., Totis, L., and Roberts, B. (1991). S. cerevisiae genes required for cell cycle arrest in response to loss of microtubule function. *Cell. , 66*, 507-17.

Huie, M.A., Scott, E.W., Drazinic, CM., Lopez, M.C., Hornstra, I.K., Yang, T.P., *et al.* (1992). Characterization of the DNA-binding activity of GCR1: in vivo evidence for two GCR1-binding sites in the upstream activating sequence of TPI of Saccharomyces cerevisiae. *Mol Cell Biol. 12*, 2690-700.

Hwang, L., Lau, L., Smith, D., Mistrot, C., Hardwick, K., Hwang, E., *et al*. (1998). Budding yeast Cdc20: a target of the spindle checkpoint. *Science , 279* , 1041-4.

Hwang, E., Kusch, J., Barral, Y., and Huffaker, T. C. (2003). Spindle orientation in Saccharomyces cerevisiae depends on the transport of microtubule ends along polarized actin cables. *J. Cell Biol, 161*, 483–488.

Hyland, K.M., Kingsbury, J., Koshland, D., and Hieter, P. (1999). Ctf19p: A novel kinetochore protein in Saccharomyces cerevisiae and a potential link between the kinetochore and mitotic spindle. *J Cell Biol., 145*, 15-28.

Inoue, Y.H., do Carmo Avides, M., Shiraki, M., Deak, P., Yamaguchi, M., Nishimoto, Y., Matsukage, A., and Glover, D.M. (2000). Orbit, a novel microtubule-associated protein essential for mitosis in Drosophila melanogaster. *J Cell Biol., 149*, 153-166.

Irazoqui, J., and Lew, D. (2004). Polarity establishment in yeast. *J Cell Sci. , 1*, 2169-2171.

Irniger S, Bäumer M, Braus GH. (2000). Glucose and ras activity influence the ubiquitin ligases APC/C and SCF in Saccharomyces cerevisiae. *Genetics.154*,1509-1521.

Iwase, M., Luo, J., Nagaraj, S., Longtine, M., Kim, H., Haarer, B., *et al*. (2006). Role of a Cdc42p effector pathway in recruitment of the yeast septins to the presumptive bud site. *Mol Biol Cell. , 17*, 1110-1125.

Jacquet, M., Renault, G., Lallet S, S., De Mey, J., and Goldbeter, A. (2003). Oscillatory

nucleocytoplasmic shuttling of the general stress response transcriptional activators Msn2 and Msn4 in Saccharomyces cerevisiae. *J Cell Biol. , 161*, 497-505.

Janke, C., Ortiz, J., Lechner, J., Shevchenko, A., Shevchenko, A., Magiera, M., *et al*. (2001). The budding yeast proteins Spc24p and Spc25p interact with Ndc80p and Nuf2p at the kinetochore and are important for kinetochore clustering and checkpoint control. *EMBO J. , 20* , 777-791.

Janke, C., Ortiz, J., Tanaka, T.U., Lechner, J. and Schiebel, E. (2002). Four new subunits of the Dam1-Duo1 complex reveal novel functions in sister kinetochore biorientation, *EMBO J. 21* 181–193.

Jaquenoud, M., and Peter, M. (2000). Gic2p may link activated Cdc42p to components involved in actin polarization, including Bni1p and Bud6p (Aip3p). *Mol Cell Biol. , 20*, 6244-6258.

Jaquenoud, M., Gulli, M., Peter, K., and Peter, M. (1998). The Cdc42p effector Gic2p is targeted for ubiquitin-dependent degradation by the SCFGrr1 complex. *EMBO J. , 17*, 5360-5373.

Jaspersen, S.L., and Winey, M. (2004). The budding yeast spindle pole body: structure, duplication, and function. *Annu Rev Cell Dev Biol., 20*, 1-28.

Joglekar, A., Bloom, K., and Salmon, E. (2009). In vivo protein architecture of the eukaryotic kinetochore with nanometer scale accuracy. *Curr Biol. , 19*, 694-9.

Joglekar, A., Bouck, D., Molk, J., Bloom, K., and Salmon, E. (2006). Molecular architecture of a kinetochore-microtubule attachment site. *Nat Cell Biol. , 8*, 581-5.

Kaiser, C., Michaelis, S., and Mitchell, A. (1994). *Methods in yeast genetics.* Cold Spring Harbor Laboratory Press: Cold Spring Harbor, N.Y.

Karimova, G., and Ladant, D. (2005). *A Bacterial Two-Hybrid System Based on a cAMP Signaling Cascade* (2 ed.). (E. Golemis, and P. Adam, Eds.) NY, USA: Cold Spring Harbor Laboratory Press.

Kawamukai, M., Gerst, J., Field, J., Riggs, M., Rodgers, L., Wigler, M., *et al*. (1992). Genetic and biochemical analysis of the adenylyl cyclase-associated protein, cap, in Schizosaccharomyces pombe. *Mol. Biol. Cell , 3*, 167-180.

Keaton, M., and Lew, D. (2006). Eavesdropping on the cytoskeleton: progress and controversy in the yeast morphogenesis checkpoint. *Curr Opin Microbiol. , 9*, 540-546.

Kelly, A., and Funabiki, H. (2009). Correcting aberrant kinetochore microtubule attachments: an Aurora B-centric view. *Curr Opin Cell Biol. , 21*, 51-58.

Kemmler, S., Stach, M., Knapp, M., Ortiz, J., Pfannstiel, J., Ruppert, T., *et al*. (2009). Mimicking Ndc80 phosphorylation triggers spindle assembly checkpoint signalling. *EMBO J , 28*, 1099-1110.

Kinoshita, M. (2006). Diversity of septin scaffolds. *Curr Opin Cell Biol. , 18*, 54-60.

Kitagawa, K., and Hieter, P. (2001). Evolutionary conservation between budding yeast and human kinetochores. *Nat Rev Mol Cell Biol. , 2*, 678-687.

Kolodner, R.D., Putnam, C.D., and Myung, K. (2002). Maintenance of genome stability in Saccharomyces cerevisiae. *Science*., *297*, 552-557.

Kosco, K.A., Pearson, C.G., Maddox, P.S., Wang, P.J., Adams, I.R., Salmon, E.D., Bloom, K., and Huffaker, T.C. (2001). Control of microtubule dynamics by Stu2p is essential for spindle orientation and metaphase chromosome alignment in yeast. *Mol Biol Cell*., *12*, 2870-2880.

Kozminski, K., Chen, A., Rodal, A., and Drubin, D. (2000). Functions and functional domains of the GTPase Cdc42p. *Mol Biol Cell. , 11*, 339-354.

Kraakman, L., Lemaire, K., Ma, P., Teunissen, A., Donaton, M., Van Dijck, P., *et al*. (1999). A Saccharomyces cerevisiae G-protein coupled receptor, Gpr1, is specifically required for glucose activation of the cAMP pathway during the transition to growth on glucose. *Mol Microbiol. , 32*, 1002-1012.

Krishnan, V., Nirantar, S., Crasta, K., Cheng, A.Y., and Surana, U. (2004). DNA replication checkpoint prevents precocious chromosome segregation by regulating spindle behavior. *Mol Cell*., *16*, 687-700.

Krishnan, V., and Surana, U. (2005). Taming the spindle for containing the chromosomes. *Cell Cycle*., *4*, 376-379.

Lampert, F., Hornung, P. and Westermann, S. (2010). The Dam1 complex confers microtubule plus end-tracking activity to the Ndc80 kinetochore complex. *J Cell Biol. 17*, 641-649.

Lappalainen, P., and Drubin, D. (1997). Cofilin promotes rapid actin filament turnover in vivo. *Nature , 388*, 78-82.

Le Masson, I., Saveanu, C., Chevalier, A., Namane, A., Gobin, R., Fromont-Racine, M., *et al*. (2002). Spc24 interacts with Mps2 and is required for chromosome segregation, but is not implicated in spindle pole body duplication. *Mol Microbiol. , 43*, 1431-1443.

Lee, K., Asano, S., Park, J., Sakchaisri, K., and Erikson, R. (2005). Monitoring the cell cycle by multi-kinase-dependent regulation of Swe1/Wee1 in budding yeast. *Cell Cycle. , 4*, 1346-1349.

Lew, D., and Burke, D. (2003). The spindle assembly and spindle position checkpoints. *Annu. Rev. Genet., 37*, 251-282.

Lew, D., and Reed, S. (1995). Cell cycle control of morphogenesis in budding yeast. *Curr. Opin. Genet. Dev. , 5*, 17-23.

Li, J., Li, Y., and Elledge, S. (2005). Genetic analysis of the kinetochore DASH complex reveals an antagonistic relationship with the ras/protein kinase A pathway and a novel subunit required for Ask1 association. *Mol Cell Biol. , 25*, 767-778.

Li, R., and Murray, A. (1991). Feedback control of mitosis in budding yeast. *Cell. , 66*, 519-31.

Li, Y., Bachant, J., Alcasabas, A., Wang, Y., Qin, J., and Elledge, S. (2002). The mitotic spindle is required for loading of the DASH complex onto the kinetochore. *Genes Dev. , 16*, 183-97.

Lin, H., de Carvalho, P., Kho, D., Tai, C.Y., Pierre, P., Fink, G.R., and Pellman, D. (2001). Polyploids require Bik1 for kinetochore-microtubule attachment. *J Cell Biol*., *155*, 1173-1184.

Lippincott, J., and Li, R. (1998). Sequential assembly of myosin II, an IQGAP-like protein, and filamentous actin, to a ring structure involved in budding yeast cytokinesis. *J. Cell Biol. , 140*, 355–366.

Liu, D., and Lampson, M. (2009). Regulation of kinetochore-microtubule attachments by Aurora B kinase. *Biochem Soc Trans. , 37*, 976-980.

Longtine, M., McKenzie, A. I., Demarini, D., Shah, N., Wach, A., Brachat, A., *et al*. (1998). Additional modules for versatile and economical PCR-based gene deletion and modification in Saccharomyces cerevisiae. *Yeast , 14*, 953–961.

Lopes, M., Cotta-Ramusino, C., Pellicioli, A., Liberi, G., Plevani, P., Muzi-Falconi, M., Newlon, C.S., and Foiani, M. (2001). The DNA replication checkpoint response stabilizes stalled replication forks. *Nature, 412*, 557-561.

Ma, L., McQueen, J., Cuschieri, L., Vogel, J., and Measday, V. (2007). Spc24 and Stu2 Promote Spindle Integrity When DNA Replication Is Stalled. *Mol Bio Cell , 8*, 2805-2816.

Ma, P., Wera, S., Van Dijck, P., and Thevelein, J. (1999). The PDE1-encoded Low-Affinity Phosphodiesterase in the Yeast Saccharomyces cerevisiae Has a Specific Function in Controlling Agonist-induced cAMP Signaling. *Mol. Biol. Cell , 10*, 91–104.

Maddox PS, Oegema K, Desai A, Cheeseman IM. (2004). "Holo"er than thou: chromosome segregation and kinetochore function in C. elegans. *Chromosome Res.*12, 641-653.

Maiato, H., Sampaio, P., and Sunkel, C. (2004). Microtubule-associated proteins and their essential roles during mitosis. *Int Rev Cytol. , 241*, 53-153.

Maiolica, A., Cittaro, D., Borsotti, D., Sennels, L., Ciferri, C., Tarricone, C., *et al.* (2007). Structural analysis of multiprotein complexes by cross-linking, mass spectrometry, and database searching. *Mol Cell Proteomics*. *12*, 2200-11.

Maney, T., Ginkel, L., Hunter, A., and Wordeman, L. (2000). The kinetochore of higher eucaryotes: a molecular view. *Int Rev Cytol. , 194*, 67-131.

Martin-Lluesma, S., Stucke, V., and Nigg, E. (2002). Role of Hec1 in spindle checkpoint signaling and kinetochore recruitment of Mad1/Mad2. *Science. , 297*, 2267-2270.

Matsumoto, K., Yoshimatsu, T., and Oshima, Y. (1983). Recessive mutations conferring resistance to carbon catabolite repression of galactokinase synthesis in Saccharomyces cerevisiae. *J Bacteriol. , 153*, 1405-1414.

Mattila, P., Quintero-Monzon, O., Kugler, J., Moseley, J., Almo, S., Lappalainen, P., *et al*. (2004). A high affinity interaction with ADP-actin monomers underlies the mechanism and in vivo function of Srv2/cyclase-associated protein. *Mol. Biol. Cell , 15*, 2324-2334.

Mbonyi, K., van Aelst, L., Argüelles, J., Jans, A., and Thevelein, J. (1990). Glucose-induced hyperaccumulation of cyclic AMP and defective glucose repression in yeast strains with reduced activity of cyclic AMP-dependent protein kinase. *Mol Cell Biol., 10*, 4518-4523.

McAinsh, A., Tytell, J., and Sorger, P. (2003). Structure, function, and regulation of budding yeast kinetochores. *Annu Rev Cell Dev Biol. , 19*, 519-539.

McCleland, M., Gardner, R., Kallio, M., Daum, J., Gorbsky, G., Burke, D., *et al*. (2003). The highly conserved Ndc80 complex is required for kinetochore assembly, chromosome congression,

and spindle checkpoint activity. *Genes Dev. , 17*, 101-114.

McCleland, M., Kallio, M., Barrett-Wilt, G., Kestner, C., Shabanowitz, J., Hunt, D., *et al*. (2004). The vertebrate Ndc80 complex contains Spc24 and Spc25 homologs, which are required to establish and maintain kinetochore-microtubule attachment. *Curr Biol. , 14*, 131-137.

McMillan, J., Sia, R., and Lew, D. (1998). A morphogenesis checkpoint monitors the actin cytoskeleton in yeast. *J Cell Biol. , 142*, 1487-1499.

McNulty, J., and Lew, D. (2005). Swe1p responds to cytoskeletal perturbation, not bud size, in S. cerevisiae. *Curr Biol , 15*, 2190–2198.

Measday, V., Hailey, D.W., Pot, I., Givan, S.A., Hyland, K.M., Cagney, G., Fields, S., Davis, T.N., and Hieter, P. (2002). Ctf3p, the Mis6 budding yeast homolog, interacts with Mcm22p and Mcm16p at the yeast outer kinetochore. *Genes Dev*., *16*, 101-113.

Meraldi, P., Draviam, V., and Sorger, P. (2004). Timing and checkpoints in the regulation of mitotic progression. *Dev Cell. , 7*, 45-60.

Miller, R. K., D'Silva, S., Moore, J. K., and Goodson, H. V. (2006). The CLIP-170 orthologue Bik1p and positioning the mitotic spindle in yeast. *Curr. Top. Dev. Biol, 76*,49–87.

Miller, S., Johnson, M., and Stukenberg, P. (2008). Kinetochore attachments require an interaction between unstructured tails on microtubules and Ndc80(Hec1). *Curr Biol. , 18*, 1785-1791.

Miranda, J.J., De Wulf, P., Sorger, P.K., and Harrison, S.C. (2005). The yeast DASH complex forms closed rings on microtubules. *Nat Struct Mol Biol*., *12*, 138-143.

Moffat, j., and Andrews, B. (2004). Late-G1 cyclin-CDK activity is essential for control of cell morphogenesis in budding yeast. *Nat Cell Biol. , 6*, 59-66.

Montpetit, B., Thorne, K., Barrett, I., Andrews, K., Jadusingh, R., Hieter, P., *et al*. (2005). Genome-wide synthetic lethal screens identify an interaction between the nuclear envelope protein, Apq12p, and the kinetochore in Saccharomyces cerevisiae. *Genetics , 171*, 489-501.

Morgan, D. O. (2007). *The cell cycle*. New Science Press.

Mösch, H., and Fink, G. (1997). Dissection of filamentous growth by transposon mutagenesis in Saccharomyces cerevisiae. *Genetics , 145*, 671-684.

Mösch, H., Roberts, R., and Fink, G. (1996). Ras2 signals via the Cdc42/Ste20/mitogen-activated protein kinase module to induce filamentous growth in Saccharomyces cerevisiae. *Proc Natl Acad Sci , 93*, 5352-5356.

Moseley, J., and Goode, B. (2005). Differential activities and regulation of Saccharomyces cerevisiae formin proteins Bni1 and Bnr1 by Bud6. *J Biol Chem. , 280*, 28023-28033.

Moseley, J., and Goode, B. (2006). The yeast actin cytoskeleton: from cellular function to biochemical mechanism. *Microbiol Mol Biol Rev. , 70*, 605-645.

Moseley, J., Okada, K., Balcer, H., Kovar, D., Pollard, T., and Goode, B. (2006). Twinfilin is an actin-filament-severing protein and promotes rapid turnover of actin structures in vivo. *J Cell Sci. , 119*, 1547-1557.

Musacchio, A., and Salmon, E. (2007). The spindle-assembly checkpoint in space and time. *Nat Rev Mol Cell Biol. , 8*, 379-93.

Neigeborn, L., and Mitchell, A.P. (1991). The yeast MCK1 gene encodes a protein kinase homolog that activates early meiotic gene expression. *Genes Dev*., *5*, 533-548.

Nekrasov, V.S., Smith, M.A., Peak-Chew, S. and Kilmartin, J.V. (2003). Interactions between centromere complexes in Saccharomyces cerevisiae. *Mol Biol Cell. 14*, 4931–4946

Newman, J., Wolf, E., and Kim, P. (2000). A computationally directed screen identifying interacting coiled coils from Saccharomyces cerevisiae. *Proc Natl Acad Sci., 97*, 13203-13208.

Ng, T.M., Waples, W.G., Lavoie, B.D. and Biggins, S. (2009). Pericentromeric sister chromatid cohesion promotes kinetochore biorientation. *Mol Biol Cell*., 20, 3818-27.

Nikawa, J., Cameron, S., Toda, T., and Ferguson, K. (1987). Rigorous feedback control of cAMP levels in Saccharomyces cerevisiae. *Genes Dev , 1*, 931-937.

Pagliuca, C., Draviam, V., Marco, E., Sorger, P., and De Wulf, P. (2009). Roles for the conserved spc105p/kre28p complex in kinetochore-microtubule binding and the spindle assembly checkpoint. *PLoS One. , 4*, e7640.

Park, H., and Bi, E. (2007). Central roles of small GTPases in the development of cell polarity in yeast and beyond. *Microbiol Mol Biol Rev. , 71*, 48-96.

Park, J., Grant, C., and Dawes, I. (2005). The high-affinity cAMP phosphodiesterase of Saccharomyces cerevisiae is the major determinant of cAMP levels in stationary phase: involvement of different branches of the Ras-cyclic AMP pathway in stress responses. *Biochem. Biophys. Res. Commun. , 327*, 311-319.

Parrou, J., and Fran ̧ois, J. (1997). A simplified procedure for a rapid and reliable assay of both glycogen and trehalose in whole yeast cells. *Anal Biochem. , 248*, 186-188.

Pasqualone, D., and Huffaker, T.C. (1994). STU1, a suppressor of a beta-tubulin mutation, encodes a novel and essential component of the yeast mitotic spindle. *J Cell Biol*., *127*, 1973-1984.

Pearson, C.G., Maddox, P.S., Salmon, E.D., and Bloom, K. (2001). Budding yeast chromosome structure and dynamics during mitosis. *J Cell Biol*., *152*, 1255-1266.

Perlman, P. S., and Mahler, H. R. (1974) Derepression of mitochondria and their enzymes in yeast: Regulatory aspects. *Arch. Biochem. Biophys. 162*,248–271

Peters, J., Tedeschi, A., and Schmitz, J. (2008). The cohesin complex and its roles in chromosome biology. *Genes Dev. , 22*, 3089-3114.

Pinsky, B.A. and Biggins, S. (2005). The spindle checkpoint: tension versus attachment. *Trends Cell Biol.,* 15, 486-493.

Pinsky, B.A., Kung, C., Shokat, K.M., and Biggins, S. (2006). The Ipl1-Aurora protein kinase activates the spindle checkpoint by creating unattached kinetochores. *Nat Cell Biol*., *8*, 78-83.

Pot, I., Knockleby, J., Aneliunas, V., Nguyen, T., Ah-Kye, S., Liszt, G., Snyder, M., Hieter, P., and Vogel, J. (2005). Spindle checkpoint maintenance requires Ame1 and Okp1. *Cell Cycle , 4*, 1448-1456.

Pot, I., Measday, V., Snydsman, B., Cagney, G., Fields, S., Davis, T.N., Muller, E.G., and Hieter, P. (2003). Chl4p and iml3p are two new members of the budding yeast outer kinetochore. *Mol Biol Cell*, *14*, 460-476.

Powers, A., Franck, A., Gestaut, D., Cooper, J., Gracyzk, B., Wei, R., *et al*. (2009). he Ndc80 kinetochore complex forms load-bearing attachments to dynamic microtubule tips via biased diffusion. *Cell , 136*, 865–875.

Pramila, T., Wu, W., Miles, S., Noble, W.S., and Breeden, L.L. (2006). The Forkhead

transcription factor Hcm1 regulates chromosome segregation genes and fills the S-phase gap in the transcriptional circuitry of the cell cycle. *Genes Dev*., *20*, 2266-2278.

Pruyne, D. W., Schott, D. H. and Bretscher, A. (1998). Tropomyosin-containing actin cables direct the Myo2p-dependent polarized delivery of secretory vesicles in budding yeast. *J Cell Biol 143*, 1931–1945

Pruyne, D., Evangelista, M., Yang, C., Bi, E., Zigmond, S., Bretscher, A., *et al*. (2002). Role of formins in actin assembly: nucleation and barbed-end association. *Science, 297*, 612-615.

Przewloka, M., and Glover, D. (2009). The kinetochore and the centromere: a working long distance relationship. *Annu Rev Genet. , 43*, 439-465.

Quintero-Monzon, O., Jonasson, E., Bertling, E., Talarico, L., Chaudhry, F., Sihvo, M., *et al*. (2009). Reconstitution and dissection of the 600-kDa Srv2/CAP complex: roles for oligomerization and cofilin-actin binding in driving actin turnover. *J Biol Chem. , 284*, 10923-10934.

Rolland, F., De Winde, J., Lemaire, K., Boles, E., Thevelein, J., and Winderickx, J. (2000). Glucose-induced cAMP signalling in yeast requires both a G-protein coupled receptor system for extracellular glucose detection and a separable hexose kinase-dependent sensing process. *Mol Microbiol. , 38*, 348-358.

Rolland, F., Wanke, V., Cauwenberg, L., Ma, P., Boles, E., Vanoni, M., *et al*. (2001). The role of hexose transport and phosphorylation in cAMP signalling in the yeast Saccharomyces cerevisiae. *FEMS Yeast Res. , 1*, 33-45.

Ronne, H. (1995). Glucose repression in fungi. *Trends Genet. 11*, 12–17.

Roof, D.M., Meluh, P.B., and Rose, M.D. (1992). Kinesin-related proteins required for assembly of the mitotic spindle. *J Cell Biol*., *118*, 95-108.

Rudoni, S., Colombo, S., Coccetti, P., and Martegani, E. (2001). Role of guanine nucleotides in the regulation of the Ras/cAMP pathway in Saccharomyces cerevisiae. *Biochim Biophys Acta. , 1538*, 181-189.

Sagot, I., Klee, S., and Pellman, D. (2002a). Yeast formins regulate cell polarity by controlling the assembly of actin cables. *Nat. Cell Biol. , 4*, 42-50.

Sagot, I., Rodal, A., Moseley, J., Goode, B., and Pellman, D. (2002b). An actin nucleation

mechanism mediated by Bni1 and profilin. *Nat. Cell Biol. , 4*, 626-631.

Santaguida, S., and Musacchio, A. (2009). The life and miracles of kinetochores. *EMBO J. , 28*, 2511-2531.

Sarin, S., Ross, K.E., Boucher, L., Green, Y., Tyers, M., and Cohen-Fix, O. (2004). Uncovering novel cell cycle players through the inactivation of securin in budding yeast. *Genetics*, *168*, 1763-1771.

Schittenhelm, R., Chaleckis, R., and Lehner, C. (2009). Intrakinetochore localization and essential functional domains of Drosophila Spc105. *EMBO J. , 28*, 2374-2386.

Scholz, O., Thiel, A., Hillen, W., and Niederweis, M. (2000). Quantitative analysis of gene expression with an improved green fluorescent protein. *Eur J Biochem , 267*, 1565-1570.

Schwartz, K., Richards, K., and Botstein, D. (1997). BIM1 encodes a microtubule-binding protein in yeast. *Mol. Biol. Cell, 8,* 2677–2691.

Segal, M., Bloom, K., and Reed, S. (2000). Bud6 directs sequential microtubule interactions with the bud tip and bud neck during spindle morphogenesis in Saccharomyces cerevisiae. *Mol Biol Cell. , 11*, 3689-702.

Severin, F., Habermann, B., Huffaker, T., and Hyman, T. (2001). Stu2 promotes mitotic spindle elongation in anaphase. *J Cell Biol*., *153*, 435-442.

Shero, J.H., and Hieter, P. (1991). A suppressor of a centromere DNA mutation encodes a putative protein kinase (MCK1). *Genes Dev*., *5*, 549-560.

Shimogawa, M.M., Graczyk, B., Gardner, M.K., Francis, S.E., White, E.A., Ess, M., Molk, J.N., Ruse, C., Niessen, S., Yates, J.R., 3rd, Muller, E.G., Bloom, K., Odde, D.J., and Davis, T.N. (2006). Mps1 phosphorylation of dam1 couples kinetochores to microtubule plus ends at metaphase. *Curr Biol*., *16*, 1489-1501.

Straight, A. (1997). Cell cycle: checkpoint proteins and kinetochores. *Curr Biol., 7*, R613-6.

Tanaka, K., Matsumoto, K., and Toh-E, A. (1989). IRA1, an inhibitory regulator of the RAS-cyclic AMP pathway in Saccharomyces cerevisiae. *Mol Cell Biol. , 9*, 757-768.

Tanaka, K., Mukae, N., Dewar, H., van Breugel, M., James, E.K., Prescott, A.R., Antony, C., and Tanaka, T.U. (2005). Molecular mechanisms of kinetochore capture by spindle microtubules.

Nature, 434, 987-994.

Tanaka, T., and Desai, A. (2008). Kinetochore-microtubule interactions: the means to the end. *Curr Opin Cell Biol. , 20*, 53-63.

Tanaka, T., Rachidi, N., Janke, C., Pereira, G., Galova, M., Schiebel, E., *et al*. (2002). Evidence that the Ipl1-Sli15 (Aurora kinase-INCENP) complex promotes chromosome bi-orientation by altering kinetochore-spindle pole connections. *Cell. , 108*, 317-329.

Tanaka, T., Stark, M., and Tanaka, K. (2005). Kinetochore capture and bi-orientation on the mitotic spindle. *Nat Rev Mol Cell Biol. , 6*, 929-942.

Taylor, S.S., and McKeon, F. (1997) Kinetochore localization of murine Bub1 is required for normal mitotic timing and checkpoint response to spindle damage. *Cell,* 89, 727–735.

Tcheperegine, S., Gao, X., and Bi, E. (2005). Regulation of cell polarity by interactions of Msb3 and Msb4 with Cdc42 and polarisome components. *Mol. Cell. Biol. , 25*, 8567-8580.

Thevelein, J. (1984). Regulation of trehalose mobilization in fungi. *Microbiol Rev. , 48*, 42-59.

Thevelein, J., Bonini, B., Castermans, D., Haesendonckx, S., Kriel, J., Louwet, W., *et al*. (2008). Novel mechanisms in nutrient activation of the yeast protein kinase A pathway. *Acta Microbiol Immunol Hung. , 55*, 75-89.

Tien, JF., Umbreit, NT., Gestaut, DR., Franck, AD., Cooper, J., Wordeman, L., *et al*. (2010). Cooperation of the Dam1 and Ndc80 kinetochore complexes enhances microtubule coupling and is regulated by aurora B. *J Cell Biol., 189*, 713-723.

Tirnauer, J. S., O'Toole, E., Berrueta, L., Bierer, B. E., and Pellman, D. (1999). Yeast Bim1p promotes the G1-specific dynamics of microtubules. *J. Cell Biol, 145*, 993–1007.

Toda, T., Uno, I., Ishikawa, T., Powers, S., Kataoka, T., Broek, D., *et al*. (1985). In yeast, RAS proteins are controlling elements of adenylate cyclase. *Cell , 40*, 27-36.

Tolliday, N., VerPlank, L., and Li, R. (2002). Rho1 directs formin-mediated actin ring assembly during budding yeast cytokinesis. *Curr Biol. , 12*, 1864-1870.

Trott, A., Shaner, L., and Morano, K. (2005). The molecular chaperone Sse1 and the growth control protein kinase Sch9 collaborate to regulate protein kinase A activity in Saccharomyces cerevisiae. *Genetics. , 170*, 1009-1021.

Tytell, J.D., and Sorger, P.K. (2006). Analysis of kinesin motor function at budding yeast kinetochores. *J Cell Biol., 172*, 861-874.

van Drogen, F., and Peter, M. (2002). Spa2p functions as a scaffold-like protein to recruit the Mpk1p MAP kinase module to sites of polarized growth. *Curr. Biol. , 12*, 1698-1703.

Wan X, X., O'Quinn, R., Pierce, H., Joglekar, A., Gall, W., DeLuca, J., *et al*. (2009). Protein architecture of the human kinetochore microtubule attachment site. *Cell. , 137*, 672-84.

Wang, H., Ramey, V., Westermann, S., Leschziner, A., Welburn, J., Nakajima, Y., *et al*. (2007). Architecture of the Dam1 kinetochore ring complex and implications for microtubule-driven assembly and force-coupling mechanisms. *Nat Struct Mol Biol. , 14*, 721-726.

Wang, P.J., and Huffaker, T.C. (1997). Stu2p: A microtubule-binding protein that is an essential component of the yeast spindle pole body. *J Cell Biol*., *139*, 1271-1280.

Warren, C.D., Brady, D.M., Johnston, R.C., Hanna, J.S., Hardwick, K.G. and Spencer, F.A. (2002). Distinct chromosome segregation roles for spindle checkpoint proteins. *Mol. Biol. Cell*, 13, 3029–3041.

Wei, R., Al-Bassam, J., and Harrison, S. (2007). The Ndc80/HEC1 complex is a contact point for kinetochore-microtubule attachment. *Nat Struct Mol Biol. , 14*, 54-59.

Wei, R., Sorger, P., and Harrison, S. (2005). Molecular organization of the Ndc80 complex, an essential kinetochore component. *Proc Natl Acad Sci. , 102*, 5363-5367.

Weinert, T.A., Kiser, G.L., and Hartwell, L.H. (1994). Mitotic checkpoint genes in budding yeast and the dependence of mitosis on DNA replication and repair. *Genes Dev*., *8*, 652-665.

Weiss, E., and Winey, M. (1996). The Saccharomyces cerevisiae spindle pole body duplication gene MPS1 is part of a mitotic checkpoint. *J Cell Biol. , 132*, 11-23.

Werner-Washburne, M., Braun, E., Crawford, M., and Peck, V. (1996). Stationary phase in Saccharomyces cerevisiae. *Mol Microbiol. , 19*, 1159-1166.

Westermann, S., Avila-Sakar, A., Wang HW, H., Niederstrasser, H., Wong, J., Drubin, D., *et al*. (2005). Formation of a dynamic kinetochore- microtubule interface through assembly of the Dam1 ring complex. *Mol Cell. , 17*, 277-290.

Westermann, S., Drubin, D., and Barnes, G. (2007). Structures and functions of yeast kinetochore complexes. *Annu Rev Biochem. , 76*, 563-591.

Wigge, P., and Kilmartin, J. (2001). The Ndc80p complex from Saccharomyces cerevisiae contains conserved centromere components and has a function in chromosome segregation. *J Cell Biol. , 152*, 349-360.

Wilson-Kubalek, E., Cheeseman, I., Yoshioka, C., Desai, A., and Milligan, R. (2008). Orientation and structure of the Ndc80 complex on the microtubule lattice. *J Cell Biol. , 182*, 1055-1061.

Wang P.J. and Huffaker T.C. (1997). Stu2p: A microtubule-binding protein that is an essential component of the yeast spindle pole body. *J Cell Biol., 139,* 1271-80.

Wong, J., Nakajima, Y., Westermann, S., Shang, C., Kang, J., Goodner, C., *et al*. (2007). A protein interaction map of the mitotic spindle. *Mol Biol Cell , 18*, 3800-3809.

Wolyniak, M.J., Blake-Hodek, K., Kosco, K., Hwang, E., You, L., and Huffaker, T.C. (2006). The regulation of microtubule dynamics in Saccharomyces cerevisiae by three interacting plus-end tracking proteins. *Mol Biol Cell., 17,* 2789-2798.

Yabuki, N., Terashima, H., and Kitada, K. (2002). Mapping of early firing origins on a replication profile of budding yeast. *Genes Cells., 7,* 781-789.

Yin, H., You, L., Pasqualone, D., Kopski, K.M., and Huffaker, T.C. (2002). Stu1p is physically associated with beta-tubulin and is required for structural integrity of the mitotic spindle. *Mol Biol Cell., 13,* 1881-1892.

Yu, J., Wang, C., Palmieri, S., Haarer, B., and Field, J. (1999). A cytoskeletal localizing domain in the cyclase-associated protein, CAP/Srv2p, regulates access to a distant SH3-binding site. *J. Biol. Chem. , 274*, 19985-19991.

Zaragoza, O., and Gancedo, J. (2000). Pseudohyphal growth is induced in Saccharomyces cerevisiae by a combination of stress and cAMP signalling. *Antonie Van Leeuwenhoek , 78*, 187-194.

Zimniak, T., Stengl, K., Mechtler, K., and Westermann, S. (2009). Phosphoregulation of the budding yeast EB1 homologue Bim1p by Aurora/Ipl1p. *J. Cell Biol, 186*, 379–391.

Zheng, L., Chen, Y., and Lee, W. (1999). Hec1p, an evolutionarily conserved coiled-coil protein, modulates chromosome segregation through interaction with SMC proteins. *Mol Cell Biol. , 19*,

5417-28.

Zhu, G., and Davis, T.N. (1998). The fork head transcription factor Hcm1p participates in the regulation of SPC110, which encodes the calmodulin-binding protein in the yeast spindle pole body. *Biochim Biophys Acta*., *1448,* 236-244.

Zhu, G., Muller, E.G., Amacher, S.L., Northrop, J.L., and Davis, T.N. (1993). A dosage-dependent suppressor of a temperature-sensitive calmodulin mutant encodes a protein related to the fork head family of DNA-binding proteins. *Mol Cell Biol*., *13,* 1779-1787.

Appendices

Appendix A *spc24-9* arrests in G1 after metaphase release

A.1 Results and Discussion

When *spc24* mutants are synchronized in G1 phase with mating pheromone and released to restrictive temperature, a variety of arrest phenotypes are detected. *spc24-8* cells are arrested in metaphase with an undivided nucleus and short spindles due to an active spindle checkpoint; *spc24-10* mutants lack a functional spindle checkpoint and as a result the spindle elongates despite the fact that chromosomes are not attached to the spindle and the DNA remains in the mother cell; *spc24-9* mutant cells undergo chromosome mis-segregation with elongated spindles which separate the DNA in the mother cell and the bud unequally, and finally have a mixture of large budded and G1 cells (Montpetit, *et al.*, 2005; Ma, *et al*., 2007). All the above phenotypes are induced after G1 phase and the defect is detected either in metaphase or anaphase. However the Ndc80 complex may also have a role after anaphase but this would not have been detected due to the G1 cell synchrony method. Therefore, I constructed a *GAL-CDC20* fusion (with the *CDC20* open reading frame fused to the *GAL1* promoter) in *spc24* mutant cells (see 4.3.2) so that the cells could be arrested in metaphase upon glucose treatment due to Cdc20 depletion. In order to compromise Spc24 function after metaphase, *spc24* ts mutants were arrested in metaphase by glucose depletion at 25℃ and then released into galactose media at the non-permissive temperature (37℃) to allow expression of *CDC20* and progression through the

cell cycle. As determined by monitoring cellular DNA content and nuclear position (Figure A.1A,B), *spc24-8* cells passed through anaphase at a similar pace to wild type cells then stalled in G1 for about an hour prior to continue the cell cycle, indicative of a delay at START. Combined with our previous data showing the phenotype after G1 release, *spc24-8* cells are expected to arrest with a 2N DNA content in metaphase which probably would have occurred if the time course had been extended for longer. s*pc24-10* cells entered G1 phase earlier than the wild type probably due to the inactivation of the spindle checkpoint. At 4 hours *spc24-10* cells mostly had 2N DNA content with an undivided nucleus in either small budded or large budded cells whereas the wild type cells had a mixture of 1N and 2N DNA content along with a mix of G1 and budded cells. When released from a G1 arrest to restrictive temperature for 2 hours, *spc24-10* also has a 2N DNA content but upon further incubation at restrictive temperature, the unsegregated DNA is replicated to 4N indicative of a defective spindle checkpoint (Montpetit, *et al*., 2005). Future work would be to determine if *spc24-10* cells released from the *GAL-CDC20* metaphase block eventually bypass the spindle checkpoint as well. Interestingly, *spc24-9* cells were arrested with 1N DNA and ~60% G1 cells after release from the Cdc20 block. Since over 90% of *spc24-9* G1 cells have unpolarized actin cables (Figure A.1C), *spc24-9* cells might have defects in bud site selection or polarity establishment. Alternatively, *spc24-9* cells might not able to pass START. In budding yeast, small daughter cells do not pass START until they have reached the size of the mother cell. PKA activity is required for cell growth in G1, but needs to be downregulated at START due to cAMP mediated repression of *CLN1,2* transcription (Baroni,

et al., 1994). Therefore, the other possibility for the G1 arrest of *spc24-9* is an inability to downregulate the PKA pathway and a lack of *CLN1,2* expression due to high cAMP levels. This possibility could be tested by performing a microarray analysis of *spc24-9* gene transcripts during a synchronous cell cycle, followed by northern blot analysis of specific transcripts.

A.2 Materials and methods

Timecourse, FACs, budding index and microscopy. Cells were grown to early-logarithmic phase in 150ml YPGal (2% galactose) at 25℃, spun down, resuspended in YPD (2% glucose) and incubated for 2 hours to arrest cells in metaphase. Cells were collected, washed once with YPGal, resuspended in prewarmed YPGal and shifted to 37℃. 10ml of culture was collected for each indicated time point. 5ml cells were fixed with 4% formaldehyde for 1hour, washed with PBS three times, resuspended in 100ul PBS plus 10ul Rhodamine Phalloidin (6.6μM in MeOH) (Molecular Probes Inc.), incubated in the dark at 4℃ overnight, then washed and resuspended with PBS/DAPI solution (1:2000) before imaging. See the details of microscopy in Chapter 4.2. FACs analysis was performed as described (Haase, *et al*., 1997).

A

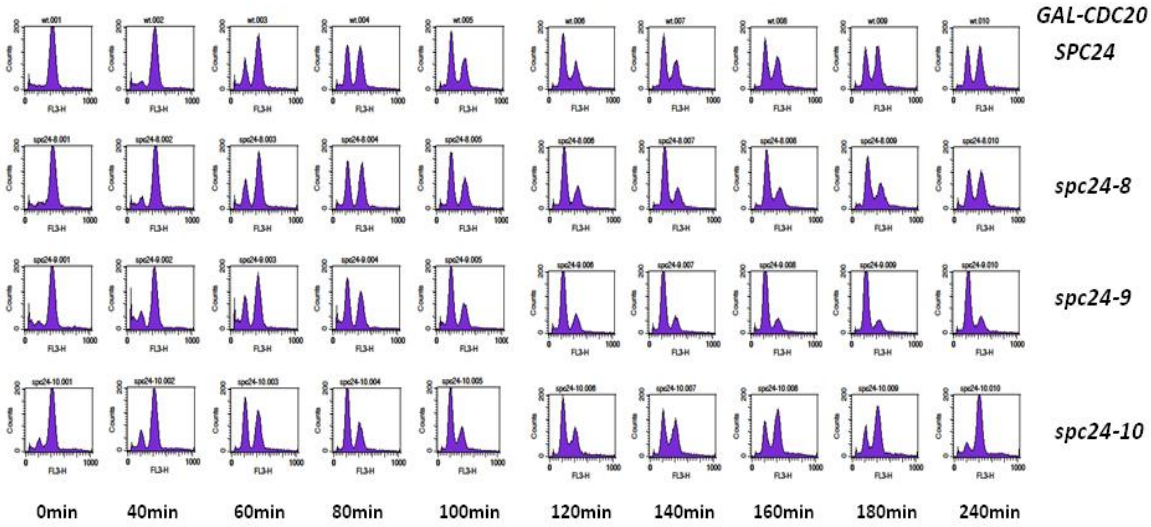
GAL-CDC20
SPC24
spc24-8
spc24-9
spc24-10
0min
40min
60min
80min
100min
120min
140min
160min
180min
240min

B

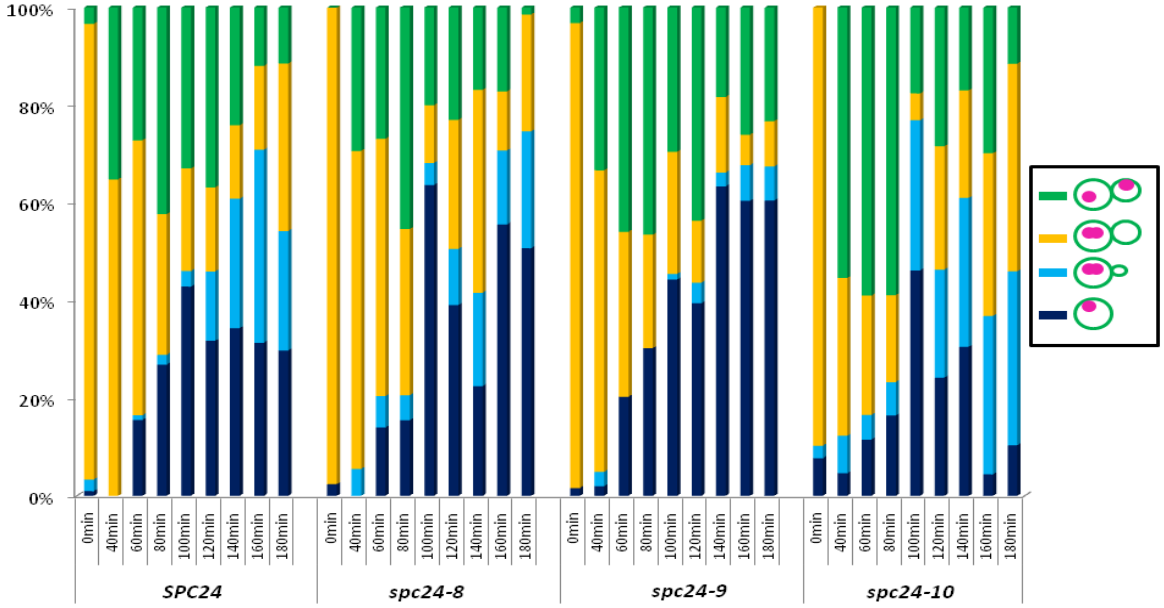
100%
80%
60%
40%
20%
0%
0min
40min
60min
80min
100min
120min
140min
160min
180min
SPC24
spc24-8
spc24-9
spc24-10

C

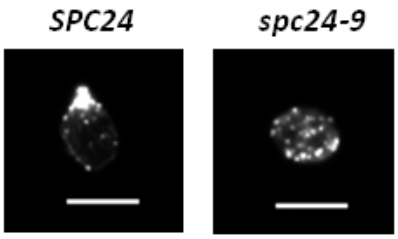
SPC24
spc24-9

Figure A.1 *spc24-9* mutants delay in G1 after a metaphase arrest

GAL-CDC20 cells were grown in galactose at 25°C, arrested in metaphase with 2% glucose (YPD) for 2h at 25 ℃, washed and resuspended with YPG and released to 37 ℃. Time points were taken at 0min, and every 20min for 4 hours. FACs (A) and budding index (B) are shown at indicated times. (C) *spc24-9* mutants have defects in polarity establishment in G1. Actin was stained with Rhodamine Phalloidin.

Appendix B Analysis of Ndc80 localization

B.1 Results and discussion

The well-known localization of the Ndc80 complex is at the kinetochore, however phenotypic analysis of mutants of this complex suggest that it might have functions at other cellular locations. I imaged Ndc80 tagged with VFP at its endogenous locus and, in addition to the well established kinetochore localization of Ndc80, I found that Ndc80 localizes along the spindle in large budded cells with an extended spindle (Figure B1.A). The spindle localization of Ndc80 has not been reported before probably because the intensity of the dots along the spindle is fairly low and therefore has likely been missed. To further characterize the minor pool of Ndc80 by amplifying the fluorescence signal, I constructed a high copy plasmid carrying Ndc80-GFP (pNdc80-GFP) and imaging of wild type cells containing this plasmid confirmed that Ndc80 localizes to punctate spots along the spindle (Figure B1.B). Several kinetochore proteins (Ndc10, Slk19), MT plus end-tracking proteins (Bim1, Bik1, Stu1 and Stu2), kinesins (Cin8, Kip3) and the Ipl1 complex have been reported to localize to the spindle midzone during anaphase and be required for anaphase spindle stability (Khmelinskii, *et al*., 2007). Therefore, Ndc80 may also have a role in anaphase spindle stability or later events.

In addition, I also detected a fainter Ndc80-GFP signal in the vicinity of the cell cortex (Figure B2.A). With time-lapse imaging, I found that the Ndc80-GFP foci localized to the cortex transiently and then moved away (arrow in Figure B2.B) which is reminiscent of the highly dynamic behavior of the plus end of cMT. Aiming to confirm the precise localization of

the non-kinetochore pool of Ndc80, I studied the localization of Ndc80 in mCherry-Tub1 wild type cells harboring pNdc80-GFP. As shown in Figure B3, the non-kinetochore pool of Ndc80 overlays with the mCherry-Tub1 signal which could be the cMT plus end. However, in some of the cells (Figure B3.C-D) there is a strong GFP foci of non-kinetochore Ndc80 that overlaps with a weaker Tub1 signal and the Tub1 signal is not at the expected location of a cMT plus end. Since Ndc80 is known to bind directly to MTs (Cheeseman *et al.* 2006; Deluca *et al.* 2006; Wei *et al.* 2007; Ciferri *et al.* 2008; Guimarase *et al.* 2008; Miller *et al.* 2008), it is possible that overexpression of Ndc80 produces excess Ndc80 that recruits free cellular tubulin which is why I detect a bright off spindle Tub1 signal colocalized with Ndc80-GFP. To clarify whether pNdc80-GFP localizes to the cMT plus end or not, I attempted imaging pNdc80-GFP with another cMT marker - Bik1-RFP. However, the Bik1-RFP signal is extremely weak and the current camera system on our miscroscope requires a 2 to 3 second exposure to detect this signal. It is therefore impossible to study the dynamics of Bik1 localization under these conditions. The lab is currently waiting to purchase a more sensitive cooled CCD camera to enable detection of weak RFP signals so that this experiment can be completed in the future.

B.2 Materials and methods

B.2.1 Strains and plasmid

The 2μ plasmid containing the *NDC80* promoter followed by the full length *NDC80* ORF (backbone p5467) was a gift from Charlie Boone's lab (University of Toronto). *pNDC80* was

tagged with GFP+ (Scholz, *et al*., 2000) by PCR-based homologous recombination (Longtine, *et al*., 1998). pRS406-mCherry-Tub1, which was a gift from Steven. I. Reed (The Scripps Research Institute), was digested with NdeI before homologous recombination in yeast. All endogenous tagging with GFP+, VFP, CFP or RFP was performed by PCR-based homologous recombination (Longtine, *et al*., 1998).

B.2.2 Microscopy

Microscopic analysis of yeast cells was performed with a Zeiss Axio Observer Inverted Microscope equipped with a Zeiss Colibri LED illuminator and a Zeiss Axiocam Ultra High Resolution Monochrome Digital Camera Rev3.0. Cells were grown to mid-log phase in SC medium at 25 ℃, resuspended with fresh media and added onto a concanavalin A coated (Nissan, *et al*., 2008) glass bottom dish (MatTek Corporation #P35G-1.5-14-C) for imaging. Imaging stacks were acquired with a 40x objective at a step of 0.2 μm to span the entire cell and images were analyzed with Zeiss Axiovision software.

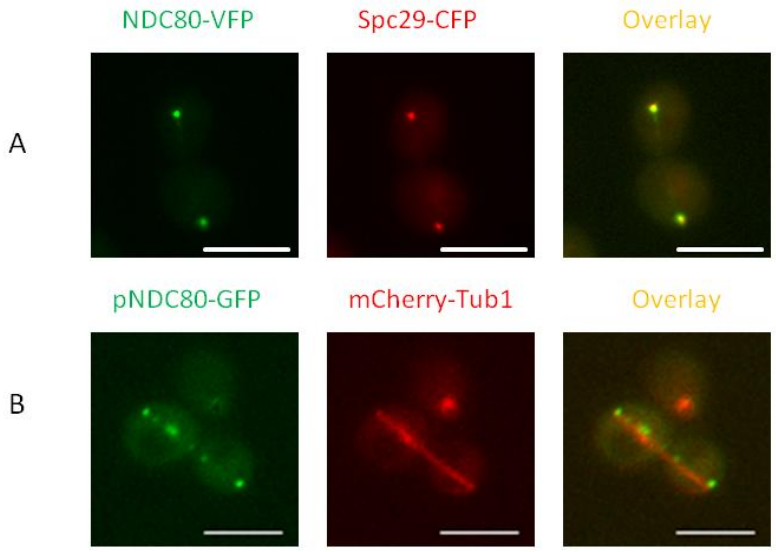

Figure B.1 Ndc80 is scattered along the spindle in anaphase

Ndc80VFP Spc29CFP cells (A) and mCherry-Tub1 cells harboring the pNdc80-GFP high copy plasmid were grown to mid-log phase in SC media at 25℃ and resuspended with fresh media for live imaging. Scale bar, 5μm.

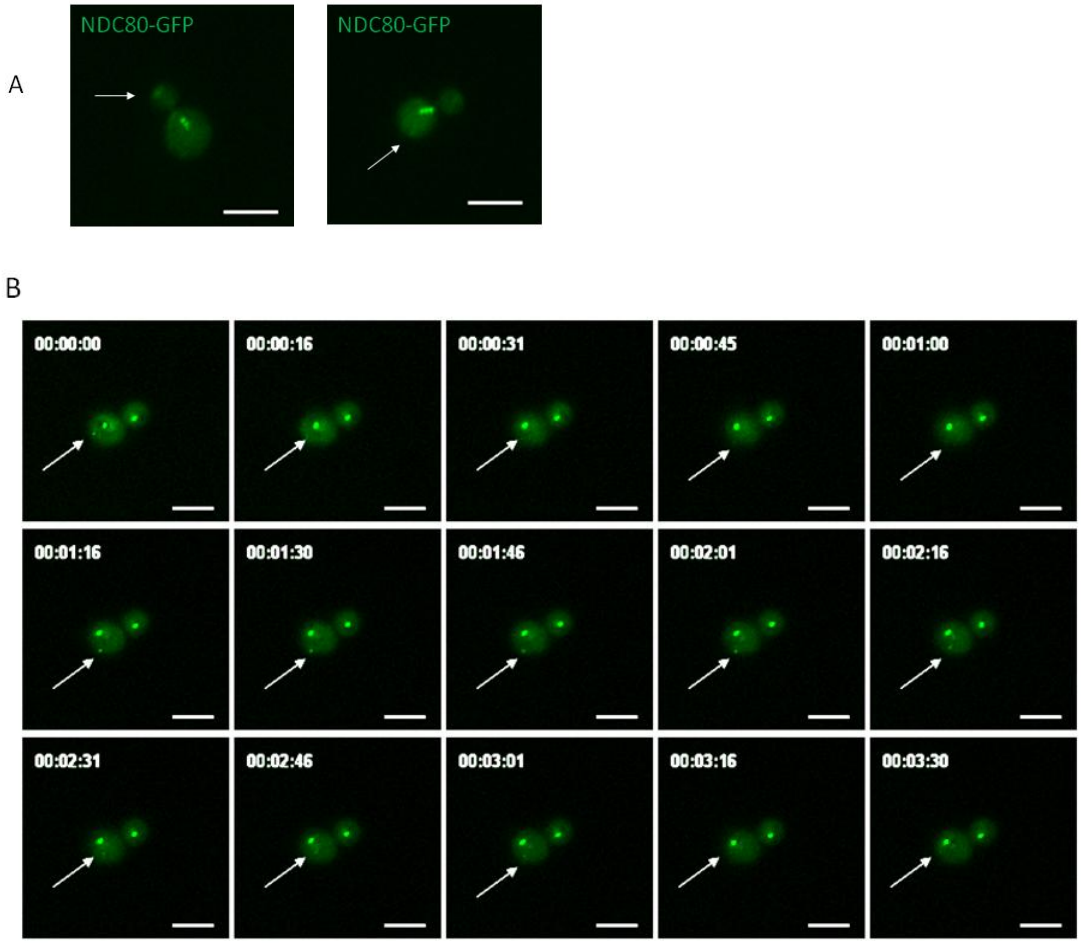

Figure B.2 Localization of Ndc80 to a non-kinetochore foci

Endogenous Ndc80-GFP cells were grown into mid-log phase in SC media at 25℃ and resuspended with fresh SC media for live imaging (A) and live imaging timelapse (B). The white arrow indicates the non-kinetochore Ndc80 foci. Scale bar, 5μm.

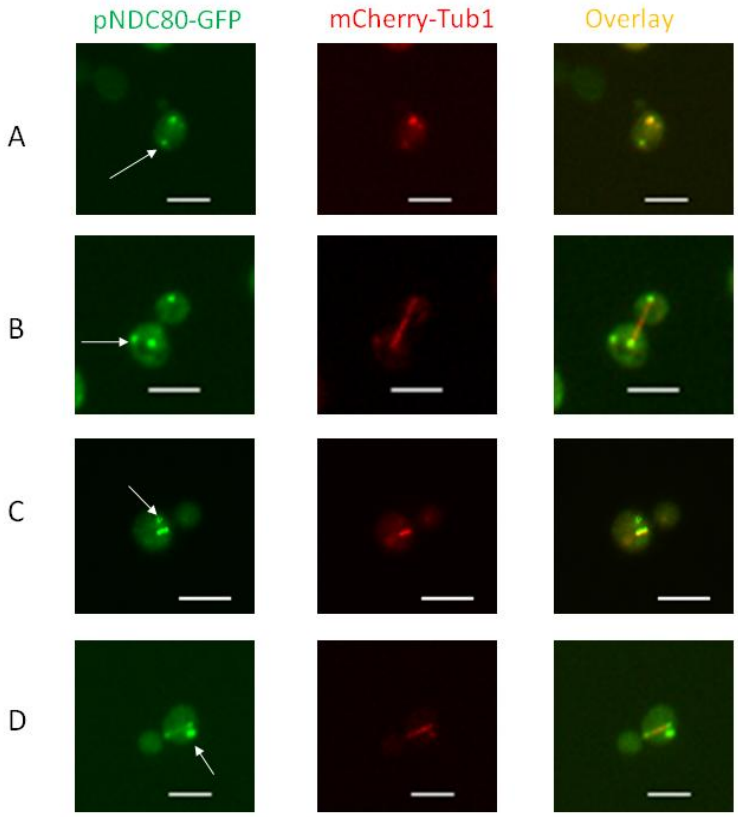

Figure B.3 Non-kinetochore pool of Ndc80 co-localizes with Tub1

mCherry-Tub1 cells harboring pNdc80GFP were grown to mid-log phase in SC media at 25℃ and resuspended with fresh SC media for live imaging. The white arrow indicates the non-kinetochore Ndc80 foci. Scale bar, 5μm.